AERODYNAMIC INVESTIGATION OF A MODEL SCALE HELICOPTER ROTOR IN GROUND EFFECT

A THESIS SUBMITTED TO
THE GRADUATE SCHOOL OF NATURAL AND APPLIED SCIENCES
OF
MIDDLE EAST TECHNICAL UNIVERSITY

BY

MEHMET ŞAHBAZ

IN PARTIAL FULFILLMENT OF THE REQUIREMENTS
FOR
THE DEGREE OF MASTER OF SCIENCE
IN
AEROSPACE ENGINEERING

OCTOBER 2017

Approval of the thesis:

AERODYNAMIC INVESTIGATION OF A MODEL SCALE HELICOPTER ROTOR IN GROUND EFFECT

Submitted by **MEHMET ŞAHBAZ** in partial fulfillment of the requirements for the degree of **Master of Science in Aerospace Engineering Department, Middle East Technical University** by,

Prof. Dr. Gülbin Dural Ünver
Dean, Graduate School of **Natural and Applied Sciences** __________________

Prof. Dr. Ozan Tekinalp
Head of Department, **Aerospace Engineering** __________________

Assoc. Prof. Dr. Dilek Funda Kurtuluş
Supervisor, **Aerospace Engineering Dept., METU** __________________

Asst. Prof. Dr. Nilay Sezer Uzol
Co-Supervisor, **Aerospace Engineering Dept., METU** __________________

Examining Committee Members:

Prof. Dr. Yusuf Özyörük
Aerospace Engineering Dept., METU __________________

Assoc. Prof. Dr. Dilek Funda Kurtuluş
Aerospace Engineering Dept., METU __________________

Prof. Dr. Ünver Kaynak
Mechanical Engineering Dept.,
TOBB University of Economics and Technology __________________

Assoc. Prof. Dr. Mehmet Metin Yavuz
Mechanical Engineering Dept., METU __________________

Asst. Prof. Dr. Nilay Sezer Uzol
Aerospace Engineering Dept., METU __________________

Date: 18.10.2017

I hereby declare that all the information in this document has been obtained and presented in accordance with academic rules and ethical conduct. I also declare that, as required by these rules and conduct, I have fully cited and referenced all material and results that are not original to this work.

Name, Last Name: Mehmet ŞAHBAZ

Signature:

ABSTRACT

AERODYNAMIC INVESTIGATION OF A MODEL SCALE HELICOPTER ROTOR IN GROUND EFFECT

Şahbaz, Mehmet
M.S., Department of Aerospace Engineering
Supervisor: Assoc. Prof. Dr. Dilek Funda Kurtuluş
Co – Supervisor: Asst. Prof. Dr. Nilay Sezer Uzol

October 2017, 126 pages

In this thesis, ground effect issue which is a vital topic for helicopter industry is investigated with model scale.For this purpose, a test setup with model helicopter rotor is established. With setup, ground effect is investigated with inclined ground and ground without inclination. Thrust and torque values are obtained for different rotation speeds with constant collective pitch. Comparison with literature is done and reliability of the test setup is proven. Inclined Ground Effect and Ground Effect with extreme proximity scenarios are tested. The proper trends of the performance parameters in these scenarios are obtained.

For the sake of performance parameter alterations, CFD (Computational Fluid Dynamics) Method is applied to analyze the rotor downwash. To model the rotating helicopter blade, Single Moving Reference Frame Method (SMRF) is used. In this method, the blade and background mesh are kept still and rotational velocity is defined at each cell in the domain. With CFD results, flow physics is studied and performance changes in ground effect are explained.

Keywords: Ground Effect, Experimental Aerodynamics, Computational Fluid Dynamics, Rotor, Helicopter, Model Scale

ÖZ

ÖLÇEKLENDİRİLMİŞ MODEL HELİKOPTER ROTORUNUN YER ETKİSİ DURUMUNDA AERODİNAMİK OLARAK INCELENMESİ

Şahbaz, Mehmet
Yüksek Lisans, Havacılık ve Uzay Mühendisliği Bölümü
Tez Yöneticisi: Doç. Dr. Dilek Funda Kurtuluş
Ortak Tez Yöneticisi: Yrd. Doç. Dr. Nilay Sezer Uzol

Ekim 2017, 126 sayfa

Bu tezde, helikopter endüstrisi için önem arzeden “yer etkisi” durumu, model ölçütlerde incelenmiştir. Bu amaçla, model bir helikopter rotorunun yer aldığı bir düzenek kurulmuş. Düzenek üzerinde yer etkisi durumu, hem düz, hem de eğimli yüzey olarak modellenmiştir. Düzenekte, farklı dönüş hızlarında, sabit kolektif açısında itki ve tork değerleri elde edilmiş, literatür ile karşılaştırılmıştır. Bu karşılaştırma sonucu düzeneğin güvenilirliği kanıtlanmıştır. Eğimli ve çok yakın mesafelerdeki yer etkisi senaryoları test edilmiş, bu senaryolarda performans parametrelerinin düzenli değişimleri saptanmıştır.

Düzenekten elde edilen değişimlere ne gibi durumların sebebiyet verdiğini öğrenebilmek adına, akış analizi için Hesaplamalı Akışkanlar Dinamiği (HAD) yöntemleri kullanılmıştır.Yazılımda, dönen helikopter palini modellemek için, Hareketli Referans Yapı yöntemi kullanılmıştır. Bu yöndemde amaç, pal ve çözüm ağının sabit tutulup, dönüş hızının her hücreye tanımlamaktır.HAD sonuçları ile akış fiziği incelenerek, yer etkisi durumundaki performans değişimlerine değişimleri işaret edilmiştir.

Anahtar Kelimeler: Yer etkisi, Deneysel Aerodinamik, Hesaplamalı Akışkanlar Dinamiği, Rotor, Helikopter, Model Ölçek

To my family

ACKNOWLEDGEMENTS

I would like to express my deepest gratitude to my supervisor, Assoc. Prof. Dr. Dilek Funda Kurtuluş for his guidance, advice, criticism, insight, and encouragement throughout the research.

I would also like to thank my superiors within the Department of Aerospace Engineering, Asst. Prof. Dr. Nilay Sezer Uzol and Assoc. Prof. Dr. Oguz Uzol, for their supports during the study.

I want to express my gratitude to my colleagues, and my other friends who were there to give me support during my study.

I would like to thank my parents, who never ceased to give me encouragement and pray for me during my graduate study.

I would also like to show my thanks to my close friends. Thank you very much for being there to support me.

I would like to thank to METU Center for Wind Energy (METUWIND) for supporting me financially and for provide me their facilities during my graduate level education.

TABLE OF CONTENTS

LIST OF TABLES

TABLES

LIST OF FIGURES

FIGURES

LIST OF SYMBOLS

A	Rotor Disk Area
C_P	Power Coefficient
C_{P_i}	Induced Power Coefficient
C_{P_p}	Profile Power Coefficient
C_Q	Torque Coefficient
C_T	Thrust Coefficient
P	Power
P_i	Induced Power
P_p	Profile Power
R	Rotor Radius
T	Thrust
T/T_{OGE}	Non – Dimensional Thrust
Q	Torque
Q/Q_{OGE}	Non- Dimensional Torque
V_{tip}	Rotor Tip Velocity
v_i	Inflow Velocity
z	Ground – Rotor Distance
z/R	Non – Dimensional Ground – Rotor Distance
β	Ground Inclination Angle
λ	Inflow
ρ	Air Density
ψ	Blade Azimuth Angle
Ω	Rotational Velocity

LIST OF ABBREVIATIONS

CFD	Computational Fluid Dynamics
IGE	In Ground Effect
OGE	Out of Ground Effect
RPM	Revolution Per Minute
SMRF	Single Moving Reference Frame
TPP	Tip Path Plane

CHAPTER 1

INTRODUCTION

1.1 Brief İnformation About Helicopters and Rotor Aerodynamics

Through the years, air transportation keeps its unique place in the history of humanity. Various aircraft types were built and used throughout the decades. The main aim of aircraft industry is always “rapid air transportation” except, for one type of aircraft, which is not valid: helicopters.

Helicopters are type of aircraft that can hover in the air. This feature separates helicopter from other aircraft. Since all other aircraft are designed for horizontal flying, helicopters are designed for both vertical and horizontal flight, on the contrary. The main usage areas of helicopter are available in Figure 1.1.

Figure 1.1 Helicopters with different usages a) Resque b) Freight transport c) Law enforcement, d) Broadcasting, e) Construction, f) Fire, g) Military [1]

The most important benefit of the helicopter is capability of landing / takeoff from the place where long landing strips or airfields are impractical to build. Since helicopter can descent or climb vertically, a landing field with adequate size is enough for landing or takeoff.

The manuevers of hovering in the air and climbing/descenting vertically make helicopters unique. In order to understand the topic of this thesis accurately, the vertical and hovering flight characteristics of the helicopter must be examined in detail.

 Although a helicopter has aerodynamic lifting surfaces, the working principle of helicopters are quite different from fixed wing aircraft. What happens in fixed wings is that air is accelerated with propulsion systems and incoming air against wing/aircraft creates lift force on the wings due to their airfoil shapes that creates high pressure below the wing and low pressure above the wing. Basically this is the lift creation principle of the fixed wing aircraft. However, helicopters have different principle. Instead of fixed wings, helicopters have lifting surfaces like wings that forms the most crucial part of the helicopter which is called as “ main rotor”.

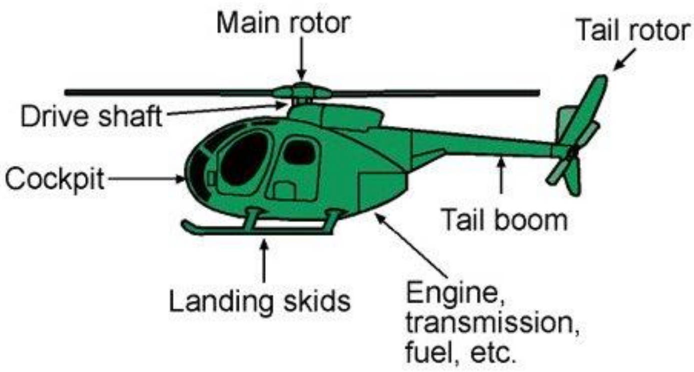

Figure 1.2 The main components of a helicopter [2]

As seen from Figure 1.2, a conventional helicopter consists of basic elements. The main rotor provides the thrust needed for the hover flight, axial climb and descent. Driving shaft connects engine and main rotor to the transmission system. Landing skids provide smooth vertical landing to the corrupted zones. Furthermore, tail rotor has a mission of balancing the main rotor rotational torque with a moment creation using tail boom as a moment arm. It is named as “anti – torque system” as shown in Figure 1.3.

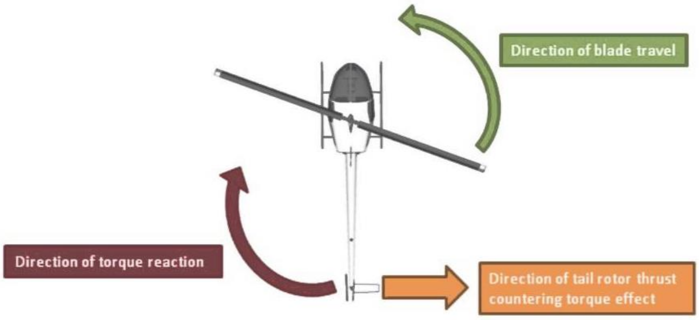

Figure 1.3 Anti torque system [3]

In Figure 1.3, tail rotor balances the torque created by the main rotor. If there is no tail rotor, helicopter does not perform hovering flight.

The scope of this thesis is the investigation of the performance of the main rotor. As defined before, helicopter is unique with its vertical flight and axial descent/climb motions. Of course, helicopter can perform forward flight with tilting the main rotor by changing the helicopter attitude by performing a low pitch down motion. But forward flight is not the main scope of this work. In this work, axial flight characterictics of helicopters are investigated.

Since main rotor provides the axial thrust for helicopters, it creates most of the unique flow features around helicopters.

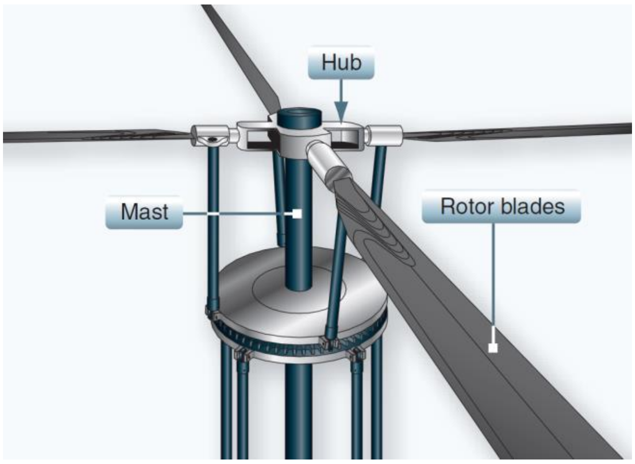

Figure 1.4 Helicopter rotor and its main components [4]

In Figure 1.4, main rotor consists of rotor blades, and hub. The rotor blades are lifting surfaces of the rotor and they are basically denoted as “rotary wings” since their sections are airfoils utilized for rotary wing applications. Rotor could have 2,3 or 5 blades depends on the type and weight capacity of the helicopter.

Rotor aerodynamics is a complex issue even in forward flight. However, for axial flight, rotor aerodynamics have some fundamental points with contribution of research and experiment in literature. Since helicopter design starts with axial flight characteristics of rotor, various scientific studies and empirical relations are available about rotor aerodynamics. Also, various mathematical models and experimental results are established about the hovering flight of helicopters.

The lifting capability of a rotor blade depends on two main parameters: local angle of attack and local dynamic pressure [1]. If rotor blade is considered as finite wing and divided into 2D stations by taking slices, every station is considered as airfoil and each one encounters to the incoming air flow created by rotation. With respect to the local angle of attack and local dynamic pressures on each station, local lift and drag generation is evident. Then, forces are integrated spanwise which is simply the contribution of one blade to the thrust of the rotor. However, there is no fixed wing situation. Here, a rotation is taken into account. Blades are deliberately rotating that means their position is changing. The blade position is denoted by azimuth angle (ψ). Azimuth angle is zero when blade tip points downstream. During force, torque calculations, another integration with respect to the azimuth angle is performed since rotor blade location is not the same. In fixed wing cases, wing encounters with the same incoming air velocity from root to tip. In rotor case, due to the rotation, the velocity profile is changing from root to tip that makes rotor flow complex hence, blade flow differs from fixed wing cases with this aspect.

The velocity described is incoming air velocity which is simply the production of rotational velocity and local radius. At the tip, this velocity is denoted as tip velocity and reaches to maximum. Tip velocity is a design parameter for rotor design.

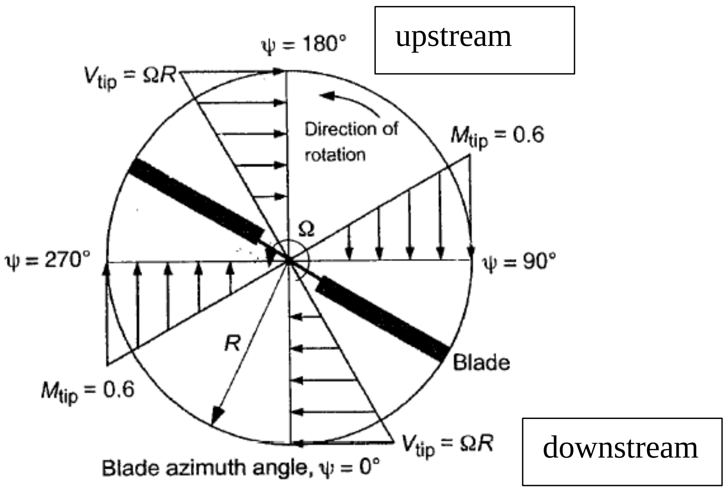

Figure 1.5 The incoming velocity distribution throug the blades for the sample 2 bladed rotor [1]

Figure 1.5 shows the incoming velocity distribution, azimuth angle and tip velocity. Since this is the hover flow, the downstream side for the blade azimuth is determined with respect to the forward flight conditions.

Another topic is the wing tip vortices. Due to the high dynamic pressure created by high velocity at the tip of the rotor blade, aerodynamic force load is collected in this region. Thus, this force load leads a vortical flow which is called as “blade tip vortex” as shown in Figure 1.6. It emerges from blade tip and continues downside from the rotor plane helically with rotation.

Figure 1.6 Blade tip vortices of Cobra helicopter visualized with vapor [5]

Blade tip vortex is significant subject for the main rotor design and rotor CFD simulations since net flow velocity and rotor wake flow distribution are strongly affected from these tip vortices [1]. For this reason, estimation of wing tip vortex path is crucial. Some empirical solutions for the tip vortex trails is available. This subject will be explained in details on following sections.

The rotor flow during the hover, axial climb/descent is called as upward or downward axisymetric flow. The rotor blades are rotating and they are interacted with air and rotational velocity creates linear local velocities from the root to tip. However, the actual rotor flow, from upside down, emerges from the upside of the rotor, air is pulled by rotor with rotation and continues at the lower side of the rotor . If rotor is considered as a disk, the actual rotor flow is shown in Figure 1.7 for hover condition.

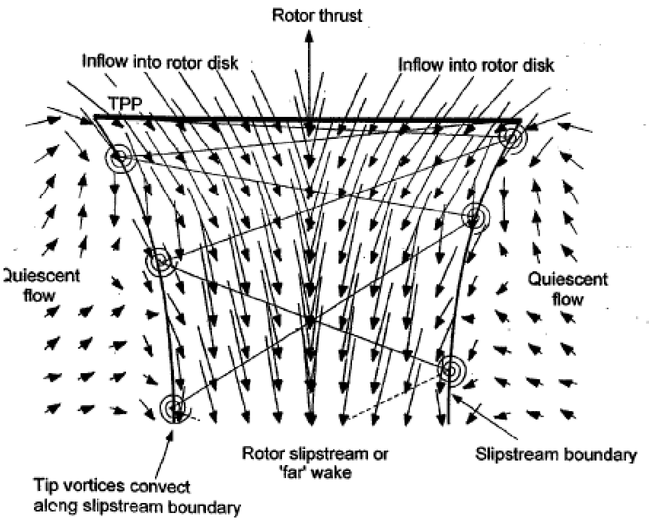

Figure 1.7 Velocity field beneath the rotor in hover [1]

Figure 1.7 shows the rotor flow at the downstream, which is called as rotor downwash. The flow which is pulled by rotor is denoted as “inflow”. The wake geometry is enclosed by the helical trails of the tip vortices and it has a contracted shape. The flow velocity increases smoothly through the rotor disk due to the rotation of blades and it exits from the disk with a higher velocity than inflow velocity. As this contracted shape is similar for every rotor flow in hover, empirical mathematical models based on some experiments were proposed.

A new velocity type takes the scene which is called as induced or inflow velocity. Inflow velocity is basically velocity belongs to the pulled air by the rotor disk. It is created with rotating blades and again, inflow velocity is distributed locally from root to tip like linear speed emerges from rotation.

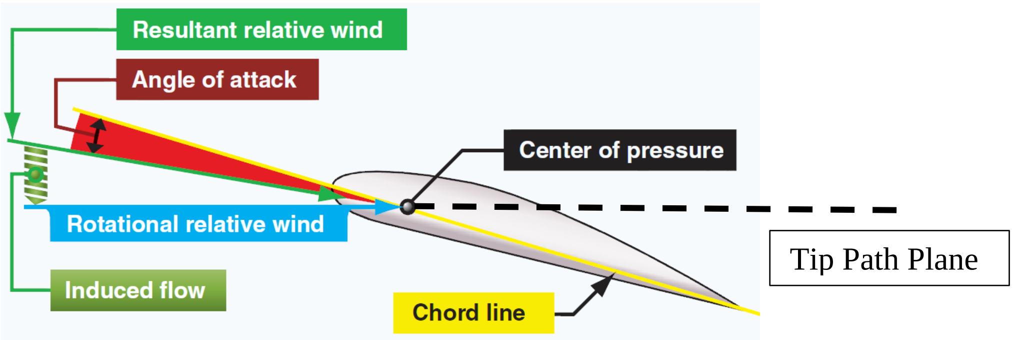

Figure 1.8 The inflow and rotational relative velocity on the section of a rotor blade [6]

In Figure 1.8, rotational relative wind is linear velocity created by rotation. Induced flow is designated by inflow velocity. It is evident that inflow changes the angle of attack. Furthermore, angle of attack changes the resultant relative wind that blade section encounters with.

The inflow velocity is not spanwisely constant. The distribution and value of the inflow velocity directly affects the rotor design parameters. There are many ways to calculate the inflow velocity distribution over the rotor disk.

The first aprroach was application of three conservation laws which are mass, momentum and energy. Application of these equations in a control volume where rotor and its downwash is enclosed is called as “Momentum Theory” developed by Rankine (1865) [1]. Then further developments were made by Froude (1878), Lanchester (1915) , Betz (1920, 1922) and Glauert (1935) [1]. In these studies, rotor was assumed as different shapes such as infinitesimal rings, actuator disk etc. But concept was only estimate the thrust and torque of the rotor rather than obtain a inflow profile.

Since, momentum theory did not take the azimuth rotation and radial distribution of one blade, it was accepted as a initial estimation tool. Then, modified methods called Blade Element Method (BEM) and Blade Element Momentum Method were introduced. They provide feasibility to calculate flow radially and azimuthally duruing the rotor flow. The sectional aerodynamic coefficients and rotational speed were taken into account. Thus, suitable substructure to calculate inflow was set. Blade Element Method simply calculates the distributed load spanwise with using inflow and relative velocity inputs or forward helicopter velocity, if exists. Gustafson and Gessow came with a new thought in order to estimate an inflow profile. Idea was combination of Momentum theory and Blade Element Method which was called as Blade Element Momentum Method. This method solves fluid continuum equations on each blade section as if they are infinitesimal rings. Advantageous point was, this method allowed a proper inflow distribution. So proper mathematical models based on some experimental corrections were implemented. The notable inflow models are, Glauert (1926),Coleman et al. (1945) , Mangler and Squire (1948) , Drees (1949), Payne (1959), White et al. (1979), Pitt and Peters (1981) , Howlett (1981) [1].

The importance of inflow parameter is, when BEMT equations are set, everytime, without any approximations, an equation with an inflow parameter (non - dimensional inflow velocity which is division of inflow velocity to the tip velocity) is emerged and it only allows numerical solution or setting some empirical coefficients with experimental results.Every inflow models contains a test setup and coefficients of inflow models were based upon the results of the tests.It is evident that, proper inflow estimation yields a proper thust torque relation for the rotors.

Today, these methods are still improved but they are limited for inflow profile estimation only. During the design process, not only the inflow profile, but also tip vortex profile and downwash profile of a rotor are also important. Because, any change in downwash could drastically change the inflow profile, which were accepted as a correction parameter for inflow profiles. In order to better inspection of rotor flow, vortex methods are introduced. The main approach is calculation of velocity field in terms of vorticity by using Biot Savart Law [7]. The vortex metholds are based on tip vortex paths gained from some experimental works. Again, these methods are helpful during the initiation of rotor design since they capture the rotor wake efficiently.

As better inspection of rotor flow issue comes to the scene, the CFD simulations are additionally applied during the rotor design process. Although they require high computational power and high amount of time, CFD simulations provide detailed flowfield solution. One can obtain every type of distribution from the CFD analyses such as, velocity profile over the blade, lift profile over the blade, path of the blade tip vortices etc. For this, CFD does not need any proposed inflow model or experimental empirical solutons. The Navier - Stokes equations are solved in the every cell of the solution domain numerically. If correct and proper grid distribution will be created with proper boundary conditions and solution techniques, then, one can obtain a reliable, accurate flow simulation for the rotary wing flows.

It is clear that, rotor flow prediction does not have a straightforward way. In order to observe the rotor flow, the inflow parameter should be accurately investigated. For this, precribed models are alternative. Implementation of CFD Simulations are another alternative or establishment of a test rig is the most exact alternative. However, rotary wing flows have complex characteristics due to the variable velocity profile on the rotating blades, the azimuthal position of the blades and interactional properties. The interactional issues are blade – blade vortex interaction and blade airframe interactions that makes the hover flow more complex to inspect. In some mathematical models, these interactional issues were defined as empirical corrections based on experiments. In helicopter aerodynamics, interaction and flow distortion is always a problem. These problems are evident during the axial flows and of course, during the forward flight.

The established mathematical models and computational methods are all utilized for pure hover flow, pure climb or forward flight with constant speed etc. The empirical outcomes must not only available for perfect scenarios but available for the extreme situations as well where, the whole flow field of helicopter is changing then, attitude and stability of helicopter is changing. Finally, fatal results may arise. In this thesis, a widespread extreme condition, which is called as “Ground Effect” will be the main scope.

1.2 Ground Effect

The flow field around the rotor is described in the previous section. Some conditions that distort the rotor inflow are summarized. The ground effect is the one of the conditions that distorts the whole rotor inflow and change the aerodynamic parameters. ground effect is basically the recirculation of rotor downwash flow from the ground to rotor, when rotor is located close to the ground.

Ground effect has a vital role in helicopters since it directly effects the helicopter performance due to the reverse flow from ground to the rotor. Helicopters encounter with the ground effect during the approaches (Landing pad, ship deck, inclined hills). Since flow becomes complex, handling the helicopter stability is the key point in order to prevent catastrophic results. The ground effect conditions are described in Figure 1.9.

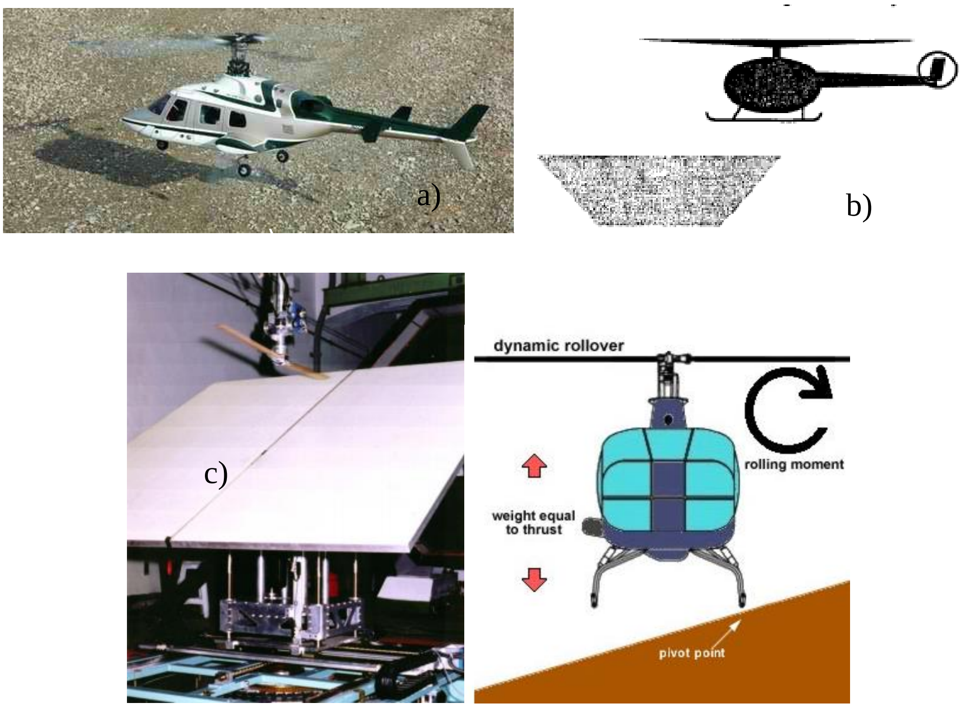

Figure 1.9 Ground effect types a) Normal b) Partial [34] c) Inclined surface [8]

Geometrically, helicopter encounters with 3 different forms in ground effect: normal, partial and inclined. The normal ground effect is observed during the every type of vertical landing. Partial ground effect is generally seen during landing onto the battleship, landing onto the building helipad and etc. The ground effect on inclined surfaces is evident during the military operations or resque operations on the mountains and on the hills.

During the close proximity of a rotor in hover, since ground must be a boundary for the streamlined characteristics of the flow, rotor downwash tends to rapidly expand as seen in Figure 1.10. This situation manipulates induced velocity and of course, induced power and thrust. On the ground, the vertical component of velocity vanishes and it is expected that induced velocity is less than in free air. The reduction of induced velocity refers to reduction of induced power for a given thrust.

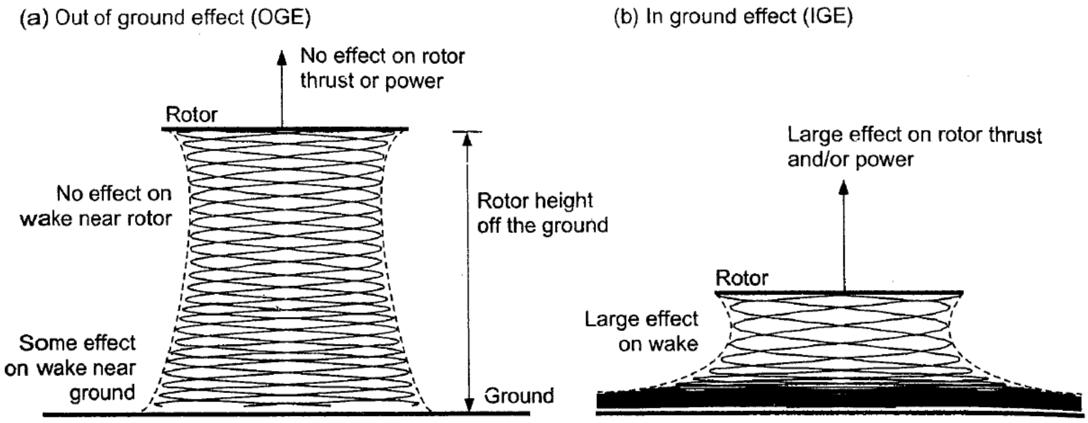

Figure 1.10 Expansion of rotor downwash [1]

1.2.1 Mirror Image Approach

The method of images provides an analytical expression for ground effect and it shows the occurence of ground effect basically. Cheeseman and Bennett (1955) firstly proposed this approach with replacing the rotor by a source and adding it a image source to define ground effect. The image of the rotor has the equal momentum terms of strength with actual rotor and distance of the image rotor is the same with the actual one. The potential flow theory [1] is referenced in order to model the image rotor. Image rotor is modeled as a fluid source and function of this source is reduction of inflow of the actual rotor flow.

Knight and Hefner [9] and Rossow (1985) [1] used vortex cylinder model in order to simulate ground effect. The theory of Knight and Hefner, includes the mirror image approach as well. In this method, 2 significant assumptions were made: the circulation around the blade is constant in order to represent blade vortex system with tip vortices only. Other assumption is, a uniform vortex cylinder is created by helical tip vortices from rotor to the ground. With respect to the ground, the image of this vortex system is defined with vortex filaments and image rotor. The wake of image rotor composes of a series of spiral vortex filaments generated from the blade tips. The image rotor inflow velocity carries these vortex filaments to the upper zone, where the actual rotor inflow velocity is reduced by the image of vortex filaments. The image and actual vorticities have equal but opposite quantities in order to eliminate normal velocity on the ground as shown in Figure 1.11.

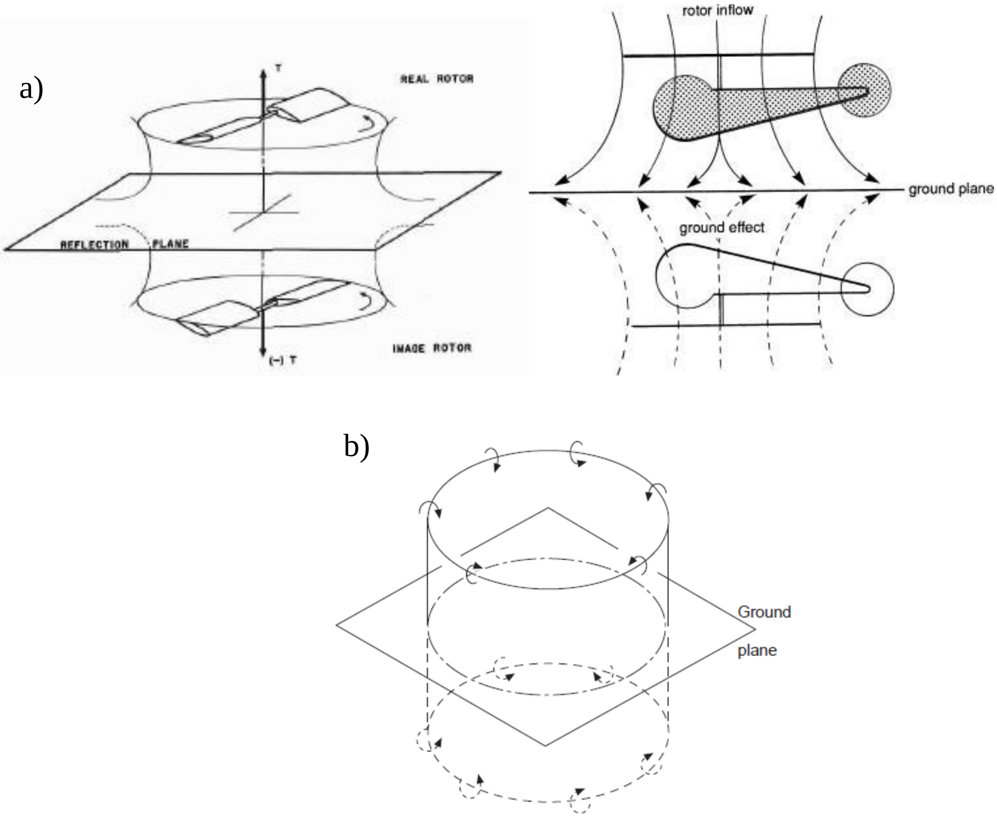

Figure 1.11 a) Mirror Image and b) Vortex Cylinder Model [1]

All in all, image system produces upflow which reduces the inflow to create the ground effect. The image vortices decrease the actual induced velocity on the actual rotor then, actual power decreases. The decrease in induced power value could be obtained as a function of rotor height above the ground mathematically. In order to create a better insight about this induced velocity reduction, it is needed to inspect the change of flow structure in the vicinity of rotor blade, where flow is pulled by rotor blades.

1.2.2 The Details of Ground Effect

This subsection is the sequel for Figure 1.8, where generation of rotor flow is explained in details. The occurence of inflow and downwash are clearly explained. Now, the effect of the addition of ground in the rotor downwash is inspected and change of inflow and flow near the blade are represented.

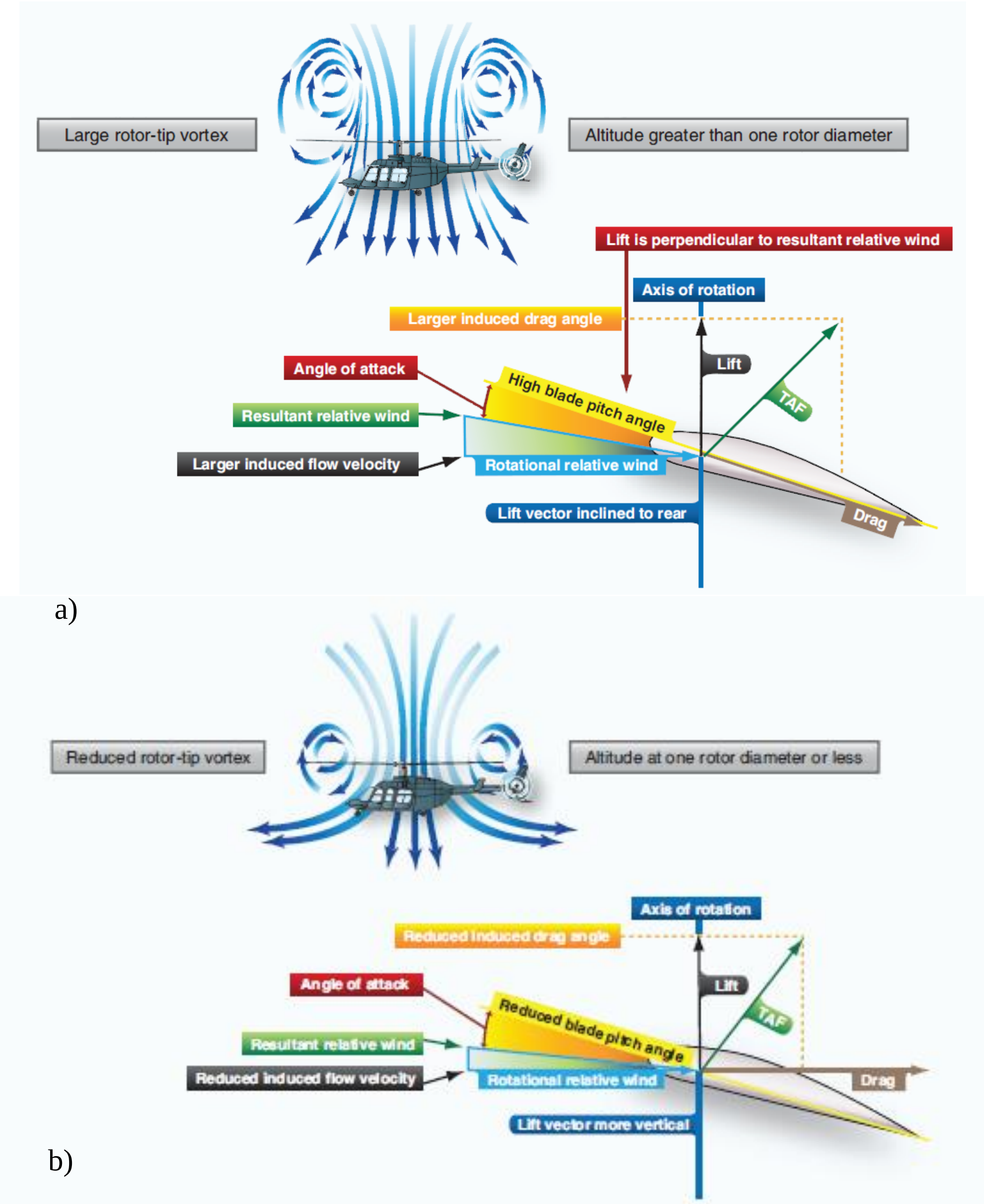

Figure 1.12 The change in induced velocity due to the ground effect [6]

Figure 1.12 a) is the extended version of Figure 1.8 where rotor flow is visualized near the blade. The blade pitch angle is high which is the angle between the blade chord and rotor tip path plane (TPP). Tip path plane is basically the plane where relative wind (linear velocity created by rotation) is parallel to it. The inflow or induced velocity is high during the out of ground effect case. The induced drag (drag due to lift) angle is high and tendency of lift vector direction is pointed to rear of the blade. For entire rotor, rotor tip vortices are larger.

When helicopter approaches to the ground, the great portion of the tip vortices pass away by transforming their flows streamlined to the ground that leads to smaller tip vortices in ground effect.

The method of the images proves that, induced velocity or inflow decreases in ground effect. The reduction in inflow creates a reduced inflow velocity. Reduced inflow velocity leads increasing angle of attack which results from the reduced blade pitch angle. The blade pitch angle reduction leads to a reduced induced drag and finally induced power is reduced which is exactly the power required to hover in ground Effect. Figure 1.13 shows this process schematically:

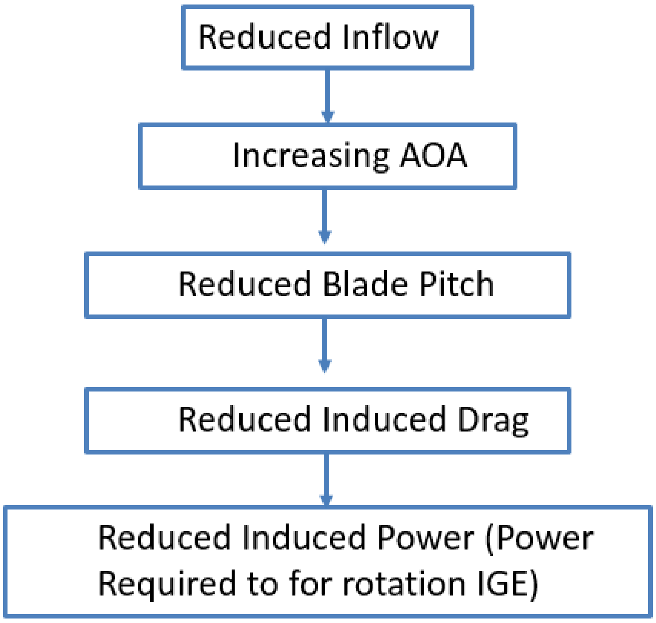

Figure 1.13 The sequence of the ground effect on the blade section

By the way, angle of attack is not actually increased. After the inflow reduction, Angle of attack has a tendency to increase. In order to keep relative wind stable and keep the total thrust constant, the blade pitch angle is reduced by pilot in order to balance this tendency with reduction. Hence, reduced inflow results in reduced blade pitch angle which creates less induced drag, since the exposed area of blade decreases with respect to the relative wind. To sum up, ground effect leads to less power requirement for rotation for the same thrust.

1.2.3 Power Reduction in Constant Thrust

Previous section depicts a power reduction in ground effect. That means a benefit in fact: The power required to operate rotor is lower in ground effect compared with out of ground effect at the same rpm and thrust value. Reduction of power required envisions that helicopter spend less energy in ground effect in order to perform hover. Another aspect is, helicopter could hover in ground effect with higher payload with consumption of less energy than the out of ground effect case.

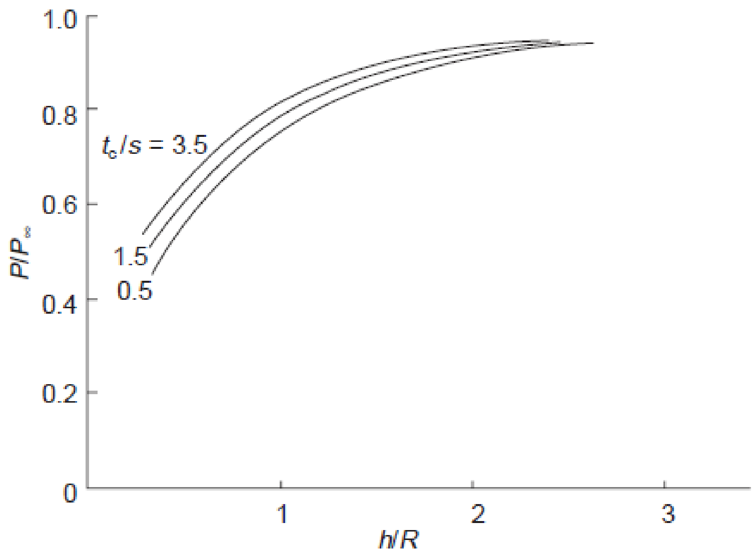

Figure 1.14 Power reduction with decreasing ground effect [1]

In Figure 1.14, height above the ground is non – dimensionalized by radius (R) . the term “h” denotes the dimensional distance between the rotor and ground. The “h/R” depicts the non – dimensional rotor distance to the ground. The power is also non – dimensionalised with power out of ground effect. It is clearly seen that with decreasing distance between the rotor and ground, the power decreases.

1.2.4 Thrust Increase in Constant Power

The ground effect leads increase in thrust when constant power is supplied as well (constant RPM). The difference of this condition from the power reduction in constant thrust is, there is no intervention to the blade pitch angle. In the ground effect, when inflow decreases and angle of attack increases with its tendency, this time, no blade pitch decrease is applied in order to set the constant thrust. Instead, pitch angle remains constant, with decreasing inflow, angle of attack increases. Thus, overall thrust increases with same power and rpm. This situation shows that, in ground effect, helicopter could gain higher thrust than the out of ground effect case, with constant power.

This thrust increase is, advantageous for helicopters especially for takeoff. During the axial climb, with the higher thrust corresponding the same power facilitates the helicopter take – off that means, helicopter could hover and climb with the help of ground. This is actually valid during the take off from the high altitudes (such as on the top of the mountain). Similarly, during the axial descent, this feature facilitates the helicopter landing and ground effect will be resembled as "cushion" to the helicopter that provides a smooth and secure landing.

There are various initial fundamental works about the ground effect in hover and these works are pionner for establishment of the mathematical relations of ground effect in hover. Zbrozek (1947) used flight test data and arranged a mathematical model in order to prove the thrust increase with constant power in ground effect. Betz (1937) applied a rotor performance study in ground effect. Fradenburgh (1960,1972) ,Stepniewski et al. (1984) ,Prouty (1985) and Hayden (1976) are all collected hover test data for the hover ground effect [1]. Various modifications were done such as, blade aspect ratio, blade twist changes etc. However, general outcome was ground effect is efficient till the rotor distance is one rotor diameter. Beyond this point, no ground effect was observed.

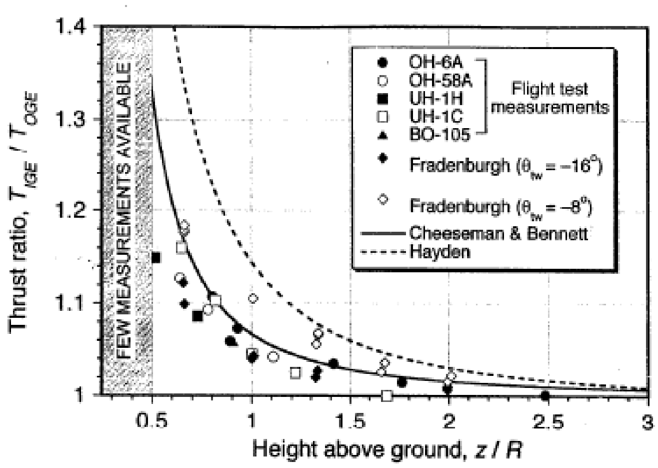

Figure 1.15 Increase of a rotor thrust with respect to the rotor distance to the ground [1]

In Figure 1.15, height above the ground is non – dimensionalized by radius (R) . the term “z” denotes the dimensional distance between the rotor and ground. The “z/R” depicts the non – dimensional rotor distance to the ground. It is evident that ground effect is valid till z/R: 2.

1.2.5 Additonal Key Points of Ground Effect

The physical type of ground has an important role on the emergence of ground effect. Maximum ground effect is achieved over the smooth and hard surfaces [1]. When hovering over the grass, bushes, water, surfaces leading brownout conditions like mud or sand, ground effect reduces [1].

The ground effect approximations and studies are generally assumed for isolated rotors. Whereas, actual helicopters have fuselage beneath the rotor and it is studied that fuselage presence below the rotor accompanies the ground effect [1]. However, general relation of thrust and power is not changed with respect to the ground proximity. For the cases with isolate rotors, generally z/R value is started from 0.5 which is the clearance for the fuselage dimensions. Below the 0.5, ground effect is denoted as “extreme ground effect”.

All in all, ground effect in hover flight have complex but understandable flow characteristics that is possible to model mathematically. Due to this feasibility, ground effect models and works were initiated with hover tests. Today, still some unknown points are available in ground effect literature, but with the help of technology, better understanding about this “complex but beneficial” case is possible.

1.2.6 Ground Effect in Forward Flight

During the transition from hover to the forward flight, helicopter reaches a forward speed that power required decreases to a lower value than the power available and forward flight is initiated. This transition and power gaining is provided by ground effect in hover.

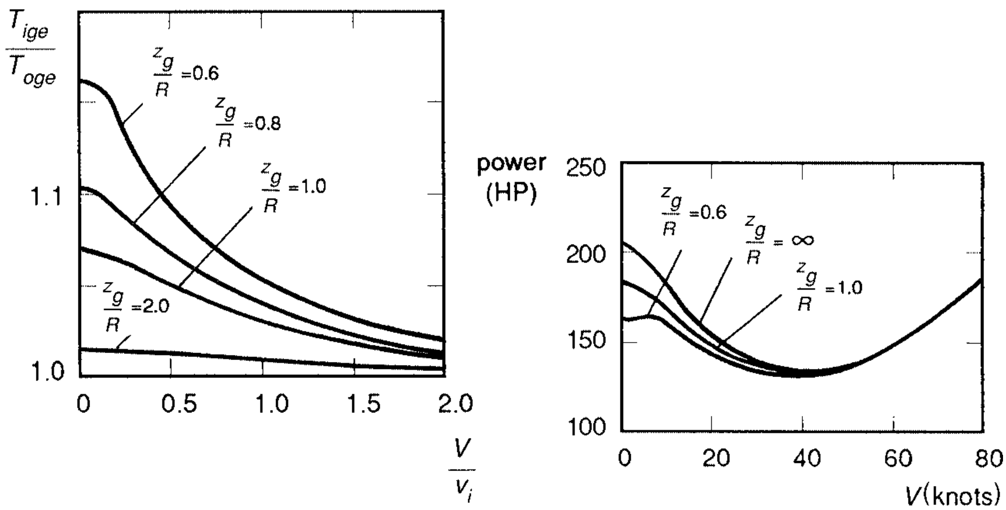

Figure 1.16. Effect of forward velocity on ground effect [1]

In both figures, V denotes the forward velocity. In Figure 1.16 a) the forward velocity breaks the ground effect regardless of the ground proximity. When forward velocity reaches to the double of the inflow velocity, there is no ground effect presence. In Figure 1.16 b), the power need for the transition to forward flight is shown. It is clearly inspected that, during out of ground effect, the power required to transition to the forward flight is higher than the in ground effect case. This figure

apparently proves the enhancement effect of ground cushion created on hover during the transition to forward flight.
To conclude, in order to perform efficient take off with helicopter, the ground effect characteristics in hover are determinant factors.

1.2.7 Main Scope of This Work

Up to that section, information about the helicopters, rotor aerodynamics in hover flight and ground effect were provided.

The aims of this thesis are summarized as:

- Establishment of a model rotor test setup in order to investigate ground effect performance of a rotor.
- Validation of the test setup with the past outcomes, such as proving the ground effect inefficiency when distance is 1 rotor diameter between the rotor and ground
- Application of a further work about the ground effect, when ground is inclined surface and depiction of a mathematical relation about this case.
- Application of extreme ground effect when z/R has a value below 0.5
- Determination of a numerical solution procedure for the rotor flow in ground effect and validation of simulations with the experimental results
- Presentation of a ground effect insight including inclined surfaces, enhanced with rotor test setup and accurate computer simulation procedure.

The test setup could not only used for ground effect cases, but also available for model scale propeller tests, visualisations etc. The establishment of a CFD solution procedure will enlights the any other rotary wing CFD simulations since ground effect is extreme case for rotorcrafts. CFD requires high computing power, fine solution domain and accurate solution procedure, in order to capture the flow beneath the rotor in ground effect, even for inclined cases.

CHAPTER 2

LITERATURE STUDY

The fundamental mathematical relations affiliated with rotorcraft aerodynamics are obtained with established test setups. In order to understand the nature of the flow, experimentation is inevitable. Especially, if issue is ground effect which is an extreme condition for rotorcraft industry, correct experimental instrumentation is needed. After establishment of initial mathematical relations and tests, some advance works were done. In this chapter, the literature experimentations about the ground effect are presented. Since construction of experimental setup is the one of the targets of this thesis, it is significant to clearly understand what had been done in the past.

2.1 Test Setups

Before the introduction of test setups, it is important to sort them by their sizes. Most of the works are done with actual rotor size, whereas, tests with scaled models are available.

2.1.1 Actual Rotor Sized Test Setups

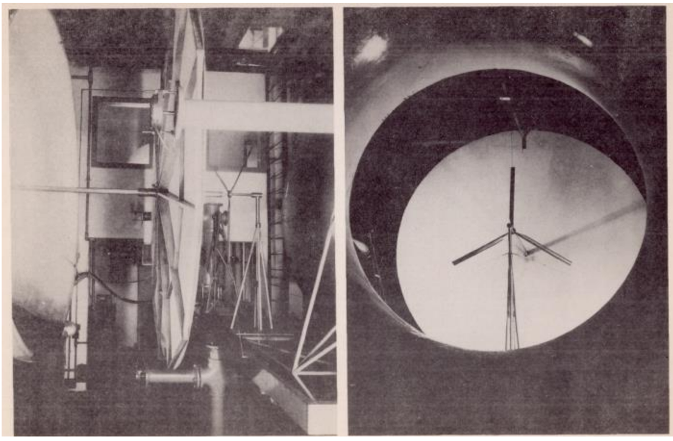

Figure 2.1 Test setup of Knight and Hefner [9]

Knight and Hefner [9] conducted a ground effect research with the help of three different helicopter rotors as seen in Figure 2.1. The effect ground presence over the rotor flow and performance was investigated. The main aim of the program was expansion of the previous works and declare a general outcomes about the ground effect issue.

Fradenburgh [10] observed the ground effect with performance effects and hover flow characteristics by utilizing a model rotor test setup. Sloped surface, power comparison during transition to forward flight issues were examined. Test setup is 2 bladed 2 ft diameter rotor with untwisted, untapered blades. Tip speed is denoted as 600 ft/s. Extreme ground effect is simulated starting from the ground proximity of z/R = 0.1.

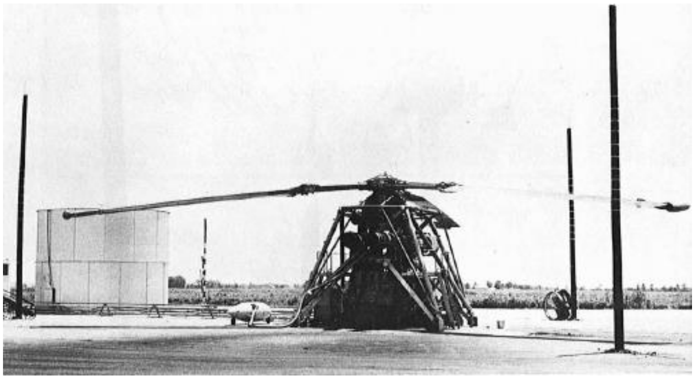

Figure 2.2 Test setup of Bolanovich et al.[11]

Bolanovich et al. [11] investigated the effect of rotor downwash to the turboshaft inlet with the test setup shown in Figure 2.2. The power supply of a helicopter is turboshaft engine which includes turbine sections. Since turbine engine is located beneath the rotor, in ground effect, some air intake problems were observed. Hence, overall performance losses are detected. To create a remedy for this problem, a velocity profile beneath the rotor in ground effect must be estimated. The main aim of this work was estimation of this type of velocity profile in order to overcome the performance losses in the vicinity of turbine engine intakes.

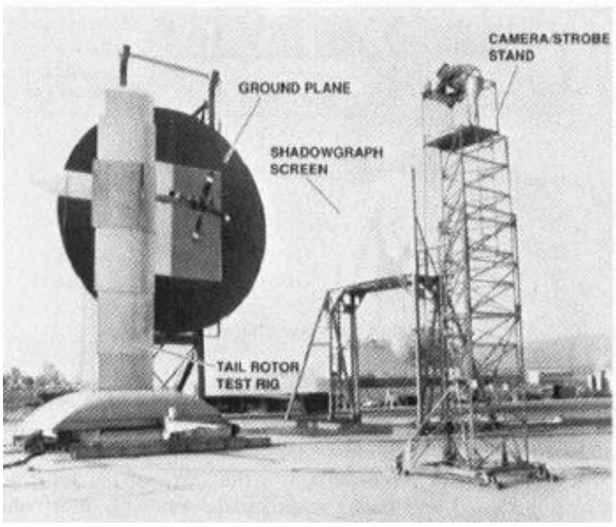

Figure 2.3 Test setup of Light [12]

The work of Light [12] has a main target of tip vortex monitoring in/out of ground effect with model tail rotor test rig. Tip vortices visualization of a hovering rotor was conducted in ground effect. The tip vortex geometry and performance data from the tests were compared with the tip vortex geometry and performance data were predicted using a free wake hover performance analysis and several computational methods. As a test setup, full scale Lynx tail rotor was mounted with a radius of 1.1 m and 0.18 m chord as shown in Figure 2.3. As a tip Mach number, 0.56 to 0.6 range was accepted .In order to visualize tip vortices, shadowgraph method was used.

Xin et al. [13] investigated partial ground effect which is clearly a portion of rotor in ground effect whereas other portion is located out of ground effect, like approach to the landing pad behind the battleship. The rotor of Yamaha R -50 unmanned helicopter was used which has a rotor diameter of 3 m and chord of 0.106 m. Reynolds is kept on 700000 around the tip region. Both full and half ground effect cases with five different ground proximities were tested.

Figure 2.4 Test setup of Tanner et al. [14]

Tanner et al. [14] observed the outwash relation during the ground effect. The outwash is clearly the turned and continued downwash flow after exposition with ground. The flow visualisation is done with phase locked PIV which is the most accurate visulatization technique for rotorcraft, rather than smoke or tuft visualization. The testing was conducted in NASA Langley Research Center. The used rotor system was Army's General Rotor Model System which includes 4 bladed rotor with 5.54 ft rotor radius and a 1150 RPM rotation as shown in Figure 2.4. A generic ROBIN fuselage is added for the interactional testings

2.2 Scaled Sized Test Setups

Iboshi et al. [8] conducted a ground effect study including the partial surface and inclined surface. The tests were conducted with moving rotor on the inclined/partial ground. The mid section of ground plane was set as a center and variations of the torque and thrusts values were detected during the center to ground edge movements of the rotor. The alterations show out of ground effect results even in “in ground effect” cases due to the distance increase occured by expanded portion of inclined surface.

Another research of Iboshi et al.[15] is the mid - size test setup for investigation of the ground effect over the confined area. The confined area is simply the plate enclosed by barriers and the effect of these barriers over the rotor performance was investigated during ground effect. The dimension of barriers, the longitudinal location of rotor with rescept to the barriers and ground proximity are the parameters of this test setup. Main approach is the helicopter condition during resque operations or law enforcement operations. In these missions, helicopter may encounter with some obstacles which are clarified as confined zones in this work. The effect of confined areas may be harmful. The rotor may enter to the vortex ring state due to the hover on the confined area. Finally, catasthropic results may be seen. In order to gain better insight about the dynamics of the helicopter, the behavior of the rotor and flow field during the confined area hovering must be estimated.

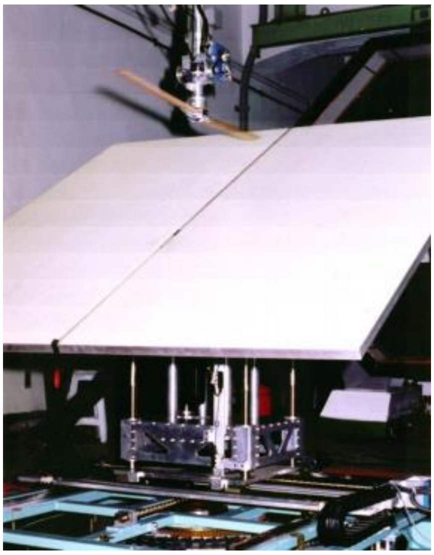

Figure 2.5 Test setup of Iboshi et al. [16]

Additional work of Iboshi et al. [16] contains a model rotor test system in order to observe the effects of ground effect with/without ground inclination as shown in Figure 2.5. The blade flapping motion of a rotor in ground effect is inspected. The hovering performance of a model scale rotor is investigated during the presence of inclined surface. Setup includes 2 bladed rotor with blade dimensions of 1.138 m diameter and 0.06 m chord. Blade sections are NACA 0015. The rotational speed is 94.2 radians per second and 2 blade pitch angles are tested.

Yeager et al. [17] performed an investigation about the directional control and performance helicopter rotor- tail-fin configuration in ground effect in Langley Full-Scale Tunnel. This work contains a ground effect study which is not only investigating the isolated rotor, but also investigate the effect of other elements of helicopter like tail fin, tail rotor, fuselage etc. in ground effect. The forward velocity effects are also included with different conditions. The results of this work investigates the modifications of the other elements of helicopter if necessary. The interaction of ground effect with the other elements are taken into account. The experiments were done with constant ground proximity value. However, this study is beneficial to show that, test setups including the other helicopter elements are available and ground effect study is extended with addition of them in order to show their effects and contributions to the ground effect test setup includes a main rotor with a diameter of 3.35 m and blade chord of 0.171 m. Tip speed is defined as 210 m/s. As a ground proximity, z/R: 0.7 is used. 7 different forward velocities are simulated as an incoming wind velocities.

Gilad et al. [18] studied ground effect on hovering rotor performance both experimentally and theoretically. The experimental cases are done with a rotor test system. The work is endorsed by the Sikorsky Human Powered Helicopter Challenge (HPH) This work contains a ground effect investigation for both elastic blades and rigid blades in order to observe the effect of blade elasticity in ground effect. Besides, test results are used in order to validate a computational method which includes structural and aerodynamic methods like CFD, finite element methods and their couplings for the prediction of elastic blade behavior in ground effect. Main approach of this work is inspection of ground effect during extreme conditions where z/R is below 0.5. For this purpose, 2 different test setups are set. First setup has a rigid untwisted untapered NACA 0012 blades as shown in Figure 2.6. The other test setup includes a rotor specified for quadrotor configuration.

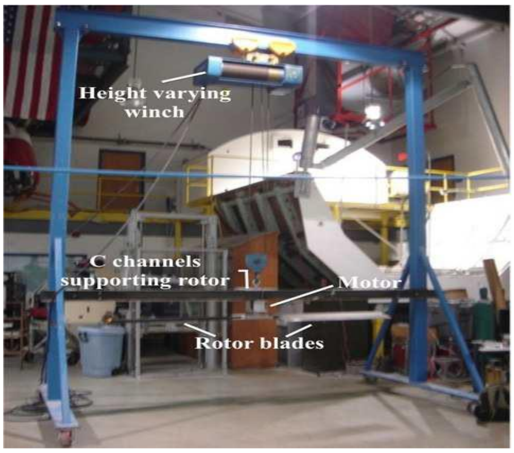

Figure 2.6 Test setup of Gilad et al. [18]

Caradonna and Tung [19] establised a rotor test system with two NACA 0012 blades as shown in Figure 2.7. This work includes information about the blade pressure measurements and tip vortex research. Besides, it is a comprehensive benchmark for CFD validation since it includes a wide range of cases such as different rpm values.

Although this work contains nothing about the ground effect, its test setup presence and well known widespread CFD validation acceptability makes this work a key reference for this thesis.

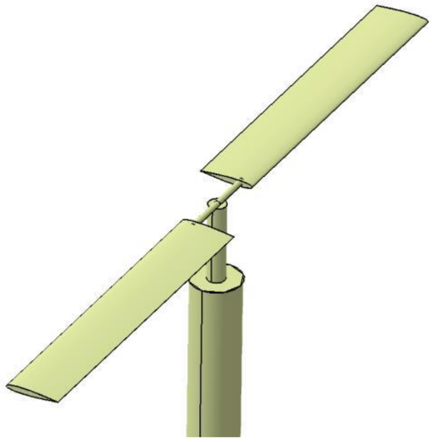

Figure 2.7 Test setup of Caradonna and Tung [19]

Leishman et al. ([20] - [23]) set up a micro rotor test system in order to investigate the rotor aerodynamics, ground effect, brownout effects and fuselage - rotor interaction as seen in Figure 2.8. For better investigation, rotor downwash and blade tip vortices are examined with both PIV (Particle Image Velocimetry) method and particle tracking velocimetry technique. During the experiments, test setup with two bladed rotor is used. Rotor has a diameter of 0.17 m and blades have 0.018 m chord. Since this setup is designed as “microscale”, there is no aerodynamic difference of airfoil section or simple arc section for the rotor blades in this Reynolds interval. Hence, blades are available with simple arc shape section. Tip Reynolds number is preserved around 200K.

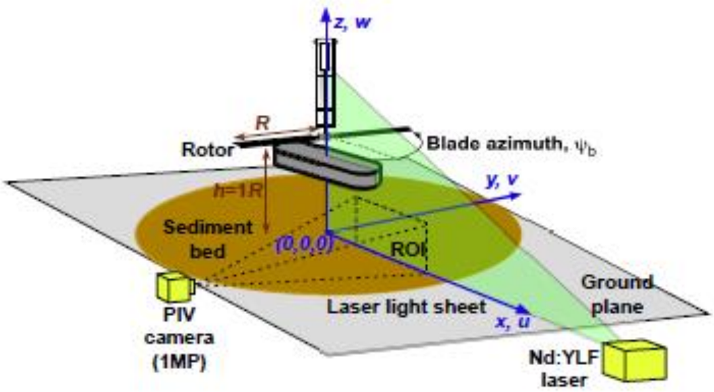

Figure 2.8 Test setup of Leishman et al. ([20] - [23])

The work of Lee et al [24] is almost similar to Leishman's test setup in terms of size as shown in Figure 2.9. In addition, this setup is used for some CFD validations to measure the capabilities of the CFD codes used for ground wake interactions, thrust and torque measurements and tip vortex flow field predictions.

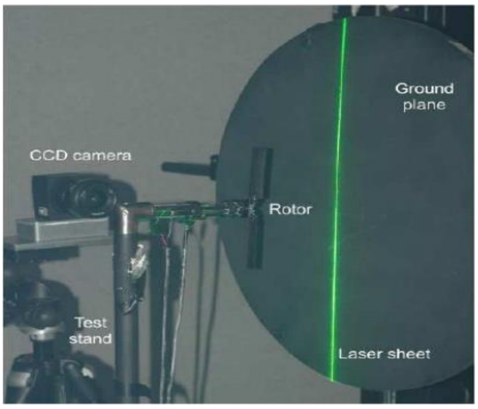

Figure 2.9 Test setup of Lee et al. [24]

The work of Hanker and Smith [25] presents an experimental investigation on a model rotor test rig in the Boeing Vertol 2041 by 2041 V/STOL wind tunnel to develop further insights into the parameters that affect helicopter interactional aerodynamics in ground effect which affects helicopter handling qualities. Interactional aerodynamics means affection between the main rotor and tail rotor etc.Test section consists of 1:4.85 scale YUH 61A Helicopter. Rotor radius is 60.62 in. and blade chord is 4.74 in. Approximately 1400 RPM is applied to main rotor. For ground effect, z/R value is determined as 0.7. The blockage ratio of tail rotor is changed and effects of this condition is studied. For detailed analysis of interaction flows, hot film and flow visualization methods are applied. Setup is shown in Figure 2.10.

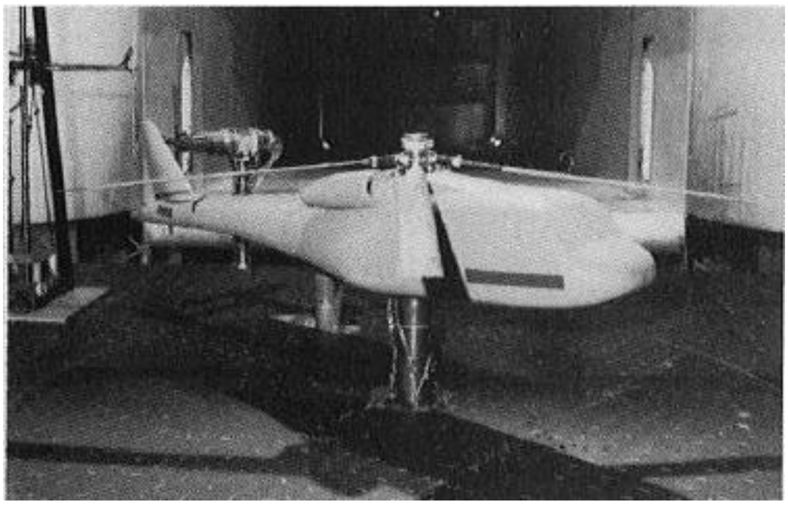

Figure 2.10 Test setup of Hanker and Smith [25]

Balch et al. [26] established a rotor test rig to observe main rotor/tail rotor/ airframe interaction. Model scale hover tests were carried out in the Sikorsky Aircraft Model Rotor Facility. The work is a comprehensive benchmark for CFD validation since it contains many main rotor cases such as in- out of ground effect, different rpm values, with/without tail rotor. Four different rotor blade sets were used on 9 ft diameter rotor rig which is not meant that all blades have span length of 4.5 ft. The rotor blades are UH60, S-76, High Solidity and H- 34 blades. The conducted combinations are, isolated main/tail rotor, main/tail rotor with fuselage, lowered rotor head with respect to the fuselage. Besides, flow visualization techniques are applied.

The research of Curtiss et al. [27] describes the results of an experimental investigation of the aerodynamic characteristics of an isolated rotor operating at low advance ratios close to the ground. The study includes flow visualization in addition to measurement of the forces and moments of the rotor as a function of collective pitch, advance ratio, and rotor height above the ground-to-diameter ratio. The experiments were conducted in the Princeton Dynamic Model Track Test Rig using a model moving over the ground. Test setup includes a 4 bladed rotor with 8 ft diameter by aapplication of a tip speed around 57 m/s. 3 different rotor heights with two blade pitch angles were tested.

Ganesh and Komerath [28] carried out a work that is basically the aerodynamic characteristics of rotor close to the ground by means of the model test rig as shown in Figure 2.11. Flow visualization was done to assess the flow characteristics in ground effect and compare it with the out of ground effect case. Force measurements were done to measure the loads at various advance ratios and yaw angles. 2 bladed rotor has 3 ft diameter with blades of 3.37 in. chord. As a blade section, NACA 0015 profile is used. 2100 rpm rotor revolution is applied. z/R = 0.72 is the only parameter for ground proximity. 7 different advance ratio values are determined as experimental parameter for forward flight.

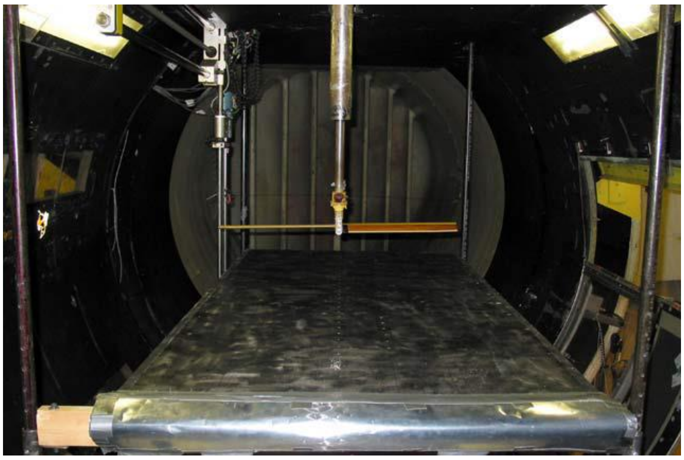

Figure 2.11 Test setup of Ganesh and Komerath [28]

2.3 Flight Tests

Figure 2.12 Flight test helicopter of Flemming et al. [29]

Flemming et al. [29] conduct flight tests where NASA 740 Helicopter configuration was used. Rotor has 31 feet radius with a blades containing NACA 0012 airfoil sections which is shown in Figure 2.12. Ground effect cases were performed at 5 different heights with a 3 knots relative wind. Besides, forward flight data were obtained with 5 different heights and 15 knots forward velocity.

Wadcock et al [30] conducts a flight test work about the ground effect. Main aim of this study is getting detailed insight about the helicopter aerodynamics in ground effect with brownout conditions. Brownout is basically the flow separation during the descent onto the sand, sea etc. In this experiment, in order to visualize ground vortex path, tuft monitoring is applied on the ground and helicopter fuselage. Tuft configurations are shown in Figure 2.13.

Figure 2.13 Tuft visualisation on a) Ground b) Flight test helicopter (S -70 Blackhawk) [30]

The outstanding concerns are mostly performance variations, flow visualizations, rotor interactional effects with the additional components of helicopter and CFD validation benchmarks. Besides, ground effect for the seperation of engine outflows, ground effect during the inclined, confined and partial surfaces, investigation of ground effect during the low forward speeds or with wind interactions, effect of blade flexibility in ground effect and investigation of ground effect during the extreme ground proximity were additional research topics in the past.

The literature study provides a competitor study for the newly designed test setup desribed in this thesis.

CHAPTER 3

TEST SETUP

The key parameters of ground effect test setup is available in this chapter. After the competitor study and size determination, the test setup was shaped, the design was freezed then produced. Test rig is located at the METUWIND Research Facility at Middle East Technical University.

During the design process of test setup, various combinations were taken into account as shown in Figure 3.1.

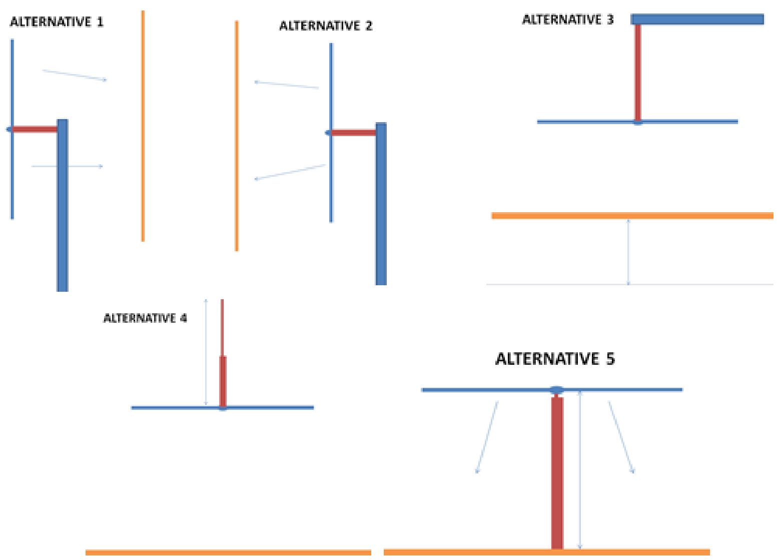

Figure 3.1 Design alternatives

In fact, first and second alternatives are same setups. The only difference is rotation direction of rotor and location of plate that represents the ground with respect to the rotor. Second alternative is more advantageous than the first one since rotor mast in the first one spoils the flow and clean flow does not provided onto the ground plate. Hence, first alternative was eliminated.

The difference of 3th, 4th and 5th concepts from the first two cases, rotor and ground are positioned in order to create the flow vertically. On alternative 3, ground plate can move vertically whereas, on 4th concept, rotor can move vertically above the floor. Although alternative 4 appears useful, it was eliminated due to the need for durable parts for the high rpm values that increase the overall cost. On alternative 5, downwash flow is interacted with the rotor mast. Due to this disadvantage, alternative 5 is eliminated. At last, alternative 2 and 3 are remained.

Since, inclined ground effect must be applied, alternative 3 requires abundantly high motor location from the ground. This condition creates difficulty for user and it increases the overall cost. After all assessements, alternative 2 was decided to produce.

Test setup is designed to create the flow parallel to the real ground in order to create downwash on the ground plate. The reason why setup is designed horizontally is, facilitate the application of inclination angle of the ground plate. The dimensions of ground plate are dimensionalized with respect to the rotor diameter. The reason of this dimensionalization is to create ground effect compherensively.

General Properties:

The dimensions and specifications of the test setup are defined in Table 3-1.

Table 3-1 General properties of test setup

Rotor Plane Center Height [mm]	1980
Plate Size [mm x mm]	2000 x 2000
Maximum Plate Distance [mm]	1500
Plate Inclination Angle Interval [°]	-25: 25 , ±5
Blade Collective Angle Interval [°]	-20: 20 , ±2
Rotor Radius [mm]	364

Figure 3.2 shows the detailed 3D Computer Aided Drawing of the test setup.

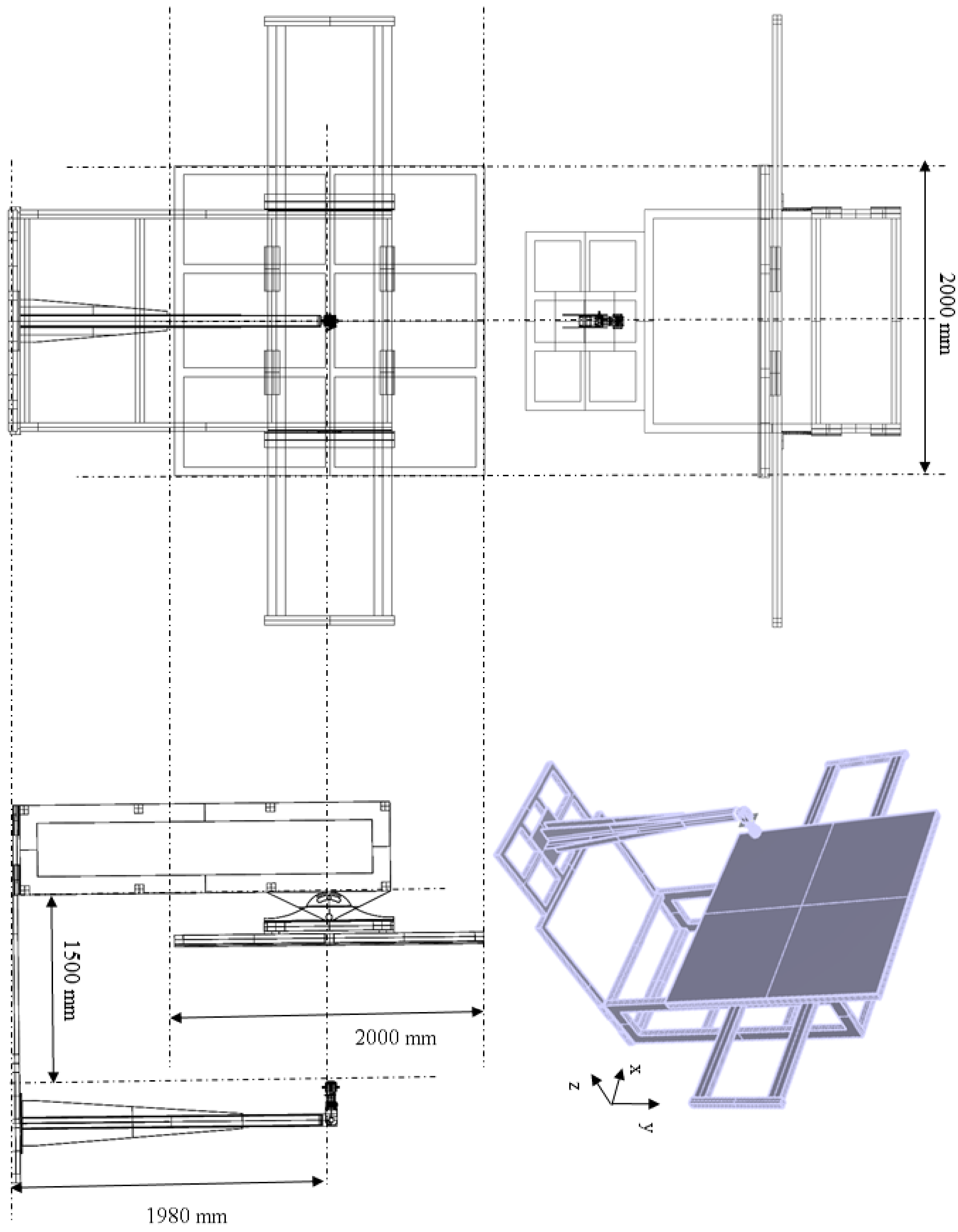

Figure 3.2 CAD of the test setup

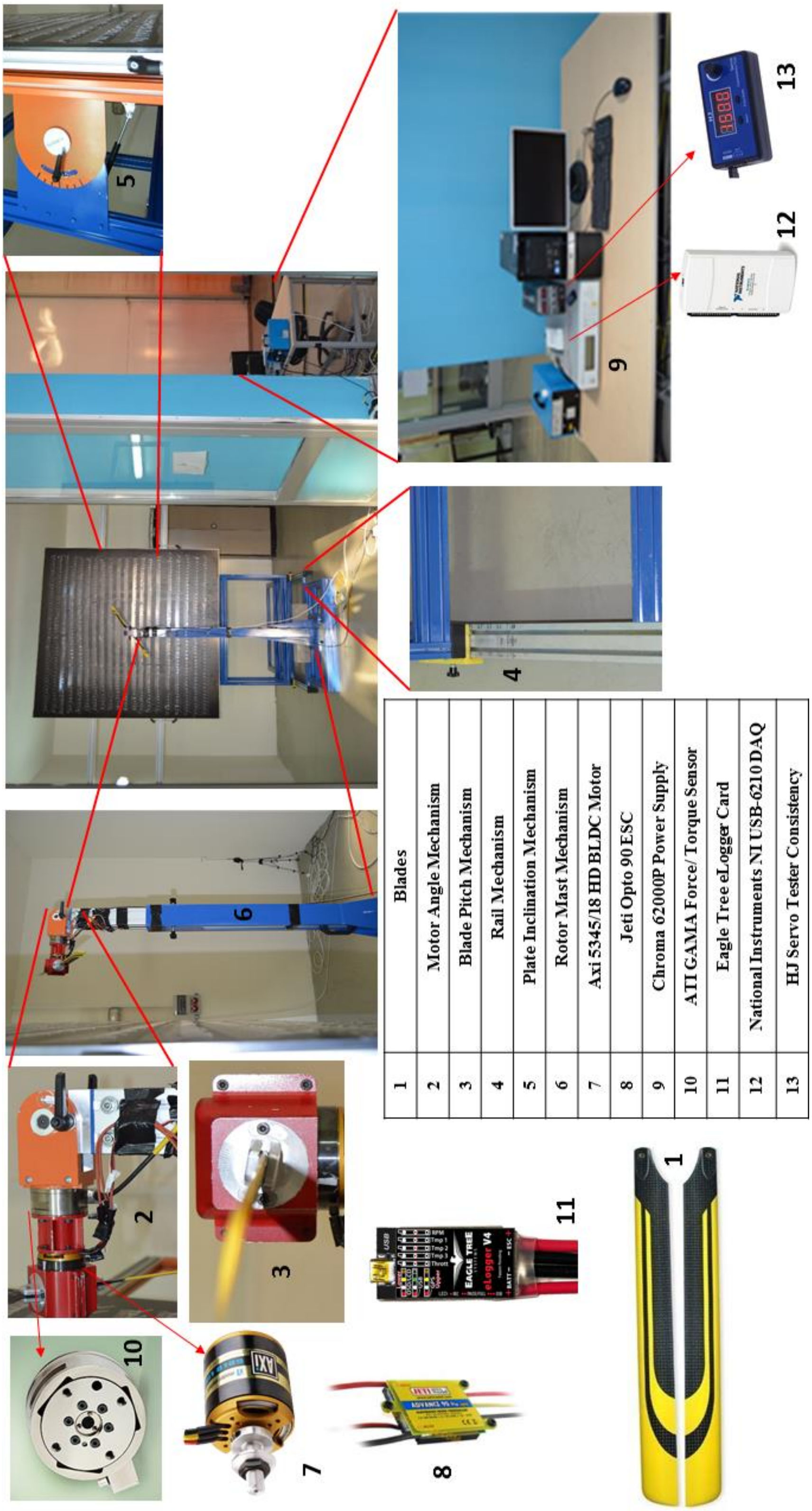

1	Blades
2	Motor Angle Mechanism
3	Blade Pitch Mechanism
4	Rail Mechanism
5	Plate Inclination Mechanism
6	Rotor Mast Mechanism
7	Axi 5345/18 HD BLDC Motor
8	Jeti Opto 90 ESC
9	Chroma 62000P Power Supply
10	ATI GAMA Force/ Torque Sensor
11	Eagle Tree eLogger Card
12	National Instruments NI USB-6210 DAQ
13	HJ Servo Tester Consistency

Figure 3.3 Breakdown of the test setup [58]

Figure 3.3 is the breakdown of entire test setup including mechanisms, propulsion and data acquisition elements.

3.1 The Mechanisms of Test Setup

3K Carbon Fiber RC Helicopter blades are specially designed for RC helicopters. Each blade has 325 mm span withy 3K carbon fiber degree. With this feature, blades are durable for high rpm values. Blades have symmetric airfoil section which is not belong to any known airfoil family. No twist and taper are available. The blade tip is sharp and aft swept. Blades are mounted from the real ground with a height of 3 diameter similar to setup of reference [12].

Motor angle mechanism provides a rotation for rotor hub. Maximum 90° rotation is available. The advantage of this mechanism is, rotor could be operated vertically to the real ground. Vertical ground effect and rotor tests could be initiated with this mechanism. Besides, Inclined ground effect tests could be done with changing the angle of rotor with respect to the ground plate.

Collective mechanism provides changing the blade collective or pitch angle. Its range starts from -20° to 20° with increment of 2°. Collective mechanism does not change automatically during the tests. It is adjusted when rotor does not work and tests are done .

The ground plate rail mechanism arranges the distance between the ground plate and rotor

Ground plate inclination mechanism is located behind the ground plate. With the help of this mechanism, the angle of plate with respect to the rotor could be arranged. The piston bars are mounted in order to reinforce the heavy ground plate during the inclined cases.

The rotor mast mechanism is located below the rotor hub. Rotor hub could move vertically by means of this mechanism. It provides centering the rotor with respect to the midpoint of ground plate. Besides, when rotor hub is rotated in order to create vertical flow, this mechanism works as a ground proximity adjuster.

3.2 Propulsion and Power Elements

These elements supply the power and rotational energy needed for rotation. Simply motor, electronic speed controller and power supply forms this section.

The AXI 5345/18 Brushless Motor is utilized model for aircrafts up to 15 kg in weight. Due to its high current capacity and RPM/V ratio, motor can work with high rpm values utp to 6000 and can generate high thrust values with connected blades.

The purpose of electronic speed controller is controlling the speed of motor with available power supply and voltage limit. Motor gains voltage with respect to the desired rpm values with ESC. Jeti Opto 90 is a fully programmable brushless motor controller and it provides smooth throttle response and motor cutoff in case of danger or low battery voltage.

DC power supply defined in Figure 3.3 is programmable to desired voltage or current which is easy to use. Up to 600 V voltage could be reachable. With the current choice, at most 5000 W power is gained.

3.3 Data Acquisition Elements

Data Acquisition system is responsible for obtain the experimental outputs with converting them from analog to digital values. This conversion is necessary in order to process experimental outputs with computer. Data Acquisition classify the test outputs like forces and moments on 3 axis, RPM, Voltage, Current and Power. For force and torque, force torque sensor is utilized. For rpm, current and voltage, elogger and rpm sensor is used.

ATI GAMA F/T Sensor, which is mounted on the test set-up in Figure 3.3, could be used in order to obtain force and torque values of the rotor in all three cartesian coordinates. Six seperate analog signals are available (F_x, F_y,F_z, T_x,T_y,T_z) .The system consists of a sensor, shielded high-flexible cable, DAQ power supply and ethernet/device net interface or F/T controller. The sensor uses silicon strain gages to measure forces.

The system monitor clearly shows the power, voltage, current that consumpted by whole system with the elogger card. It is connected between the ESC and Battery in order to calculate how much electrical power is consumpted by system from the power supply. Besides, an additional rpm sensor that mounted below the rotor hub is also plugged to system monitor card. The Eagle Eye rpm sensor estimates the rpm. It is “white colour” sensitive sensor. That is, a tiny white strip drawn on the rotating part of the motor. On every revolution, sensor detects this white strip and counts the rpm as shown in Figure 3.4. Then, Eagle tree card transmit this rpm signal to the computer instantly. In addition, throttle controller is also connected to a elogger card which will be explained on following sections. System monitor is only affiliated with electrical power and rpm signals. It does not transmit a signal from the force/torque transducer. However, additonal power and torque calculation could be made from system monitor electrical power output.

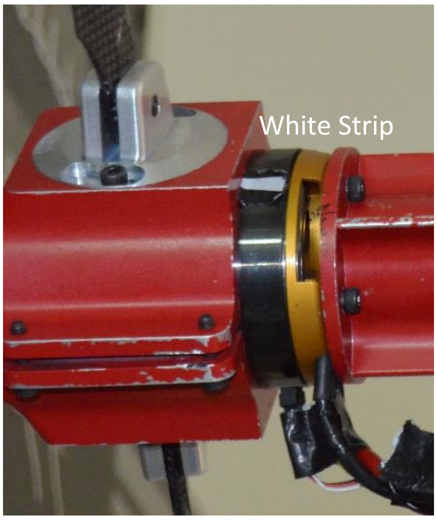

Figure 3.4 Working principle of rpm sensor

National Instruments NI USB-6210 DAQ Hardware collects the signals from the force/torque sensor and digitize them in order to use on a computer. The LabView Software on computer shows the signals digitized by DAQ. With LabView, outputs could be obtained with different frequencies and time intervals.

HJ Servo tester consistency is basically the throttle controller. With the fuse on it, the RPM could be adjustable hence, thrust and torque values are altered. Servo tester consistency is connected to a elogger card.

Each element of test setup is introduced. However, the significant point is the explanation of how entire system works. A sample diagram which includes the elements could clearly represent the working principle of test setup in Figure 3.5.

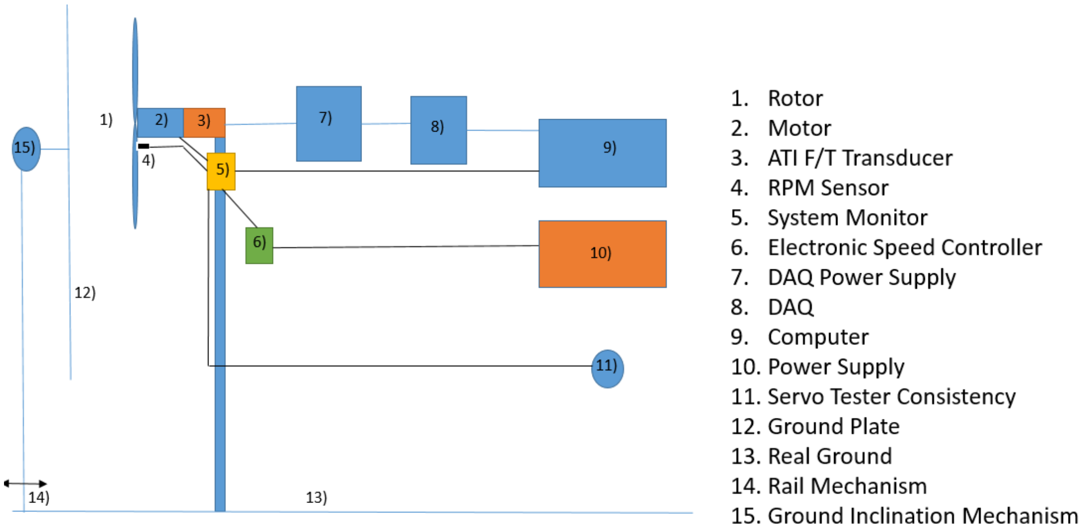

Figure 3.5 The diagram of the test setup

As seen from Figure 3.5, rotor is connected to the motor and motor is connected to the F/T Sensor. During the rotation, F/T Sensor gathers the force and torque with the strain gages inside. Rotor creates force on the sensor. The sensor transmits the signals to the DAQ hardware which needs extra power supply to work. In DAQ, force and torque signals converted into digital outputs then they are transmitted to the computer. Furthermore, system monitor is located between the motor and ESC. System monitor collects the consumpted voltage, current and power data by motor. Then, it transmits these signals to the computer. Besides, system monitor gathers the rpm data with RPM sensor below the rotating part of the motor and this signal is also transmitted to the computer. In order to start the system setup, power supply is activated. Then rotation is started by using the fuse of the Servo Tester Consistency. With the signal coming from Servo Tester Consistency, system monitor obtains signal then corresponding voltage is gained from the power supply with the usage of

ESC, finally, rotor is rotated with desired rpm related to voltage value. The ground plate is moved on the rail system for the sake of ground proximity creation. In addition, ground could be rotated with inclination mechanism.

Additionally, for tuft monitoring, tuft particles are glued onto the ground in order to visualize the flow path on the ground plate. The ground plate is painted with black in order to be compatible with PIV (Particle Image Velocimetry) flow visualizations.

CHAPTER 4

THEORY

This thesis contains both experimental and numerical study about a model scale helicopter rotor. In order to clearly justify the results and make logical comments, it is important to explain the theories behind them. Both experimental and numerical methods includes a systematic equations system and theories based upon past mathematical studies.

4.1 Experimental Data Analysis

The experimental data analysis contains the error source detection, classification and management.

4.1.1 Classification and Management of Experimental Data

The test setups introduces outputs with defined inputs. However, a perfect experimentation could not be seen in literature. Every experiment contains errors and it is the nature of experimentation. The main target in experimentation is “minimizing” the errors in order to obtain closer results to the perfect one. However, the sources of the errors must be clearly understood in order to minimize them. They are classified as follows:

4.1.1.1 Sources of Random Errors

Random errors are unpredictible and could be encountered in all experiments due to the imperfections. Basically, random errors occur during the repeat of experiments. When data is obtained with time, stopwach may be stopped early or late in time. These time exceedings may depict a value that is below the mean or above the mean. The remedy of this error is gathering data in a long time period or applicating several repeats then taking their mean values. If most of the mean values of repeats are accurate around a value, then random error is prevented.

As an example, changing the air humidity or automobile passing near the test facility could be apparent. The force sensor is sensitive to the outside sound level. This could be prevented by doing the tests on fully silent place, or stopping the data grabbing procedure temporarily when car is passing. Air humidity or density may cause random errors. For this reason, experiments will be made if there is no additional smoke generator or density altering element around the facility since multiple experiments may be done in the laboratory. The instrumental resolution is additional random error source. For instance, measurement of RPM for the ground effect test setup could be defined as a resolution error. However, this error is valid if little change could lead a high difference. For this experiment, since RPM's with 10^3 scales are taken into account, the differences of +-5 could not drastically change the result. So resolution is not important for this study.

4.1.1.2 Human Error Sources

Human error is simply the errors created by researcher. For instance, wrong establishment of setup, wrong reading of an output value or wrong management of experimental data after the data acquisition. Important point is, human errors are not defined as a error due to the nature of experiment. They could be denoted as external effect. In addition, due to the sensitivity of force torque sensor, walking or talking during the experiment could create an error. These errors could be denoted as human errors.

4.1.1.3 Systematic Error Sources

Systematic errors are basically errors created by the nature of the experiment, or the malfunction, wrong design of an experimental element. For example, for the ground effect test setup, the blade pitch angles must be equally arranged for both of the blades. If there is a little difference observed, this will monitor wrong results diverging from the mean value, on every repeat. For the prevention of systematic error, experimental setup must be consistent with its all elements. Another example is calibration. For instance, the setup used for this thesis includes a force torque transducer. Before experiments, it must be calibrated to the “zero value”, when there is no thrust. Calibrations are done with putting weight on the force sensor to investigate if it monitors the correct force value or not.

Another systematic error source is hysteresis which is clearly to reach a equilibrium value during experimentation. For this study, the thrust and torque values could not be obtained immediately after the motor starting. Approximately 5 minutes, it is waited until rotor downwash completely reach the ground then return the rotor to create ground effect completely.

It is clear that, errors have different reasons. There is not a strict classification, for example walking during the data grabbing may defined as random error for some issues. Definition of error type is important but, minimizing it in order to gain more reliable data is much more important. For the sake of experimental accuracy, all possible experimental error sources must be foresought and setup must be designed in order to remove or minimize this error sources. For example, on the previous chapter, the clean downwash flow creation was said to be main target. For this reason, alternatives include additional part except ground plate was eliminated to reduce the errors.

If multiple testing depicts the close value to the true value, that experiment could be defined as “accurate”. If multiple testing depicts the close values without taking true value into the accont, that experiment could be denoted as “precise”.

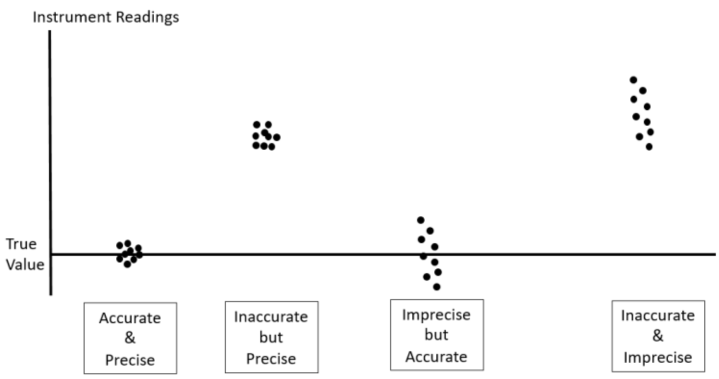

Figure 4.1 Precision and accuracy definitions [57]

Figure 4.1 defines the precision and accuracy terms. These terms creates the error types and detailed error analysis for the experimental data.

4.2 Computational Fluid Dynamics

Computational Fluid Dynamics is a branch of the calculation and observation of fluid flow physics. The reaction of fluid to the solid interfaces, the total force over a defined body etc. are all the subparts of Computational Fluid Dynamics. Viscous flow simulations are done with the numerical solution of special types of partial differential equations which are called as Navier – Stokes Equations.

4.2.1 Navier Stokes Equations

Navier Stokes equations are the set of coupled partial differential equations solved for the understanding the insight of the viscous fluid flow. These equations define the density, velocity, pressure and temperature variations of the fluid.

Under N-S equations, conservation of mass (continuity), momentum and energy equations are given in Eq. (5-9).

$$\frac{\partial \rho}{\partial t}+\frac{\partial(\rho u)}{\partial x}+\frac{\partial(\rho v)}{\partial y}+\frac{\partial(\rho w)}{\partial z}=0 \tag{4.1}$$

$$\frac{\partial(\rho u)}{\partial t}+\frac{\partial(\rho u^2)}{\partial x}+\frac{\partial(\rho uv)}{\partial y}+\frac{\partial(\rho uw)}{\partial z}=-\frac{\partial p}{\partial x}+\frac{1}{Re_r}\left(\frac{\partial \tau_{xx}}{\partial x}+\frac{\partial \tau_{xy}}{\partial y}+\frac{\partial \tau_{xz}}{\partial z}\right) \tag{4.2}$$

$$\frac{\partial(\rho v)}{\partial t}+\frac{\partial(\rho uv)}{\partial x}+\frac{\partial(\rho v^2)}{\partial y}+\frac{\partial(\rho vw)}{\partial z}=-\frac{\partial p}{\partial y}+\frac{1}{Re_r}\left(\frac{\partial \tau_{xy}}{\partial x}+\frac{\partial \tau_{yy}}{\partial y}+\frac{\partial \tau_{yz}}{\partial z}\right) \tag{4.3}$$

$$\frac{\partial(\rho w)}{\partial t}+\frac{\partial(\rho uw)}{\partial x}+\frac{\partial(\rho vw)}{\partial y}+\frac{\partial(\rho w^2)}{\partial z}=-\frac{\partial p}{\partial z}+\frac{1}{Re_r}\left(\frac{\partial \tau_{xz}}{\partial x}+\frac{\partial \tau_{yz}}{\partial y}+\frac{\partial \tau_{zz}}{\partial z}\right) \tag{4.4}$$

$$\frac{\partial(E_t)}{\partial t}+\frac{\partial(uE_t)}{\partial x}+\frac{\partial(vE_t)}{\partial y}+\frac{\partial(wE_t)}{\partial z}=-\frac{\partial(up)}{\partial x}-\frac{\partial(vp)}{\partial y}-\frac{\partial(wp)}{\partial z}$$

$$-\frac{1}{Pr_r\,Re_r}\left(\frac{\partial(q_x)}{\partial x}+\frac{\partial(q_y)}{\partial y}+\frac{\partial(q_z)}{\partial z}\right)+\frac{1}{Re_r}\left(\frac{\partial}{\partial x}(u\tau_{xx}+v\tau_{xy}+w\tau_{xz})+\frac{\partial}{\partial y}(u\tau_{xy}+v\tau_{yy}+w\tau_{yz})\right.$$

$$\left.+\frac{\partial}{\partial z}(u\tau_{xz}+v\tau_{yz}+w\tau_{zz})\right) \tag{4.5}$$

The above set of partial differential equations are solved numerically with various methods: finite element, finite volume method or spectral approaches. In this thesis, Finite Volume Method is utilized in order to solve numerically the flow of the rotor in ground effect.

The independent variables of equations are spectral coordinates *x,y,z* and time *t*. The dependent variables of equations are velocity in x direction(u), velocity in y direction(v) ,velocity in z direction (w), pressure, density ρ and Total Energy (e) . These dependent variables are functions of the independent variables that constitute Navier Stokes equations.

The left hand side of the momentum equations are called as "convection" terms. Convection is a process of the property transportation by systematic motion of fluid flow. The right hand side of the momentum equations are denoted as "diffusion" terms. Diffusion is a property transportation process with random molecular motion in gaseous flow. The terms including stress tensors and fluid viscosity (τ) are related to diffusion. Turbulence and boundary layer are created by the diffusion of flow.

4.2.1.1 Solution Procedure of the N-S Equation

The five equations (mass, momentum and energy) must be solved simultaneously which is denoted as coupled solution procedure. In order to equate the number of unknowns with number of equations, equation of state is taken as the 6th equation:

$$p = \rho R T \tag{4.6}$$

Perfect gas assumption with Sutherland Law is used for the solution algorithm of Navier Stokes Equations [31].

Finally, the stress tensor terms are specified which are approximated by turbulence model. Most of the rotary wing flow simulations implement NS equations as observed in the study of Kim et al. [32]. The vortex structure passed parallel to the ground must be fully resolved which requires a full NS Equation solution, as discussed by Kang et al. [33].

4.2.2 Reynolds Averaged Navier Stokes Equations

In the previous section, it is stated that viscous stress fluctuations are approximated by the turbulence model. In other words, turbulence is integrated to the NS equations under viscous terms. In order to better understanding of this phenomenon, Reynolds Averaging definiton must be stated.

As flat plate assumption is made, the flow becomes turbulent when Reynolds number is around 10^4 - 10^6. Thus, a laminar flow assumption could not be made and, turbulent characteristics of fluid flow must be taken into account. The turbulent flow is shown in Figure 4.2.

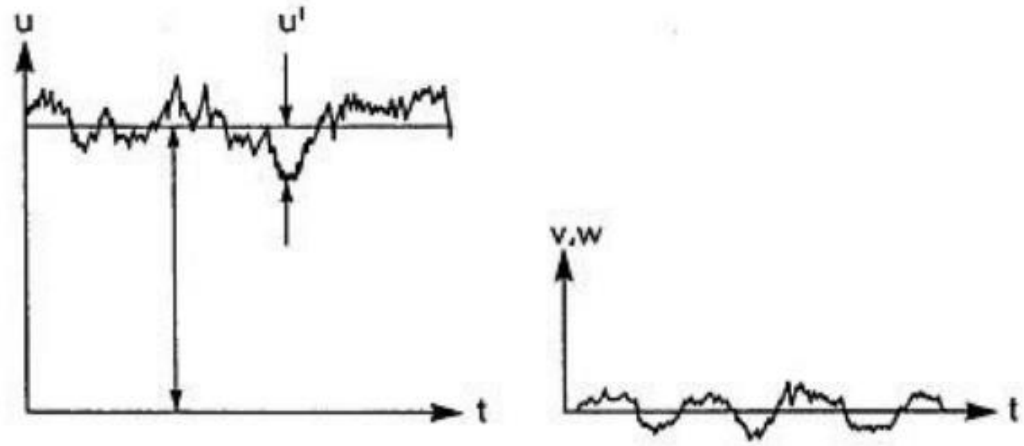

Figure 4.2. Turbulent velocity fluctuation with respect to the time [34]

As seen in Figure 4.2, turbulent flow velocity has mean value and fluctuating value. Each variable could be written analogously with its time averaged value and fluctuated value. Define u as a primitive variable:

$$u = \overline{u} + u' \tag{4.7}$$

Afterwards, above variable is plugged into Navier Stokes equations with a systematic procedure. After certain steps, total shear stress term has an additional term when compared to original Navier Stokes equation.

Additional stress term: $\rho\overline{u_i'u_j'}$

This stress term is called as the Reynolds stress, turbulent shear stress or eddy viscosity which is the 7th unknown variable for the set of NS equations. This nonlinear stress term requires additional equation which is estimated by modelling to solve the set of RANS equations. For this purpose, various turbulence stress models are available in the literature.

4.2.3 Turbulence Modelling

As turbulence model, two equation SST k-ω Turbulence Model of Menter [35] is selected. This model could also be utilized as Low Reynolds Turbulence model due to the the usage of k and ω (omega) functions in the inner parts of boundary layer. The past experiences show that SST Model could handle the flow separations and adverse pressure gradients.

Basically, in this model, for inner parts of the boundary layer, original k- ω Model is applied. Then, for outer parts of the boundary layer, k-ϵ Model is utilized.

The k equation designates the turbulence kinetic energy equation. On the other hand, ω equation is denoted as specific dissipation rate.

Transport equation of k (Turbulence Kinetic Energy)

$$\frac{Dk}{Dt} = \frac{\partial k}{\partial t} + u_j \frac{\partial k}{\partial x_j} = P_k - \beta^* k\omega \ \frac{\partial}{\partial x_j}\left[(\upsilon + \sigma_k \upsilon_T)\frac{\partial k}{\partial x_j}\right] \tag{4.8}$$

Transport equation of ω (Specific Dissipation Rate)

$$\frac{D\omega}{Dt} = \frac{\partial \omega}{\partial t} + u_j \frac{\partial \omega}{\partial x_j} = \alpha S^2 - \beta^* \omega^2 \ \frac{\partial}{\partial x_j}\left[(\upsilon + \sigma_\omega \upsilon_T)\frac{\partial \omega}{\partial x_j}\right] + 2(1 - F_1)\sigma_{\omega 2}\frac{1}{\omega}\frac{\partial k}{\partial x_i}\frac{\partial \omega}{\partial x_i} \tag{4.9}$$

The terms $F_2, P_k, F1, \alpha, \beta, \beta^*, \sigma_{k1}\ and\ \sigma_{k2}$ are auxillary closure coefficients established by Menter [35] .

The co-operation of two models is achieved with addition of blending terms obtained by the transport equation of the turbulent shear stress which is defined as the Shear Stress Transport (SST) [35].

$$\frac{D\tau}{Dt} = \frac{\partial \tau}{\partial t} + u_j \frac{\partial \tau}{\partial x_j} \tag{4.10}$$

Turbulence model selection is based on similar literature studies explained in references [36], [37] and [38].

4.2.4 Finite Volume Method

The finite volume method is a discretization method in order to solve the Navier Stokes equations in a control volume. The control volume is created by "cells" in CFD simulations. The flow field is discritized by amount of cells.

Suppose a conservation equation with a primitive variable of *Q* in integral form:

$$\frac{\partial}{\partial t} \int_{\Omega} \vec{Q}\, d\Omega + \oint_{S} \vec{F}.\vec{ds} = \oint_{S} \vec{G}.\vec{ds} \tag{4.11}$$

The *Q* is a matrix composed of conservative variables:

$$\vec{Q} = \begin{Bmatrix} \rho \\ \rho u \\ \rho v \\ \rho w \\ \rho e_T \end{Bmatrix} \tag{4.12}$$

F is a vector of inviscid flux (convective flux) term.

$$\vec{F} = \begin{Bmatrix} \rho \\ \rho u \\ \rho v \\ \rho w \\ \rho e_T \end{Bmatrix} \vec{V} + \begin{Bmatrix} 0 \\ i \\ j \\ k \\ \vec{V} \end{Bmatrix} p \tag{4.13}$$

G is a vector term of viscous flux term given by Eqn (4.14).

$$\vec{G} = \begin{Bmatrix} 0 \\ \tau_{xx} \\ \tau_{yx} \\ \tau_{zx} \\ u\tau_{xx} + v\tau_{yx} + w\tau_{zx} \end{Bmatrix} i + \begin{Bmatrix} 0 \\ \tau_{xy} \\ \tau_{yy} \\ \tau_{zy} \\ u\tau_{xy} + v\tau_{yy} + w\tau_{zy} \end{Bmatrix} j + \begin{Bmatrix} 0 \\ \tau_{xz} \\ \tau_{yz} \\ \tau_{zz} \\ u\tau_{xz} + v\tau_{yz} + w\tau_{zz} \end{Bmatrix} k \tag{4.14}$$

For steady state process where dt =0, conservation equation is shown in Eqn. 4.15.

$$\oint_S \vec{F}.\overrightarrow{ds} = \oint_S \overrightarrow{G}.\overrightarrow{ds} \tag{4.15}$$

When conservation equation is applied to a sample tetrahedral cell as shown in Figure 4.3, equation is discretized as given in Eqn.4.16.

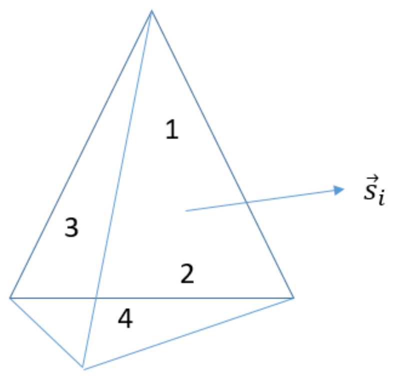

Figure 4.3 Tetrahedral control volume

$$\sum_{j=1}^{4} F_{ij}S_{ij} = \sum_{j=1}^{4} G_{ij}S_{ij} \tag{4.16}$$

Rearranging the terms on left hand side:

$$\sum_{j=1}^{4} (F_{ij} - G_{ij})S_{ij} = 0 \tag{4.17}$$

For farfield cells, convective flux terms are calculated. For wall boundary cells, both convective and viscous fluxes are calculated. Eqn. 4.17 is defined for one cell as shown in Figure 4.3. For each cell in grid system, flux computations are made.

The flux calculation is the key issue of the CFD. The ongoing flow characteristics are calculated by the flux computations in which the cells located through the flow path. All flux variables are defined at cell center.

However, the continuity of the flow and variations of flow characteristics are changing from one cell to the another contiguous cell. The variation of the flow characteristics are determined by calculation of fluxes over the cell faces. Various flux calculation methods are available in literature. The criteria like the type of flow, fluid, compressibilty effects etc. could be a reason for the development of the different flux calculation methods. The relation between the two contiguous cells are identified by face flux computation.

The term $(F_{ij} - G_{ij})$ is denoted as "residual" and main target is reach a residual value of "0" or very close value to the "0" in order to satisfy the equation. The closer equation reaches "0", the higher accuracy is. In order to reach a residual value close to zero, proper flux calculation method must be selected. As a solver, CFD++ software is used.

4.2.5 Solution Algorithm

Implicit Forward Euler Scheme is utilized since it is a stable method and provides better stability rather than the explicit methods. Inviscid terms are computed by using 2nd order discretization polynomial scheme as available in the work of Doerffer et al. [31] and in the study of Kao et al. [36].

4.2.6 Total Variation Diminishing (TVD) Scheme

TVD flux calculation method is efficient and accurate implicit stable high-resolution scheme to steady-state calculations. It is a member of a one-parameter family of explicit and implicit second-order accurate schemes developed by Harten et. al. [39]. Numerical experiments show that this scheme not only has a rapid convergence rate, but also generates a highly resolved approximation to the steady-state solution.

4.2.7 Preconditioning Methods

Various numerical solution algorithms for the solution of Navier Stokes equations are available in literature. Two main widespread solution algorithms are pressure based algorithm and density based algorithm. The pressure based solvers are "segregated" solvers where, governing equations are solved sequentially, whereas, density based solvers are “coupled” solvers where coupled system of governing equations is solved. Since momentum and continuity equations are solved in a coupled manner, the convergence rate is higher when compared with the pressure based algorithm. For this reason, density based algorithm is selected for rotary wing simulations [31] .

However, density based scheme is specialized for solutions of compressible Navier Stokes equations where flow may have a velocity value of Mach > 0.45. The maximum velocity of the rotor simulations are around mach 0.3 which is calculated from tip velocity. If density based algorithm is solved for incompressible cases, numerical errors called “diffusion” arise. Since convergence rate is much more important for rotary wing cases, density based algorithm must be re - arranged to the rotor flow with incompressible regime. Solving incompressible flow with density based algorithm is called as “preconditioning” which is developed by Turkel [40].

4.2.8 Mesh Generation

The finite volume method is applicable when the solution domain and path of flow is definite. In order to solve the flow accurately, discretization with multiple control volumes must be applied which is denoted as mesh generation. For this purpose, the flow domain is partitioned with a number of control volumes which are denoted as “cells”. First of all, surface grids are meshed as shown in Figure 4.4.

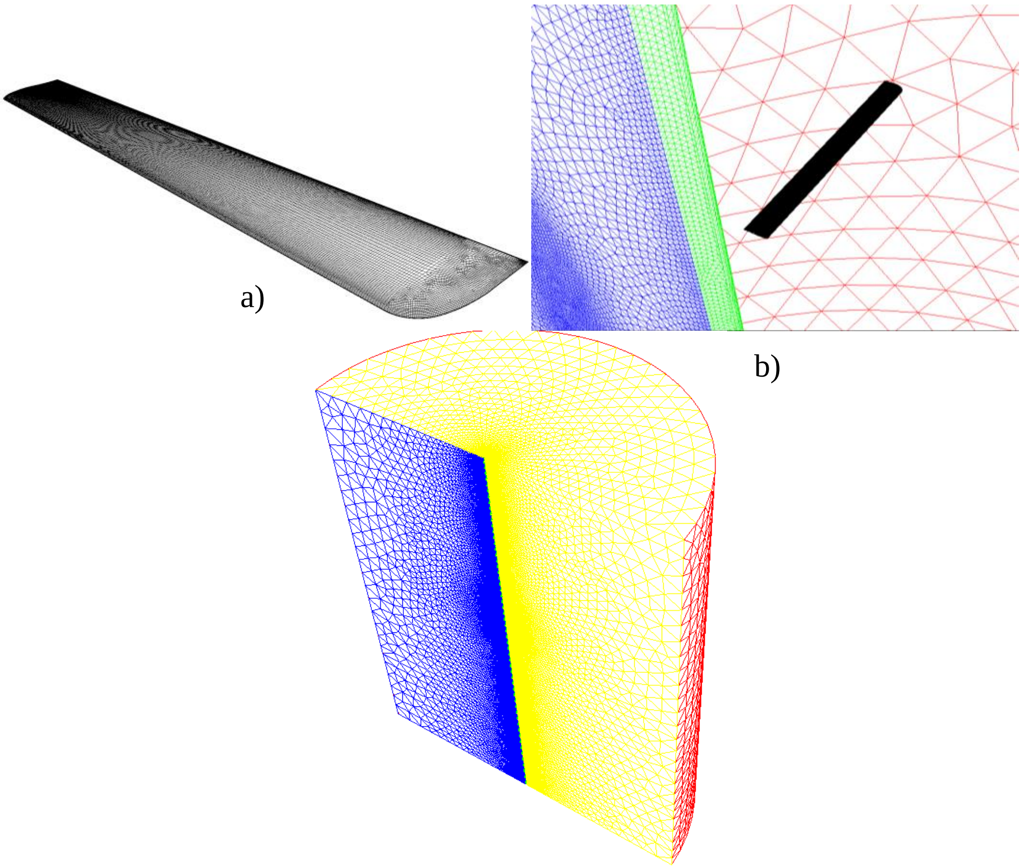

Figure 4.4 a) Surface grid of blade and b) Farfield surface grids

The surface grid could be created either with quad elements or triangle elements. In Figure 4.4, boundary grid surfaces are available for blade and farfield. The surface mesh of rotor blade is generated with quad elements. During the mesh generation process, the root cut-out section is ignored since it has no aerodynamic force contribution to the overall thrust. The zone with lifting capability is meshed. On the surface of tip region, additional refinement is done in order to capture tip vortex initiation accurately.

Secondly, the space between the blade and farfield will be filled with volume grid which is created by discretization of space with cell elements as shown in Figure 4.5.

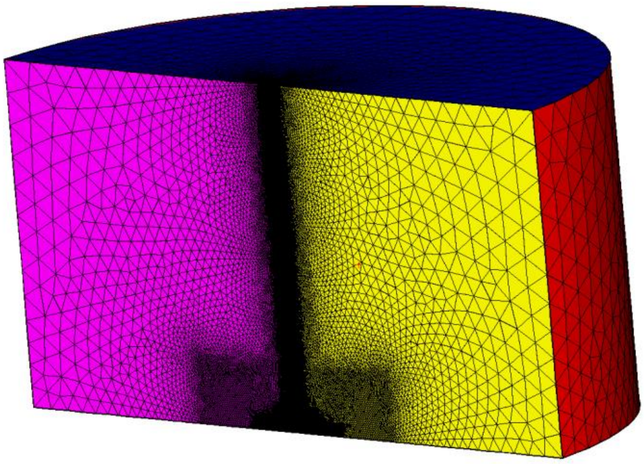

Figure 4.5 Volume grid for z/R: 0.8

In order to solve the viscous fluxes on the blade surface, boundary layer must be fully resolved. To do this, boundary layer mesh generation is done on the blade surface mesh. Boundary layer mesh is created by inflation of blade surface mesh with defined initial spacing, growth rate and number of layers.

Finally, remaining space is filled with tetrahedral elements. In this phase, local grid refinements for tip vortex visualization are done. Grid refinement is simply refinement of a specified zone with smaller cells. For ground effect without inclined surface cases, grid with one rotor blade is created. For inclined cases, volume grid containing two subblocks is created. The details will be explained on MRF section.

4.2.9 Boundary Conditions

Boundary condition implementation is done for cases of ground effect with no inclination and inclined ground effect cases seperately.

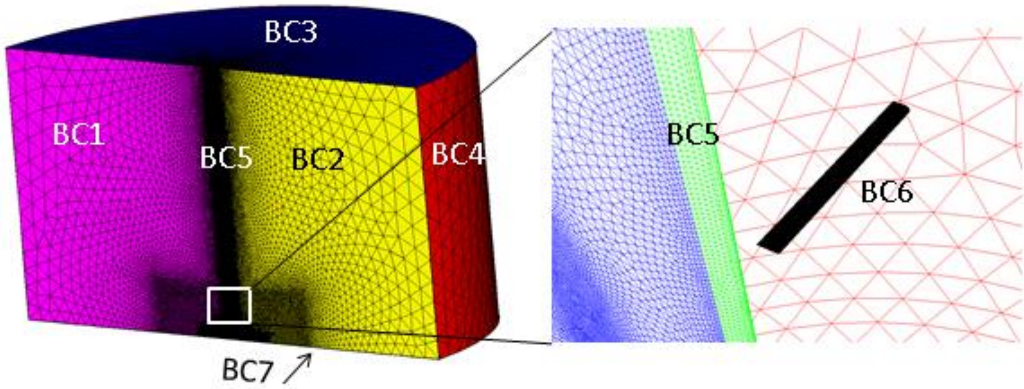

Figure 4.6 Boundary conditions of ground effect with no inclination

On account of the definition of the periodicity of the rotational motion of the blade, periodicity is imposed to the boundaries #1 and #2 as shown in Figure 4.6. In order to achieve mesh reduction for computational time saving, modelling one of the the two blades is adequate. The working principle of periodic boundary condition is interpolation of variables between the periodic boundary conditions with given rotational offset. For this case, rotational offset is 180° since it is the angle between the two periodic faces. Hence rotation of the blade is adequately modelled. Finally, the net thrust and torque values are multiplied by 2 since one blade is modelled and 2-bladed rotor is available.

Periodic boundary condition is implemented in the similar work of Thomas et al. [41].

For farfield boundaries (BC3 and BC4), a specialized boundary condition called "Inflow/outflow – Pressure Temperature using inside velocity" is imposed. The key features of this boundary condition are:

- Outer region of the flow has zero velocity
- Direction of the flow is not known due to the rotary wing simulation

Both of the features are compatible to the CFD case of the rotor simulation. The ambient pressure and temperature values are defined to this boundary condition

BC5 designates the mid root wall and BC7 designates the ground as shown in Figure 4.6. The flow velocity has a free slip at the boundary and it becomes tangential to the surface. For ground, the boundary layer solution is not applied since tip vortex and the ground boundary layer interaction are not the issues of this thesis. Due to that point, no boundary layer grid is generated on the ground and ground is defined as "Slip Wall". Slip Wall Boundary Condition approach is available in literature namely in the study of Filippone et al. [42] and in the work of Tanabe et al. [43]. In addition, the volume mesh without the ground wall boundary layer reduces the computational time [31]. For BC5,comments made for BC7-Ground are valid as well.

For no slip condition, v = 0 for stationary walls. In rotor CFD cases, rotor blade is stationary but flow moves around it. The turbulence related variables and the wall limiting parameters are implemented into this boundary condition with exact turbulence model selection.

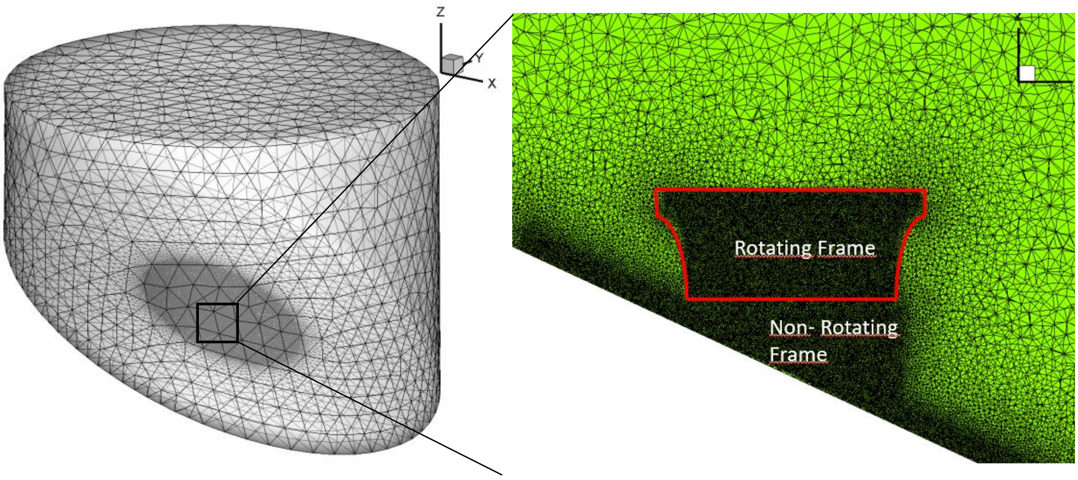

Figure 4.7 Rotating and non- rotating frames for inclined ground effect case

For inclined cases, no slip boundary condition is imposed to blades, slip wall condition is imposed to ground and "inflow/outflow, using inside velocity " condition is imposed to the farfield, similar to the ground effect without inclination cases. Main differences are described as:

- Periodicity fails when ground inclination is taken into account. Hence both of the blades are meshed and number of elements in the volume grid increases as shown in Figure 4.7.

- Unlike the cases of ground effect without inclination, two subblocks are created as shown in Figure 4.7. Inner block encapsulates the rotor blades and wake region. Outer block is the remaining block between the wake outer boundary and farfield. The reason of this block division is, rotation definition fails when one block is created for inclined cases. The rotation definition will be explained in details on MRF section.

Hence, new boundary condition emerges: Zonal Interference. The boundary between the two blocks which is the outer boundary of the wake region provides the information exchange between the rotating inner frame and non- rotating outer frame. It is in Figure 4.7 with red coloured bounds.

4.2.10 Volume Grid Generation

The volume mesh is composed of unstructured tetrahedral grids for farfield mesh and prismatic elements for the boundary layer mesh. Similar approach is observable in the work of Abras et al. [44]. The volume grid generation could be divided into two parts: Grid of ground effect without inclination and grid of ground effect with inclination.

For cases without inclination, in order to achieve grid size saving, only one of the two blades is meshed. In the end, total thrust and torque are computed as doubling of the result due to the single blade simulation.

For cases with inclination, as defined in Figure 4.7, it is impossible to define a periodicity due to the unsymmetry of the rotating flow. Hence, both of the blades are modelled and grid generation is performed due to that point.

For all cases, grid refinement study is done for the accurate visualization of the tip vortices. A tip vortex grid refinement study is available in the work of Kutz et al. [37]. In order to determine the possible tip vortex path, the path of tip vortices is generated by Kocureks' Method [45] as shown in Figure 4.8.

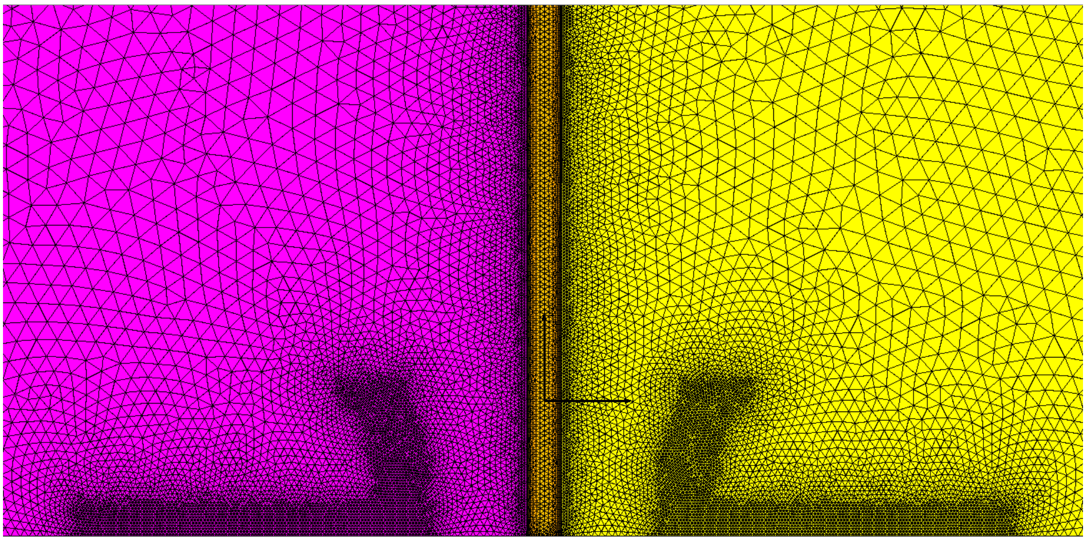

Figure 4.8 Tip Vortex Refinement on Volume Grid for z/R: 0.8

4.2.11 Kocurek - Tangler Prescribed Wake Model [45]

The helicopter in hover condition creates a severe downwash flow either in the vicinity of the blades or downside from the rotor tip path plane. The tip vortices emerged from blade tip, affect the aerodynamics of the succeeding rotor blade which causes local inflow and angle of attack change. For this reason, it is significant that, rotor wake and tip vortices must be captured accurately in order to achieve a satisfactory rotor flow simulation. Hence, possible path of tip vortices must be refined during mesh generation.

The volume grid refinement is done according as the possible blade tip vortex path. In order to define the path of the refinement, a prescribed wake model derived by Kocurek and Tangler [45] is used.

In literature, Abras et al. [44] implement a grid refinement study in order to satisfy the wake vortex preservation. Blade tip vortex path is valid only for the region between the rotor and ground. On the ground, mesh refinement continues parallel to the ground with one rotor diameter distance from the end of the tip vortice path to the farfield. Additional mesh refinement is performed approximately 10 radius apart from the helicopter blade. Figure 4.8 shows the refinement zone for z/R=0.8 case and Figure 4.9 presents the tip vortex refinement zone for OGE case.

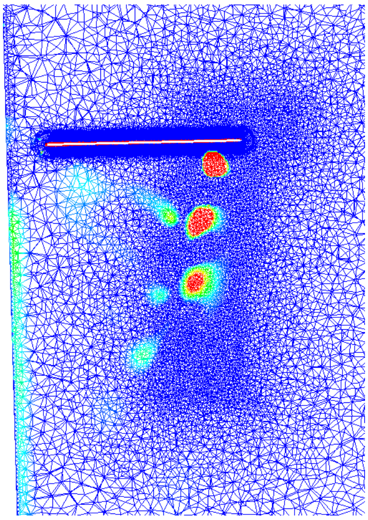

Figure 4.9 Tip vortex path created by Kocurek Tangler Method and captured tip vortices

4.2.12 Q Criterion

When tip vortices are captured with grid refinement, they could be clearly visualized with specialized variable called Q Criterion [46]. Tip vortices are accurately visualized in the defined wake region which is an indicator for the rotor CFD solution accuracy.

Q criterion is simply the second invariant of the velocity gradient tensor.

Velocity gradient tensor $\overline{D}$ is given by eqn. 4.18.

$$D_{ij} = \frac{\partial u_i}{\partial x_j} \tag{4.18}$$

Since this is a second order tensor, it could be seperated into a symmetric and skew-symmetric parts as given by Eqn. 4.19.

$$D_{ij} = S_{ij} + \Omega_{ij} \tag{4.19}$$

$$S_{ij} = \frac{1}{2}\left(\frac{\partial u_i}{\partial x_j} + \frac{\partial u_j}{\partial x_i}\right) = rate\ of\ strain\ tensor \tag{4.20}$$

$$\Omega_{ij} = \frac{1}{2}\left(\frac{\partial u_i}{\partial x_j} - \frac{\partial u_j}{\partial x_i}\right) = vorticity\ tensor \tag{4.21}$$

The characteristic equation of $\vec{\nabla}u$ (velocity gradient) is given by Eqn 4.22.

$$\lambda^3 + P\lambda^2 + Q\lambda + R = 0 \tag{4.22}$$

The P,Q,R are three invariants of the velocity gradient tensor. By symmmetric –anti symmetric decomposition, they are defined by eqns. 4.23, 4.24 and 4.25.

$$P = -tr(\,\overline{D}) \tag{4.23}$$

$$Q = \frac{1}{2}\left\|\overline{\Omega}\right\|^2 - \left\|\overline{S}\right\|^2 \tag{4.24}$$

$$R = -det(\,\overline{D}) \tag{4.25}$$

The second invariant which is denoted by Q is the Q criterion. When definition of Q is inspected, it provides a balance between the rate of shear strain and vorticity magnitude. The positive values of Q denotes the zones with high vorticity whereas negative values of Q denotes the the zone with high strain rate. Hence, with positive values of Q, tip vortices could be clearly decomposed and visualized as shown in Figure 4.9.

Baeder et al. [47] implies that, Q Criterion presentation is useful for vorticity dominated flowfields like rotor flows. For this reason, rotary wing Q Criterion applications are widespread as practiced by Kao et al. [36] , Kalra et al. [48] and Baeder et al. [49] .

4.2.13 Moving Reference Frame

For rotary wing flow simulation applications, rotation could be implemented in various ways. One way is to define a rotation to the grid where specified grid block rotates. The simulations with actual grid rotation are generally transient and consumes high amount of computational power and time. Another and simpler approach is definition of rotational velocity to the each cell of the grid. In this aprroach, grid is not rotating but rotational velocity is added as an additional source term into the RANS equations. When the rotor simulation is considered, this approach could be named as “frozen rotor” for rotary wing simulations. This approach is much more time and computational power saving since unsteady flow simulations are conducted with steady state, time invariant analyses. The general definition of this method is called as “Moving Reference Frame”.

In MRF approach, it is possible to transform the NS equations into a rotating reference frame when single rotating geometry is taken into account. During the rotation, to an observer in global referance frame, flow appears unsteady. However, when observer is moving with the rotating frame the flow appears steady.

When rotational velocity is added in MRF approach, flow equations are redefined in rotating frame. The rotation of frame is accounted for the relative velocities and additional coriolis force source terms addition to the Navier Stokes equations. Besides, flux terms are relative to the defined rotational velocity.

For ground effect cases without inclination, rotation is defined to entire frame and satisfactory results are obtained. Whereas, for cases with ground effect inclination, definition of rotation to the entire grid fails and it prompts unrealistic solutions. When volume grid is divided into two parts as defined in Figure 4.7, the rotational velocity is redefined to the inner block only. Hence, results close to the experimental results are obtained. It is assessed that, MRF approach is invalid when asymmetric features are taken into accound i.e. inclined surfaces.

All simulations are done with isolated rotor. No interface effects of any other part of the test setup is added except ground surface. The study of Pandey et al. [50] includes the MRF implementation for isolated rotor CFD solutions.

4.2.14 Computational Hardware

CFD cases were run at the Poyraz High Performance Computer located in METUWIND Facilities. The HPC has 8 nodes. Each node includes 4 AMD Opteron 6276 2.3 GHz. CPUs with 16 cores and a 256 Gb of shared memory.

CHAPTER 5

TEST CAMPAIGN, RESULTS

This chapter explains the test campaign and results in details. As mentioned before, tests were conducted to obtain force and torque values at different ground distances with respect to the rotor plane. The test campaign is shown in Table 5-1.

Table 5-1 Test parameters and number of cases

RPM	2000, 2500, 3000	3
Tip Mach Number	0.22, 0.28, 0.34	3
Tip Reynolds Number	112K, 140K, 170K	3
Non – Dimensional Distance (z/R)	0.25, 0.3, 0.4, 0.5, 0.6, 0.7, 0.8, 0.9 1, 1.2, 1.4, 1.6, 1.8, 2, 2.5, 3	16
Ground Inclination Angle (β)	$0°, 5°, 10°, 15°, 20°, 25°$	6
# of repeat		3
Total # of cases		864
Data Collection Frequency [Hz]		10000

As shown in Table 5-1, 3 different RPM, 16 non - dimensional distance and 6 ground inclination angles are tested. In order to validate the repeatibility of the experiments, each case is repeated 3 times. Data collection frequency is simply how many thrust and torque value is obtained per second for one case. The non- dimensional distance is distance of the rotor tip path plane (TPP) with respect to the ground plate divided by rotor radius. If inclination is taken into account, the z/R distance is accepted as the distance between the TPP and ground plate along the hub axis as shown in Figure 5.1.

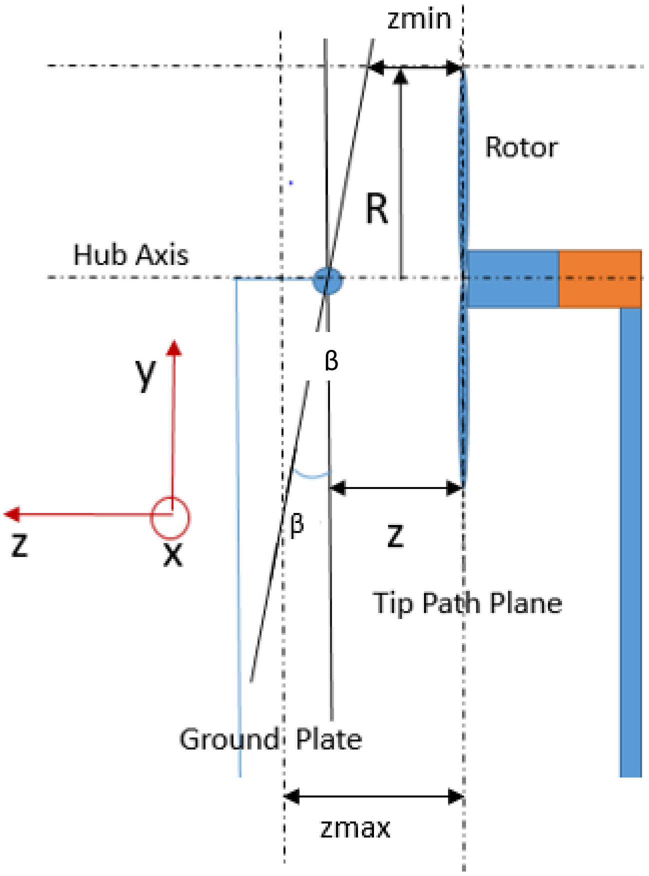

Figure 5.1. The Ground plate and rotor axes

Figure 5.1 shows how inclination angle (β) is adjusted with respect to the rotor. The hub axis, is used as a reference which passes from the center of the rotor disk. When inclination angle is zero, it is the ground effect with no inclination.

Each test proceeds approximately 5 minutes. In this time interval, force, torque, RPM, current, and voltage values could be obtained with F/T sensor and Eagle Eye sensor. During the Force/Torque data gathering, output data is defined on 3 axes (F_x, F_y, F_z and T_x, T_y, T_z). Thrust is simply the force reading on z direction (F_z) and denoted by T. Torque is the total moment on z direction (T_z) and denoted by Q.

5.1 Data Analysis Procedure

After obtaining the output values, each output value has a dataset with respect to the time as shown in Figure 5.2.

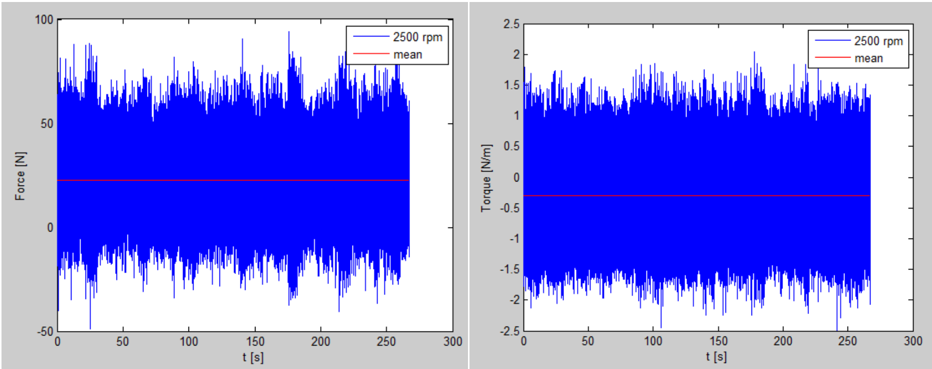

Figure 5.2 Sample a) Force and b) Torque output for the z/R = 0.25 case with 2500 RPM, with respect to time

Figure 5.2 includes vast amount of data due to the high data collection frequency. In order to identify the trend of the data, the data collection rate in one period must be plotted. Period is simply the data collection in one revolution. For 2500 RPM, the period is defined on eqn.

$$T = \frac{60\ sec/min}{2500\ rev/min} = 0.024\ sec \tag{5.1}$$

The period is 0.024 seconds which is the time interval for one rotor revolution in 2500 RPM. Figure 5.2 are replotted between the 0 - 0.025 s time interval and force and torque change in one period could be observable.

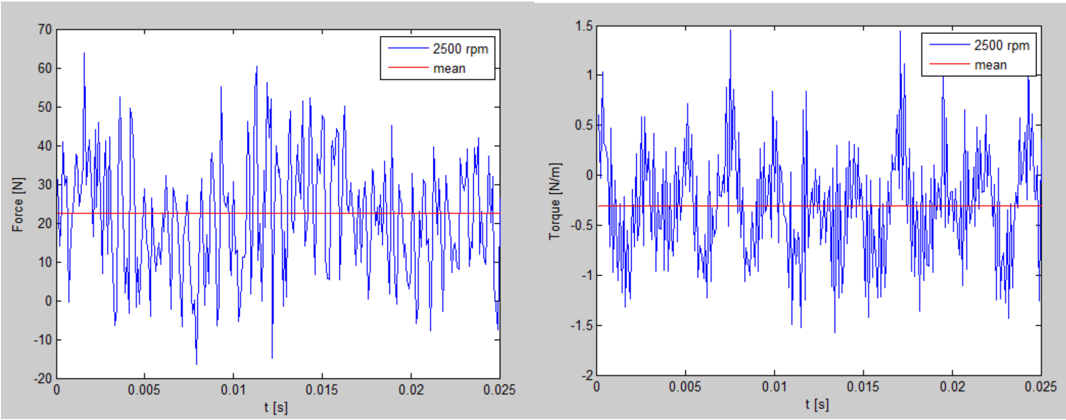

Figure 5.3 Unsteady force and torque measurements in one period

As seen from Figure 5.3, force and torque values are oscillating around the mean value without any sudden amplification. That picture proves that a clean and logical data collection procedure is done. Another key point is the precision of the F/T Sensor which is high enough.

Table 5-2 Sensor ranges [63]

Fx ,Fy [N]	Fz [N]	Tx,Ty [Nm]	Tz [Nm]
± 32	± 100	± 2.5	± 2.5

The sensor ranges defined in Table 5-2 define that force and torque variations described in Figure 5.3 have a trend in acceptable range.

After obtaining sample force and torque values, the mean and standard deviation values are calculated for all datasets in order to inspect the stability of the data obtaining process in defined time interval as shown in Figure 5.4. Besides, standart error is calculated in order to investigate the validity of the mean value in repeated cases.

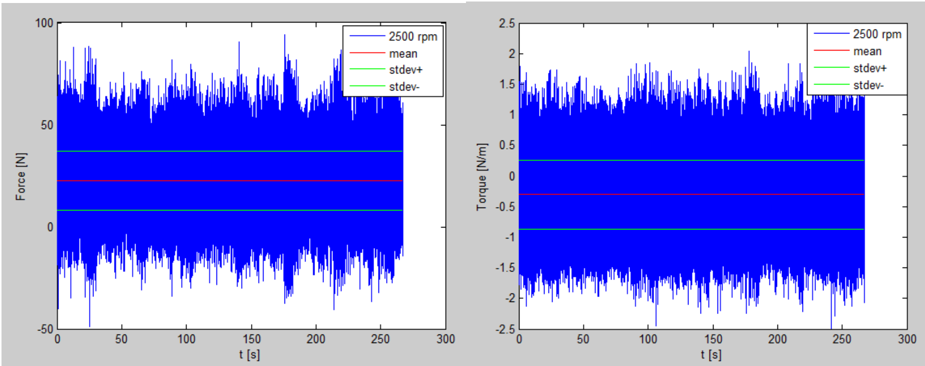

Figure 5.4 Standard Deviation and mean of sample datasets

If standard error is in the accepteble range, mean values are used for the case. If not, experimental data could not be used. For this test campaign, error range is defined as % 0.3 as a maximum. The reason of the error range selection will be explained on following sections.

The frequency check is done for each dataset in order to identify the data obtainment with defined frequency is correct or not.

Finally, each force and torque values are calculated and are written with their corresponding z/R values. Force and Torque values could be defined with 3 different definitions:

- Dimensional values:

  Thrust and torque values are defined with their dimensional values.

- Thrust and torque coefficients:

  Thrust and torque could be defined as non - dimensional thrust coefficient and torque coefficient with eqn. 5.2 and eqn 5.3.

$$C_T = \frac{T}{\rho A V_{tip}^2} \quad (5.2)$$

$$C_Q = \frac{Q}{\rho A V_{tip}^2 R} \quad (5.3)$$

  With this non – dimensionalization, the difference of the Force/Torque values arising from the RPM could be removed. Coefficient data of the Force/Torque values corresponding to different RPM values will be the same.

- Non dimensional Thrust and Torque with respect to the Out of Ground Effect Values

  This non - dimensionalization method is again similar with coefficient method. However, it is specialized non dimensionalization for ground effect studies. It is simply the division of Thrust and Torque values to the reference Out of ground effect thrust/torque value.

$$Non - Dim\,Thrust = \frac{T}{T_{oge}} \tag{5.4}$$

$$Non - Dim\,Torque = \frac{Q}{Q_{oge}} \tag{5.5}$$

  For this study, reference thrust and torque values are chosen as Thrust/Torque values of z/R : 3 since it is an “out of ground effect” case.

  The sample trend curves for Thrust and Torque are plotted with standard error bars:

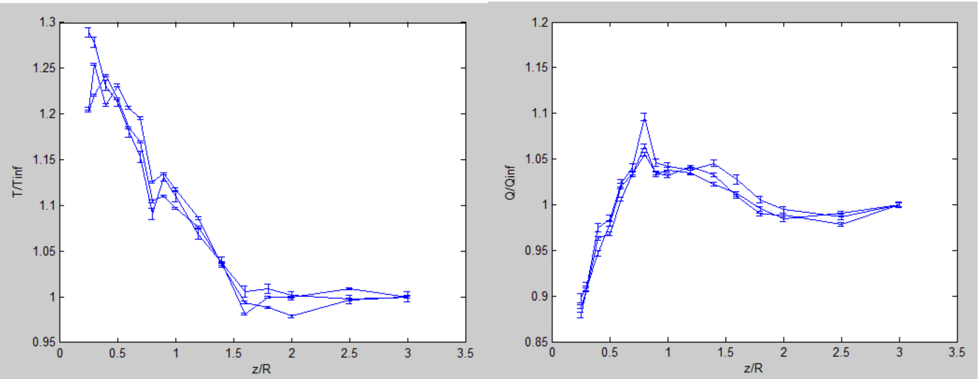

Figure 5.5 Standard error bars

In Figure 5.5, as torque curve is investigated, a peak point is available as Q/Q_{OGE} : 1.1. This value is out of trend curve. When standard error percentage of this value is investigated, it is calculated approximately 0.3%. The error range is determined with this way. Hence, cases with standard error percent higher than 0.3 % are eliminated and they cannot be placed in force and torque figures.

After elimination of values with high error percentages, trend curves of point clouds are estimated where an exact trend is observable. In addition, comparison with literature data will be introduced.

The ground effect test results could be investigated into two parts: Ground Effect with no inclination and Inclined Ground Effect.

5.2 Results of Ground Effect Without Inclination

This section of the test campaign includes thrust and torque relations for ground plate distances defined on Table 5-1 with 3 different RPM values. Thrust and Torque values are shown in Figure 5.6.

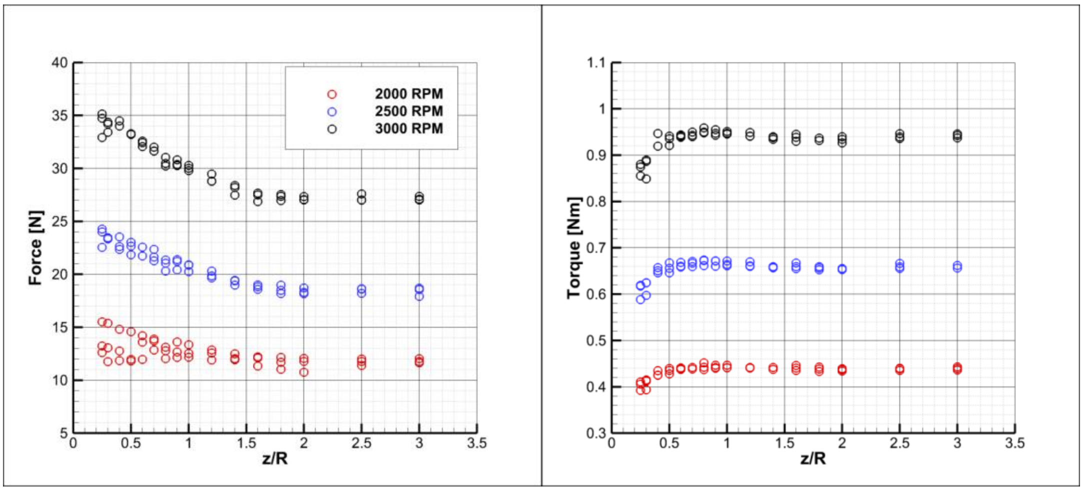

Figure 5.6 .Dimensional thrust and torque values

As seen from Figure 5.6, thrust values converges a steady value between z/R 1.8 and 2. Since power is constant for each RPM, constant torque profile is observed between z/R 0.5 and z/R: 3. Test runs are repeated 3 times. The above figure includes 3 repeats for each RPM.

Another important issue is, the thrust values of 2000 RPM do not represent the desired trend. It is evident when nondimensional thrust values are plotted in Figure 5.7.

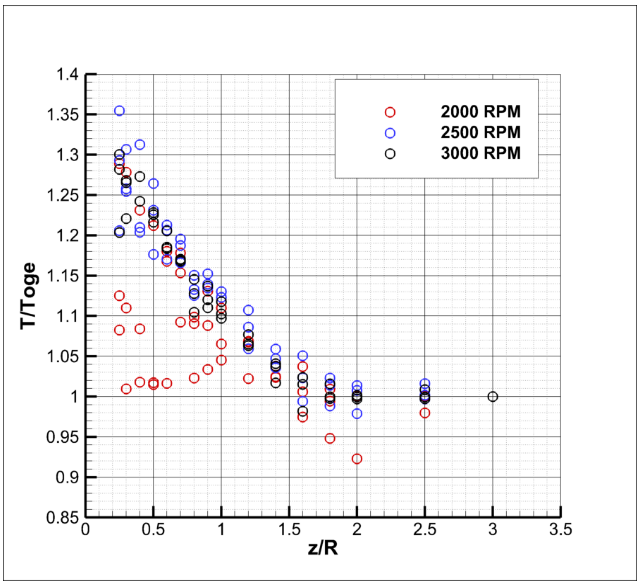

Figure 5.7. In ground effect non – dimensional thrust for 2000 rpm, 2500 rpm and 3000 rpm

It is apparent that, rotor flow does not perform ground effect when rpm has a value of 2000. It is assessed that a rotor with a blade tip Reynolds number below 140K does not create a ground effect. Besides, the standard error percentages of 2000 RPM cases are all have a value higher than 0.3% as defined in Table 5-3:

Table 5-3 Standard error values of 2000 rpm cases

z/R	Test 1	Test 2	Test 3
0.25	0.41	0.48	0.57
0.3	0.43	0.48	0.54
0.4	0.44	0.57	0.58
0.5	0.30	0.63	0.53
0.6	0.46	0.74	0.56
0.7	0.54	0.70	0.55
0.8	0.54	0.83	0.63
0.9	0.41	0.85	0.60
1	0.49	0.79	0.61
1.2	0.53	0.58	0.63
1.4	0.57	0.57	0.60
1.6	0.63	0.56	0.57
1.8	0.50	0.59	0.61
2	0.50	0.59	0.61
2.5	0.43	0.44	0.67
3	0.53	0.59	0.61

As observed from experimental results, dataset with a standard error lower than 0.3% creates the expected thrust trend for ground effect in Figure 5.7. Data points of 2500 rpm and 3000 rpm have standard errors lower than 0.3% which means repeatability deoes not create any alteration in overall trend. However, cases with a standard error higher than 0.3% does not create a relevant trend as seen on 2000 rpm values.

At first glance, high errors may have reasons of outer effects like noise and experimental errors. However, for 3 repeats. still the same high error characteristics are evident. Hence, possible reasons are. 2000 rpm is not adequate for ground effect creation and outer error source effects are dominant when rpm has a value of 2000.

Thus, they are all eliminated and following trends are obtained for thrust and torque as non – dimensional as shown in Figure 5.8.

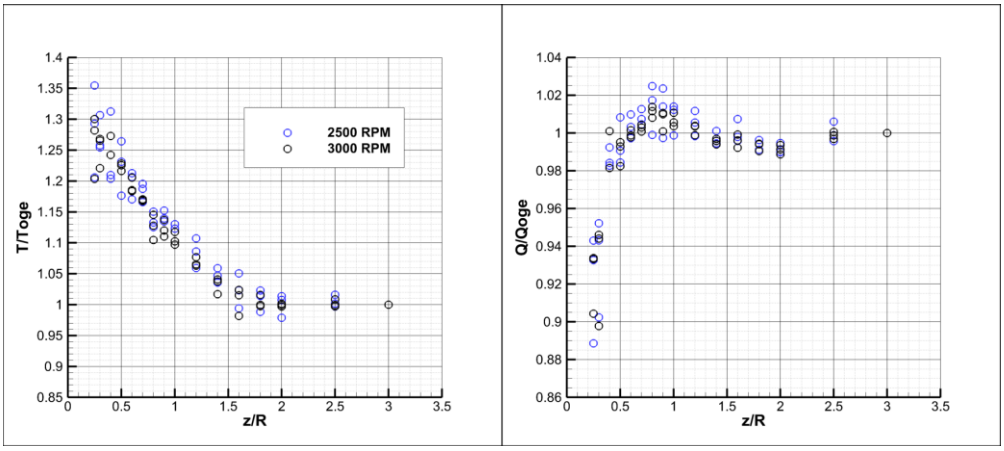

Figure 5.8 In ground effect non- dimensional thrust and torque values for 2500 rpm and 3000 rpm

The key experience is that 2000 RPM is not enough to create a ground effect for the rotor scale used in this work. Due to that reason. experiments are conducted with 2500 and 3000 RPM values.

Soon, non – dimensionalization is done, non dimensional values become independent of RPM. Hence, the values of two RPM sets could be plotted together. The thrust and torque coefficient values are shown in Figure 5.9 for 2500 and 3000 RPM values.

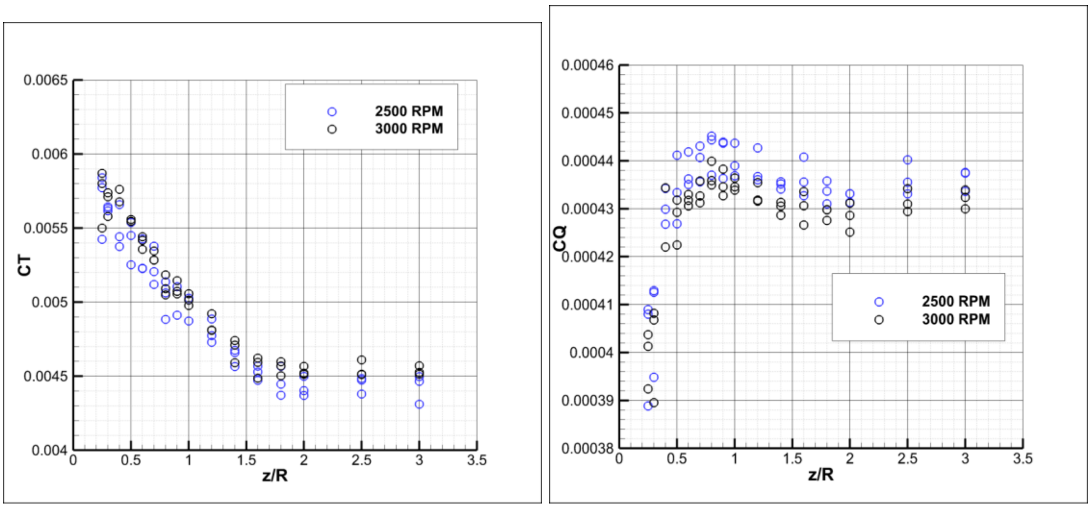

Figure 5.9 Non- dimensional thrust and torque independent of RPM

When Figure 5.9 is inspected, again, the same trends for thrust and torque are obtained as obtained with T/T_{OGE} approach.

5.2.1 Comparison with Literature

The literature data are obtained from the works of Bennett et al.[51] , study of Hayden [52] and flight test measurements retrieved from [1]. The comparison of current study with literature data is shown in Figure 5.10.

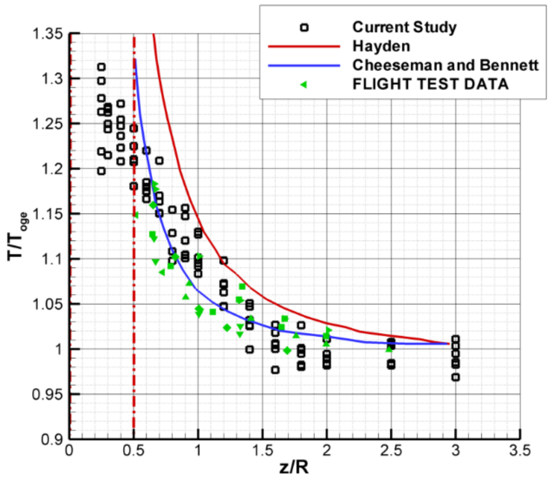

Figure 5.10 Non – dimensional thrust comparison with literature

The results of current study are relevant with literature data. This situation represents the validity of the test setup. In addition, literature includes a ground effect data with a minimum distance of z/R: 0.5. This study includes a ground effect data between the distances of z/R:0.25 and z/R: 0.5. This interval is called as “extreme ground effect” since helicopter ground effect simulations cannot include this zone due to the “fuselage clearance”. As seen from Figure 5.10, general trend is similar and thrust increases with decreasing distance in the “extreme ground effect zone”. However, when z/R is around 0.25, Thrust losses are observed. That condition tells that “actual” ground effect starts for a rotor around z/R 0.3.

Refs. [53] and [1] imply that, ground effect vanishes around z/R: 1.8 – 2. This situation is actually apparent on current study. It could be said that when the distance is z/R: 2 or higher than 1.8, thrust values are assumed to be “Out of Ground Effect” Values.

5.3 Results of Ground Effect with Inclination

The ground effect phenomena is drastically changing when ground inclination is taking the scene. Similar to ground effect without inclination, tests with standard error percent lower than 0.3% are taken. 2000 RPM does not taken into account.

During the inclination, rotor encounters with different ground proximities. as shown in Table 5-4.

Table 5-4 Ground proximity maximum and minimum values for inclined ground effect cases

	β: 5°		β: 10°		β: 15°		β: 20°		β: 25°	
z/R	**z/R_{min}**	**z/R_{max}**	**z/R_{mn}**	**z/R_{mx}**	**z/R_{mn}**	**z/R_{mx}**	**z/R_{mn}**	**z/R_{mx}**	**z/R_{mn}**	**z/R_{mx}**
0.8	0.71	0.89	0.62	0.98	0.53	1.07	0.44	1.16	0.33	1.27
1	0.91	1.09	0.82	1.18	0.73	1.27	0.64	1.36	0.53	1.47
1.2	1.11	1.29	1.02	1.38	0.93	1.47	0.84	1.56	0.73	1.67
1.4	1.31	1.49	1.22	1.58	1.13	1.67	1.04	1.76	0.93	1.87
1.6	1.51	1.69	1.42	1.78	1.33	1.87	1.24	1.96	1.13	2.07
1.8	1.71	1.89	1.62	1.98	1.53	2.07	1.44	2.16	1.33	2.27
2	1.91	2.09	1.82	2.18	1.73	2.27	1.64	2.36	1.53	2.47
2.2	2.11	2.29	2.02	2.38	1.93	2.47	1.84	2.56	1.73	2.67

The values written with red colour are IGE cases. Remaining cases are OGE cases. The minimum and maximum values are calculated by taking Figure 5.1 as a reference.

The inclined ground effect will be investigated with 2 different plotting parameters. First one is, plotting datasets with respect to the z/R, the other one is plotting datasets with respect to the inclination angle β.

5.3.1 Ground Effect Change with respect to the Ground Angle

Figure 5.11 shows the non – dimensional torque and thrust change with respect to the angle with different z/R distances.

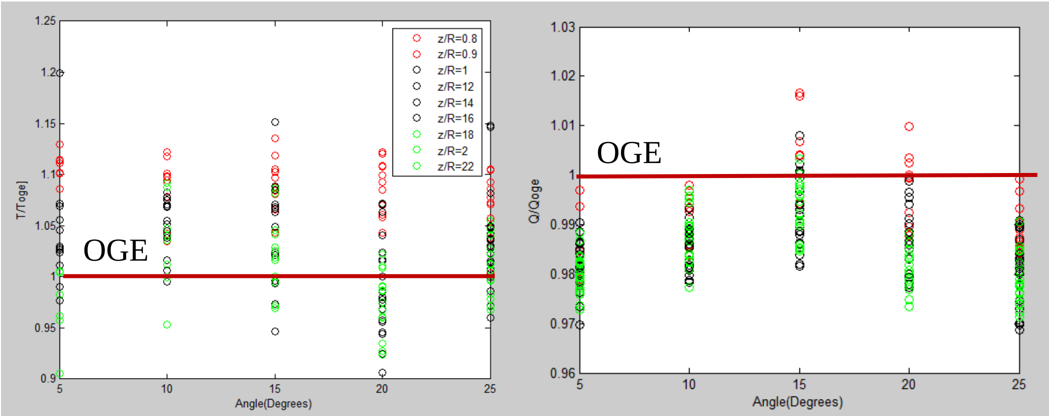

Figure 5.11 Ground effect with respect to the ground inclination angle (β)

Due to the clearance limitations, inclined ground effect cases start with z/R:0.8. The colors designate the following z/R datasets.

- Red: z/R: 0.8 and 0.9
- Black: z/R:1, 1.2, 1.4, 1.6
- Green: z/R:1.8, 2, 2.2 (OGE)

Assigning same colors to the consequent distance values provides a better insight about inclined ground effect issue.

When non dimensional thrust values are inspected, ground effect reduction is apparent when z/R: 1.8 or higher. The green points are dense on the 20° and 25° inclination zones. When z/R is 0.8 or 0.9, ground effect is apparent for all inclination angles.

The important observation about this case is. thrust reduction. During the out of ground effect, T/T_{OGE} value must be 1 or a value in the vicinity of 1. However, T/T_{OGE}: 0.9 is inspected. The possible reasons are:

1) During the inclination, rotor downwash encounters with variable proximity profile. The boundaries of the tip path plane encounter with different z/R values. This condition leads asymmetric inflow distribution. Normally, inflow decreases during the ground effect. But inclined surface may increase inflow on the half of the rotor disk if proximity of one half is out of ground effect

and other half is in ground effect. So, small but apparent thrust reductions may be observable.

2) The asymmetric inflow may cause precise but not accurate thrust values. When figure is inspected, different thrust values are detected for the same inclination angle.
3) In ground effect, the size of the tip vortices in the vicinity of blade tip, reduces. During the inclined ground effect, rotor blades may have variable tip vortice sizes with respect to the ground distance during rotation. The tip vortex change may cause strong alterations on thrust values and inflow profiles.

When torque values are inspected, better and more stable trend is available. The common explanation about torque is maximum torque is obtained when angle is 15° then it suddenly reduces. When z/R is 0.8 or 0.9. higher torque values are available. With increasing proximity, torque decreases but trend is similar as shown in Figure 5.11. However, for ground effect without inclination, torque has a stable trend when z/R > 0.8. The torque reduction defined in Figure 5.12 is almost negligible which stays around 2%. The details of this situation will be explained on following chapter (Computational Results) .

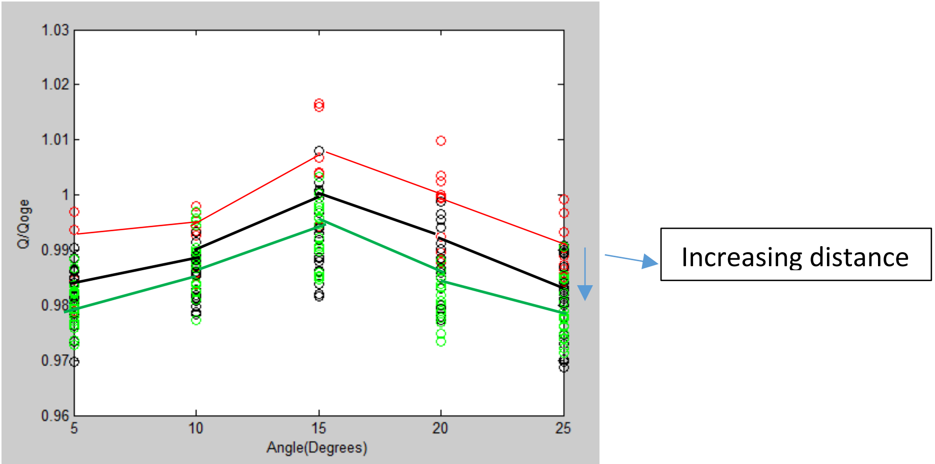

Figure 5.12 Approximate trend curves with respect to the ground inclination angle (β)

5.3.2 Ground Effect Change with respect to the Ground Distance

This part is similar with ground effect with no inclination section. The figures are plotted with respect to the z/R in Figure 5.13 and Figure 5.14.

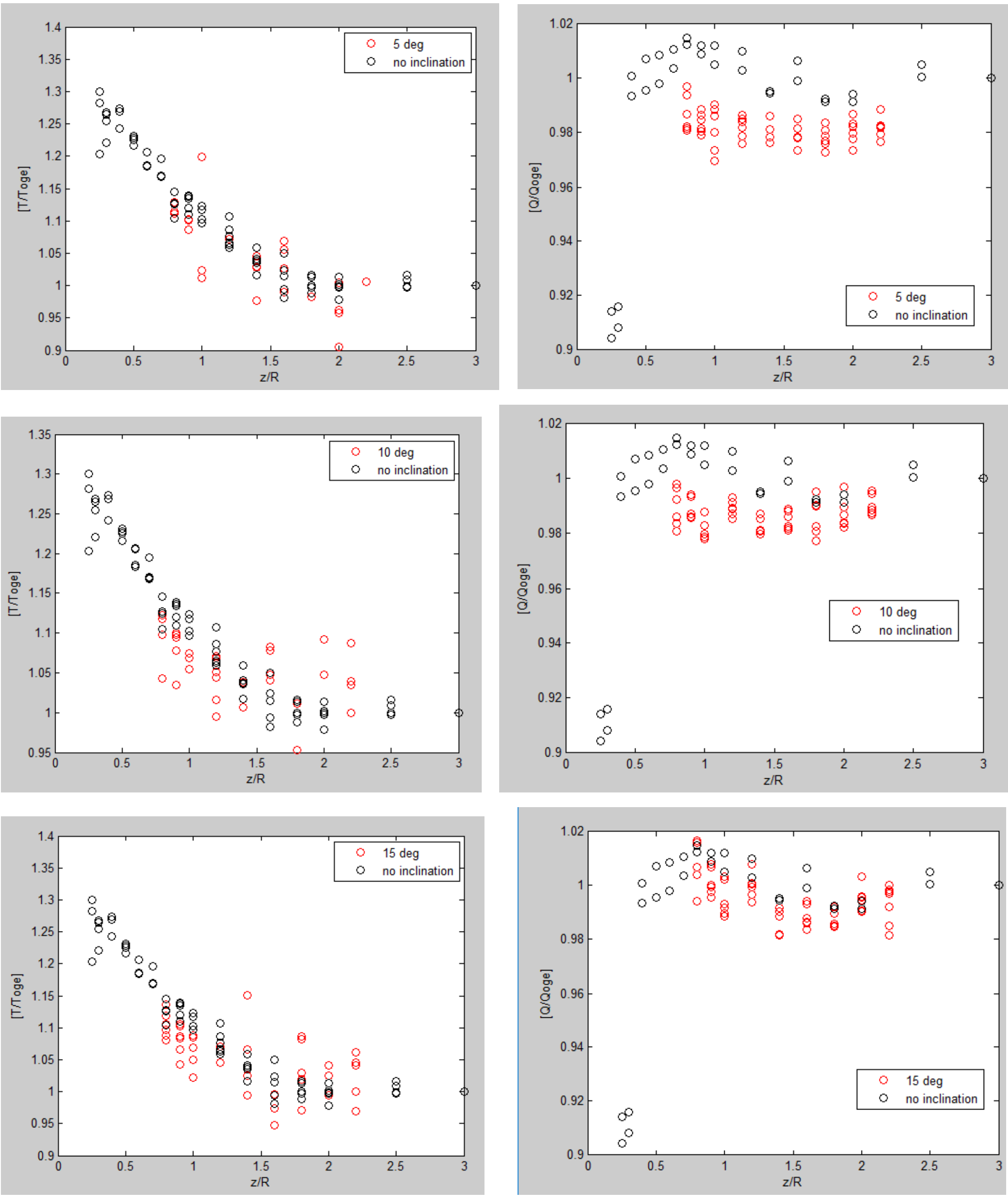

Figure 5.13 Non- dimensional force and torque values for 5°,10° and 15° inclined ground effect and comparison with no inclination

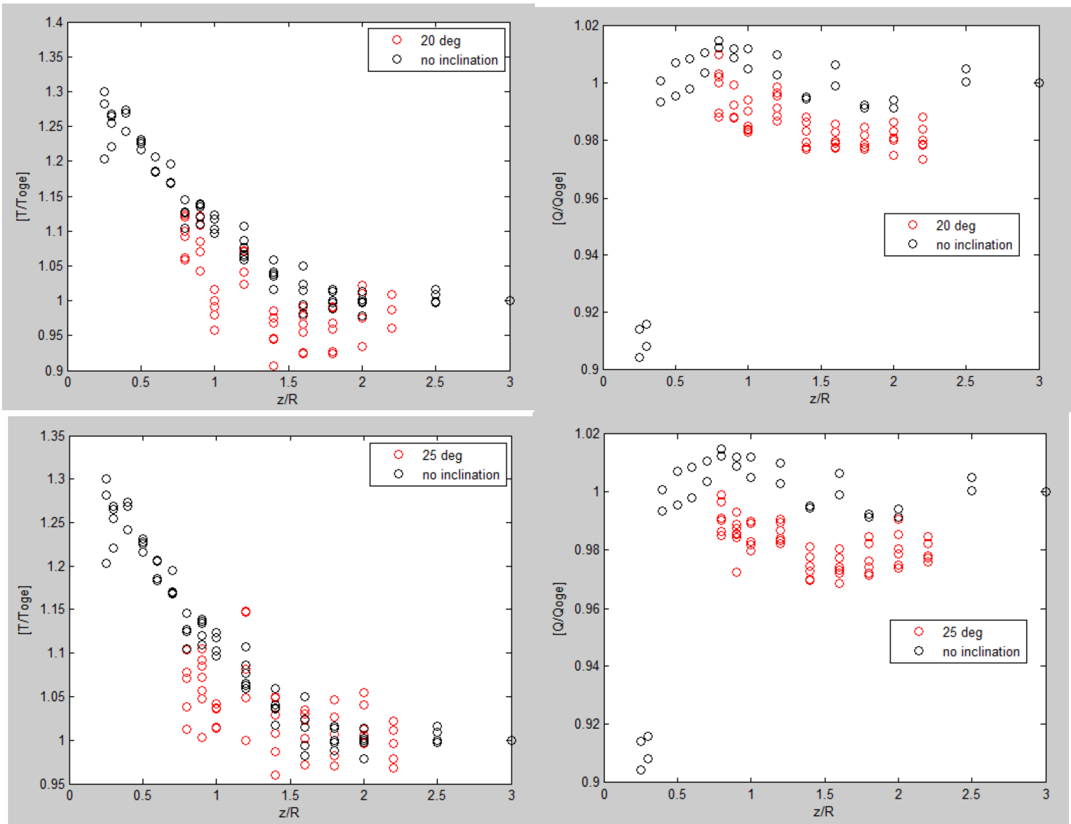

Figure 5.14. Non- dimensional force and torque values for 20° and 25° inclined ground effect and comparison with no inclination.

The outcomes of Figure 5.13 and Figure 5.14 are:

1) Increasing inclination angle reduces the thrust value for the same z/R in ground effect. Hence, thrust is not a determinant for ground effect observation.
2) Increasing angle results in increasing torque trend for the same z/R when angle changes from 5° to 15°. Due to the asymmetric inflow and tip vortex distribution. profile drag increases hence torque increases. However, from 15° inclination to 25° inclinaton, lower torque trend is obtained with respect to the ground effect with no inclination.
3) The "precise but not accurate" results are evident due to the asymmetric inflow characteristics of inclined ground effect.
4) For 20° inclination, abundant thrust loss is observed.

5) In general, thrust and torque have opposite relation. similar to ground effect with no inclination cases. The increasing thrust is the result of the decreasing inflow and increasing angle of attack. Angle of attack increment leads to local drag increment that leads to higher torque values.

5.4 Tuft Monitoring

In order to visualize the flow direction over the ground plate. tuft monitoring is applied. The importance of this modification is monitor the flow during the inclined ground effect cases. especially the close side of the ground plate to the rotor.

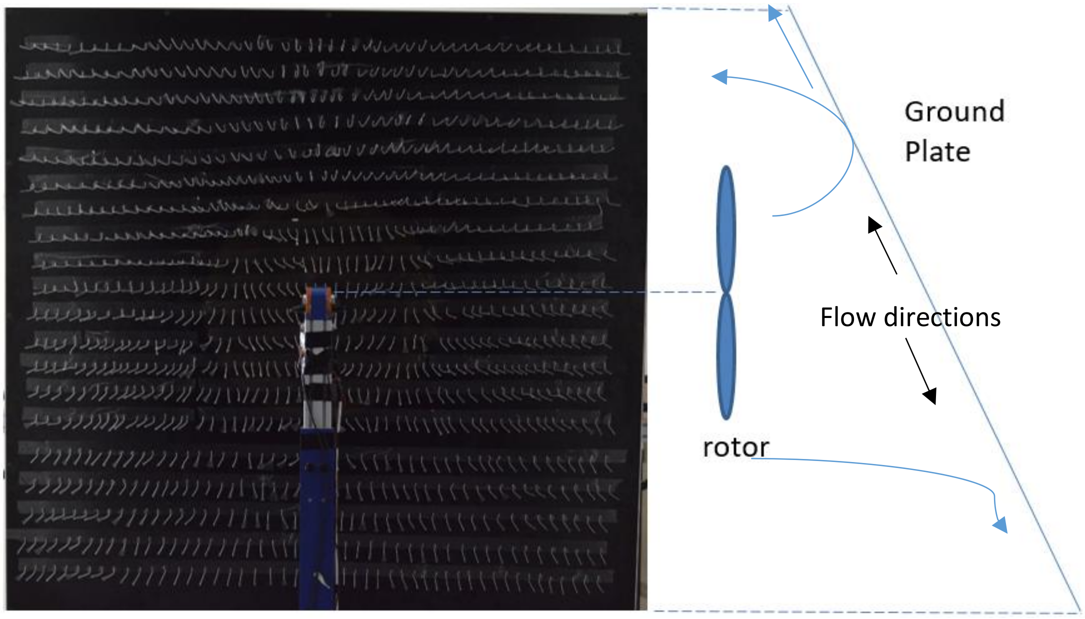

Figure 5.15 Tuft monitoring (z/R =1 , 15° Inclination)

A flow beneath the close side of the rotor could be seen by tuft monitoring as shown in Figure 5.15. Even though ground is tilted. a flow through uphill is available which is a source to create higher ground effect on the close side of the rotor to the ground.

Additional tuft figures are available in Appendix part.

CHAPTER 6

COMPUTATIONAL FLUID DYNAMICS RESULTS AND DISCUSSIONS

The ground effect test setup reveals the thrust and torque change for different ground effect conditions. However, an underlying reason of these performance changes are flow alterations around the rotor. In order to better inspection of flow, ground effect cases are simulated with CFD methods. Basically, CFD analyses could be divided into 3 parts:

- CFD Simulations of OGE case
- CFD Simulations of ground effect with no inclination
- CFD Simulations of ground effect with inclination

For the validity of CFD method, a known experimental case is used as a validation case in CFD community. The test setup used for this thesis is accepted as a validation case for proposed CFD methods at the same time. The study of Bensing et al. [54] is an example for ground effect helicopter rotor CFD application.

6.1 CFD Simulation of Out of Ground Effect Case

The out of ground effect case is simulated for validation and determination of OGE values for non – dimensionalization of thrust and torque values

6.1.1 Simulation Parameters

The simulation parameters are described in Table 6-1.

Table 6-1 CFD solution parameters

# of elements in volume grid [Millions]	10 M
# of elements on surface grid	63K
y+	≤ 1
Turbulence Model	k- ω -SST
RPM	2500
Rotor Radius [m]	0.364
Blade pitch	10°
Boundary layer initial spacing [m]	$2x10^{-6}$
# of layers in boundary layer	40
Boundary layer growth type	Geometric (First 20 step with growth rate of 1.1 . Remaining 20 step with growth rate of 1.2)
Volume Grid Type	Tetrahedral
Surface Grid Type	Quadrilateral

6.1.2 Results

The results tabulated in Table 6-2 could be denoted as a "validation case". The values for Test 1- 3 are obtained from the z/R: 3 case which is almost the out - of - ground effect scenario.

Table 6-2 CFD – experiment comparison (2500 RPM)

	Thrust (N)	Torque (Nm)
Test 1	17.9	0.656
Test 2	18.6	0.662
Test 3	18.7	0.662
CFD	18.2	0.663

As seen from values in Table 6-2, both CFD and experimental results seem relevant. This conditions prove that both CFD procedure and experimental test setup are validated.

6.1.3 Flowfield Analysis

Exact tip vortex caption leads to accurate CFD solution in rotary wing simulations in Figure 6.1.

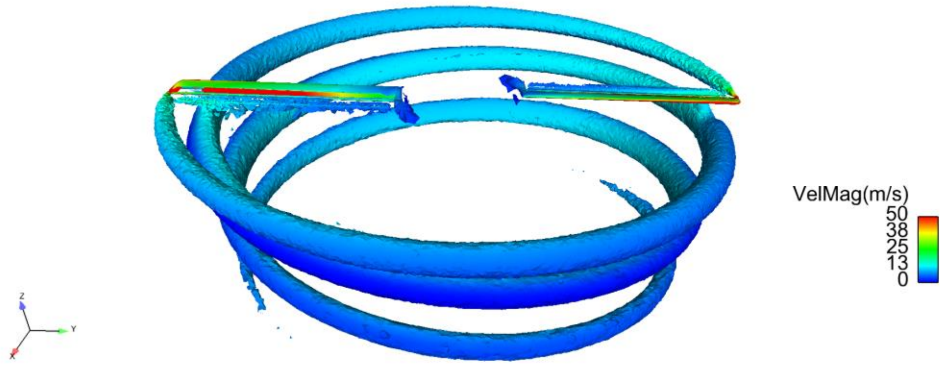

Figure 6.1 The path of tip vortices (Q criterion isosurface)

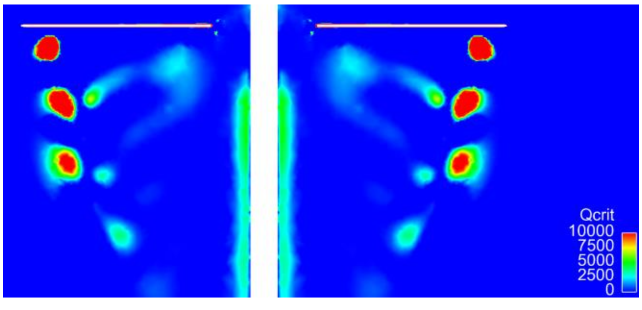

Figure 6.2 Q criterion contours [s^{-2}]

As seen from Figure 6.2, tip vortex is captured up to 270° revolution for steady state case.

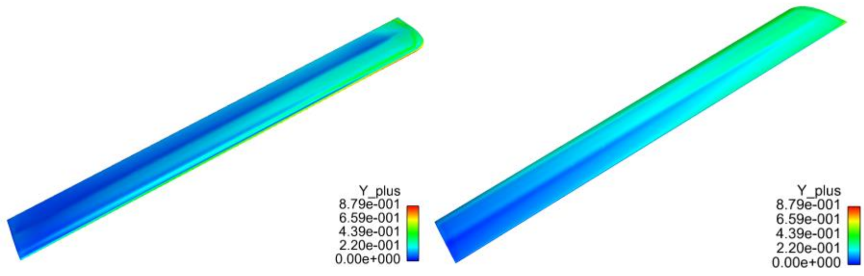

Figure 6.3 y^+ distribution a) Upper surface. b) Lower surface

In Figure 6.3, the y+ distribution on the rotor blade is almost ≤ 1 which clearly shows that the inner parts of the boundary layer is accurately resolved by provided boundary layer clustering and turbulence model. Hence, exact thrust and torque solution could be obtained

6.1.4 Convergence Check

In order to investigate the accuracy of CFD solutions, convergence check is performed.

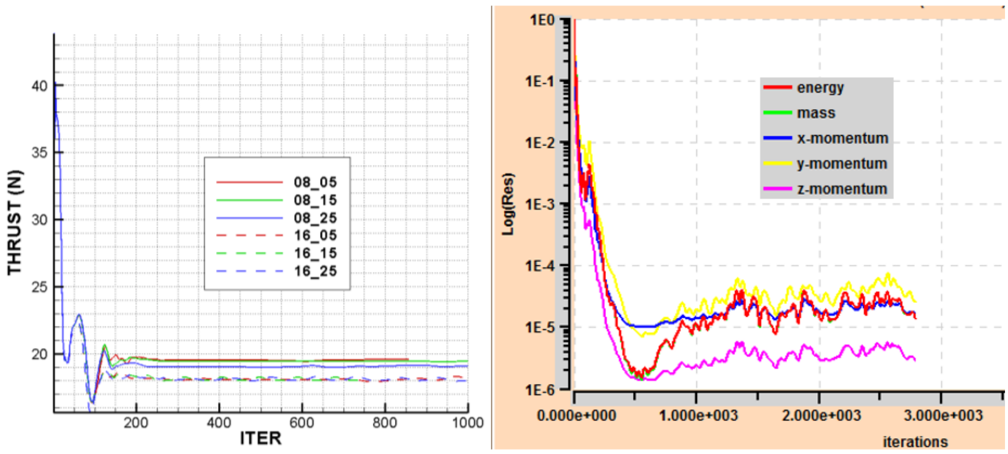

Figure 6.4 a) Convergence rates of the thrust values for inclined cases b) Residuals and their order of magnitudes

As seen in Figure 6.4 a) and b), convergence rates are at satisfactory level. Thrust values converge in 1000 iterations however, most of the cases were run till 3000th step.

The residuals reach 4th or 5th order of magnitude which are apparent indicator for convergence.

6.2 Ground Effect Cases without Inclination

The IGE Simulations are done for all of the z/R values. The parameters are shown in Table 6-3.

Table 6-3 IGE CFD cases

z/R	0.25 0.3:1 (+0.1) 1.2:1.8 (+0.2) 2, 2.5, 3
Volume Grid Sizes (Millions)	11M – 15 M

6.2.1 Results

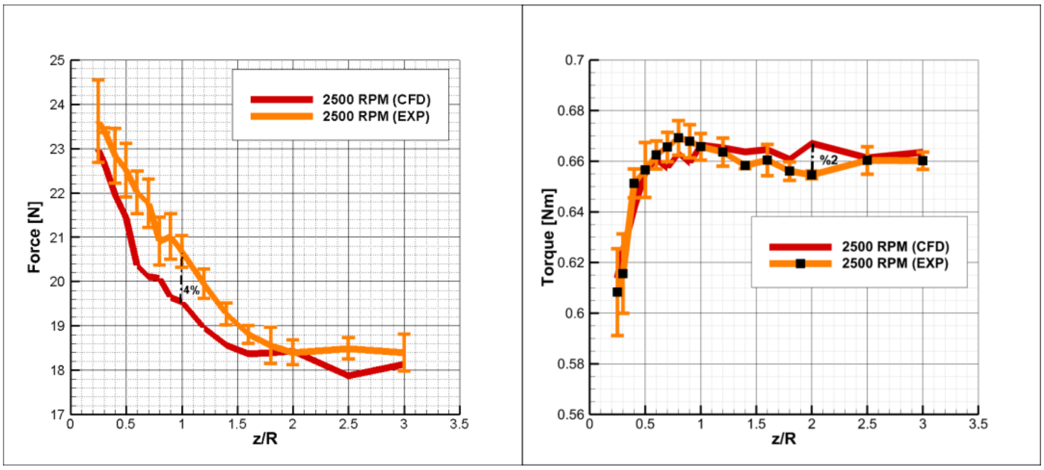

Figure 6.5 Comparison of dimensional torque and force results for 2500 RPM

Figure 6.5 clearly shows the comparison of CFD Results and test results for 2500 RPM runs. The differences between the CFD and experiments are denoted by % (percent) as a deviation from the experimental data. Experimental data is shown with mean and error bars which are calculated by standard deviation for each dataset. The maximum deviation of both thrust and torque are calculated approximately 4% which is a negligible since difference may take lower values around 2% or 1% on whole figure with respect to the error bar bounds. The maximum difference of torque is calculated around 2% when z/R = 0.25 where, modelling the flow simulation is compelling and flow is more complex when compared with other cases. When z/R value is between 0.8 and 3, steady torque trend is inpected. However, when errorbars and differences are investigated, 2% oscillations could be observable and acceptable.

The dimensional thrust values between z/R : 0.5 and z/R : 1 in Figure 6.5, are under estimated. It is an expected condition since rotor is simulated without hub in flow simulations (isolated rotor). Since blockage effect of rotor hub is not modelled which is contributor to thrust, thrust value may be obtained slightly low. This condition is encountered during the similar study of Kutz et al. [55]. Based on this comment. same explanation could be made for the little difference of the CFD and experimental torque values, since the torque formation over the blade is connected to overall thrust formation.

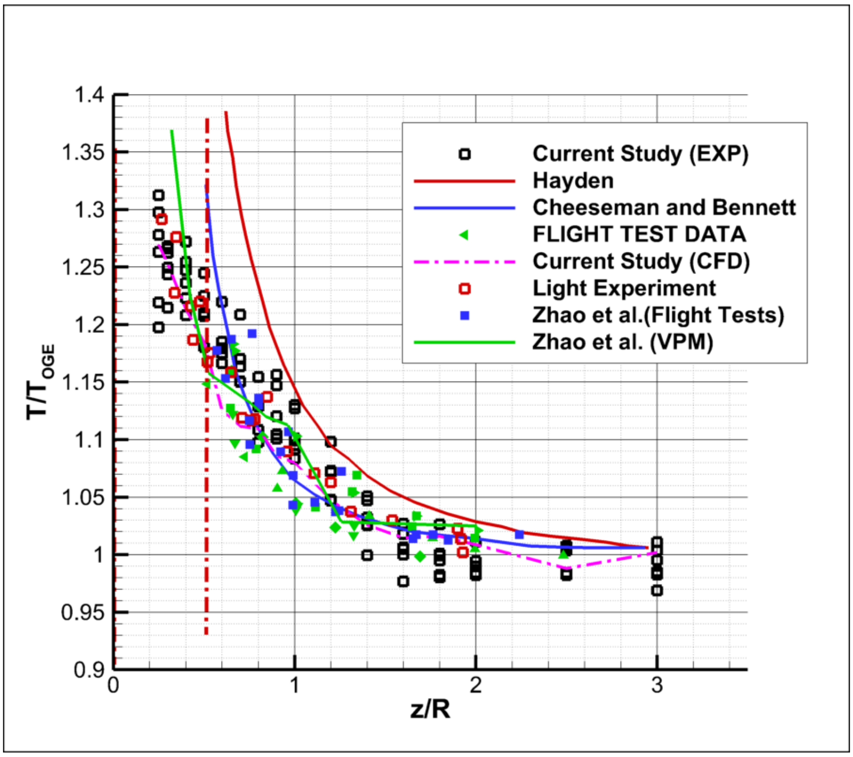

Figure 6.6 CFD result comparison with experiment (Non - dimensional thrust) [59]

In Figure 6.6, solutions are almost compatible with experimental results and literature studies occupied by flight test data, the approximation of Hayden [52] .the calculations of Cheeseman and Bennett [51], data of Zhao et al. [56] and results of Light [12]. This work includes extra information about the extreme ground effect cases where z/R value is between 0.25 and 0.5 which is denoted as “fuselage margin” by Leishman [1] .In Figure 6.6, dataset of 3000 rpm is also available since, non-dimensional values Show the same trend independent of the rpm.

When solutions are compared with literature studies and current study, they are quite compatible, even for extreme ground proximities (z/R: 0.25 – z/R: 0.5). For better comparison, all thrust values are non-dimensionalized with OGE thrust value since literature data are available with that way. It is inspected that between z/R:18 and z/R: 2, ground effect is decreasing and loses its effect over rotor performance which is declared by Leishman [1].

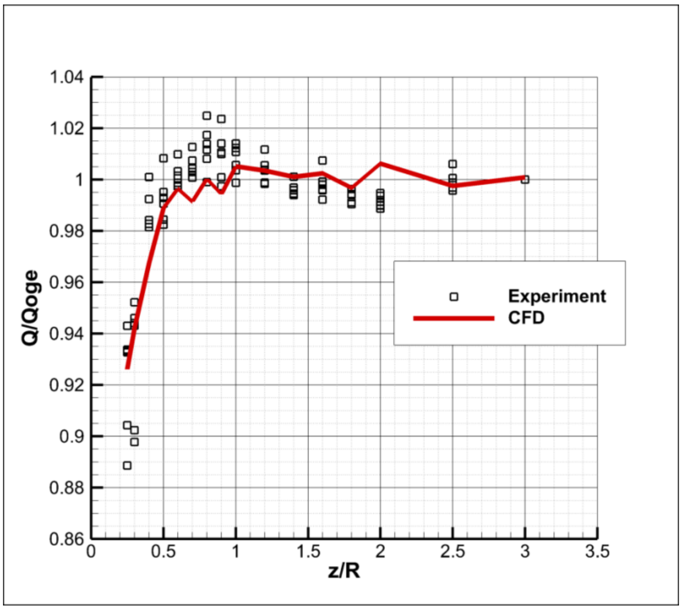

Figure 6.7 Non – dimensional torque comparison between the experiment and CFD

The overall torque relation is plotted in Figure 6.7. The non - dimensional experimental values contains both values for 2500 RPM and 3000 RPM. Normally, due to the constant RPM, torque is expected as constant. It could be accepted as correct when z/R :0.5 and higher. The total torque oscillates with $\pm$ %1 difference at that z/R interval which could be accepted as "constant power". However, when z/R < 0.5. even same power is supplied by power supply, the overall torque of the rotor decreases hence, overall power decreases as if constant thrust / decreasing power condition of ground effect is emerging. The outcome is, power could decrease when extreme ground effect occurs (z/R< 0.5)

6.2.2 Inflow

The inflow parameter variation on the rotor disk is calculated by division of inflow velocity to the tip speed. The inflow is dependent to the x and y coordinates for CFD simulations as shown in eqn 6.1.

$$\lambda_i(x.y) = \frac{v_i(x.y)}{\Omega R} \qquad (6.1)$$

The inflow parameter is integrated over the circular surface grid section which is defined close to the tip path plane (TPP) and above the rotor disk in order to obtain accurate inflow velocity distribution.

$$Mean\ Inflow : \frac{1}{A}\int \lambda_i(x.y)\,dA \tag{6.2}$$

A is, simply the disk area.

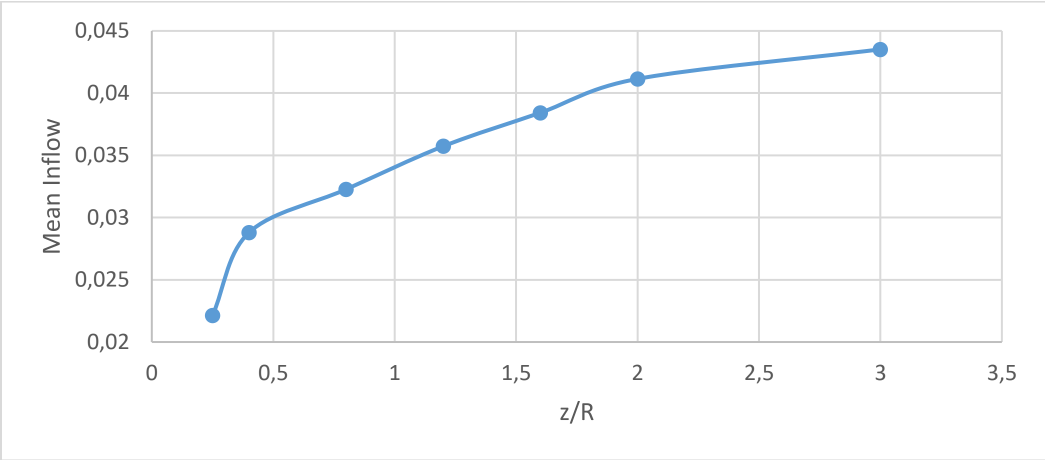

Figure 6.8 Inflow variation with increasing ground distance

Figure 6.8 clearly shows the inflow reduction with increasing ground proximity. When thrust data are inspected, ground effect ineffectivity is apparent. However, when inflow is inspected, small amount of ground effect could be is still observable since total inflow increases when ground proximity changes from z/R: 2 to z/R: 3. The contour plots of inflow distribution λ is shown in Figure 6.9 with half rotor:

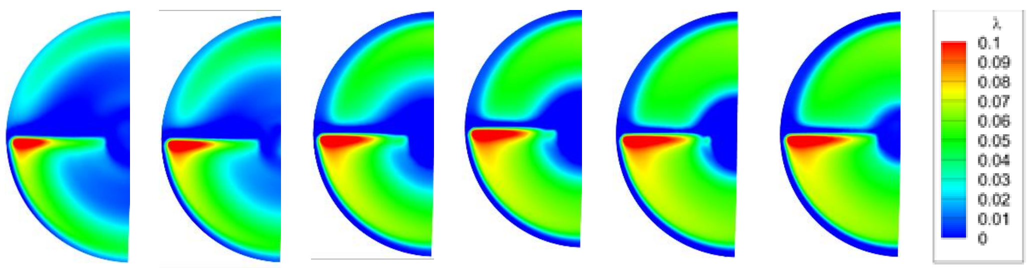

z/R 0.25 0.4 0.8 1.2 1.6 3

Figure 6.9 Inflow distribution for various ground proximities

The rotor power has two main components: Induced component and profile component as defined by eqn 6.3.

$$C_Q = C_P = C_{P_i} + C_{P_p} \tag{6.3}$$

Profile power is the power that rotor blade consumpts against incoming air drag. Induced power is the consumpted power to create inflow. The power is defined as a power coefficient which is the same with torque coefficient C_Q .In fact, rotor power has auxillary contribution called a "Ancillary power" which includes the effect of external elements like rotor hub and rotor mast. However, rotor is simulated as "isolated". Hence this portion is not available for CFD. The subscript of Power P could be replaced with torque Q. Hence, profile power coefficient will be denoted with "profile torque coefficient". Induced power coefficient could be denoted as "induced torque coefficient". As reference [1] states that, Induced power coefficient CQ_i will be simplified as defined in equation 6.4.

$$C_{Q_i} = \kappa \, \lambda \, C_T \tag{6.4}$$

The κ is the correction factor taken as 1.15 [1]. This relation is derived from the Blade Element Method [1]. Since inflow and thrust coefficient data are given in Figure 6.6 and Figure 6.8, induced power coefficient could be shown in Figure 6.10.

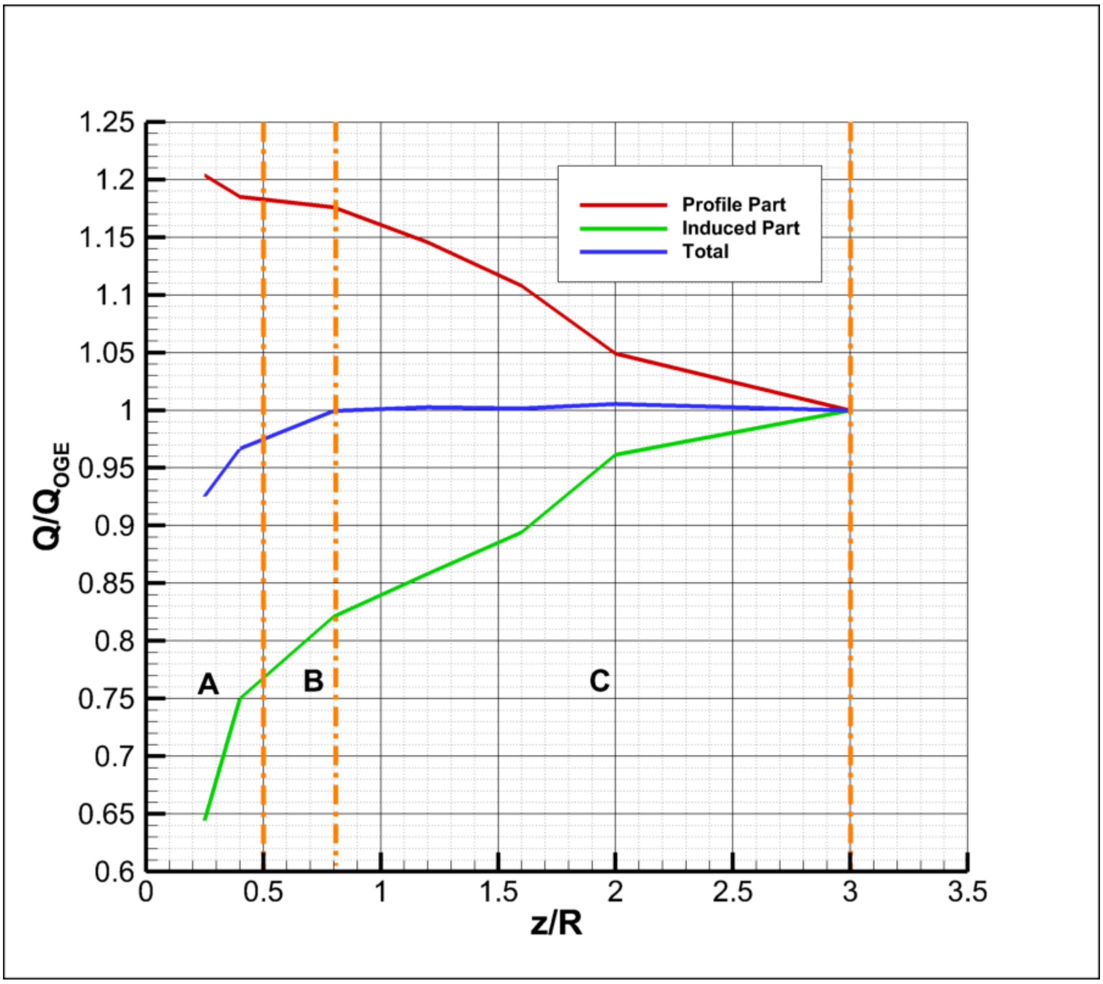

Figure 6.10 Power contributions in ground effect for constant thrust

In Figure 6.10, total power. induced power and profile power contributions are available in non - dimensional format. The total power has a stable profile when z/R > 0.8. Induced power has the same relation with inflow change as expected. The profile power, on the contrary, decreases in the region C between z/R: 0.8 and z/R:3. In the extreme ground effect zone (region A) which is the region between z/R: 0.25 and z/R:0.5. induced contribution is dominant whereas when z/R is higher than 0.5, power contributions begin to balance each other in order to keep total power constant for the same rpm input.

Table 6-4 Power coefficient contributions as a percentage of total power coefficient in ground effect

z/R	$C_{Q_i}\%$	$C_{Q_p}\%$
0.25	34.66	65.34
0.4	41.25	58.75
0.8	40.89	59.11
1.2	42.60	57.40
1.6	44.43	55.57
2	47.59	52.41
3	49.77	50.23

Table 6-4 reveals that, profile drag is dominant in extreme ground effect. The term "dominance" must not to be mixed with the "contribution".To illustrate, when z/R: 0.25, profile power contribution is higher than induced contributor. However. when overall power curve is investigated, the extreme induced power loss is dominant on total power curve when total power of the z/R:0.25 is lower than the any other power values.

For ground effect studies in literature, induced power term is often used since the nature of ground effect flow arises from the inflow change. However, the profile power change must also be considered. The induced power is affiliated with the pulled and released flow with rotor. In ground effect, released flow leads a reduction in inflow. In addition. The recirculating flow from ground to the blades create extra drag on rotor blades, especially in extreme ground effect cases. With increasing distance, drag contribution decreases due to the decrease of the recirculating flow. Even for out of ground effect case (z/R:0.3) the profile power contribution is half of the total power. However, induced power starts to be half of the total power with increasing ground distance where rotor is out of ground effect and in hover condition as stated in reference [52] .

The profile contribution of rotor power is also strongly dependent with blade airfoil, #of blades and rotational velocity in hover flight. In ground effect with the same power input, inflow decreases however, angle of attack increases since blade pitch is constant. The increasing angle of attack creates the thrust increase in ground effect. However. this angle of attack increase leads to higher drag force hence, higher profile power, as well. The profile power increase in Figure 6.10 is the proof for drag increase since profile power is directly proportional with drag. In order to increase the efficiency of rotor blade, drag characteristics of blade airfoil must handle the complex flow environment in ground effect.

Figure 6.11 shows the non dimensional induced torque coefficients. The non-dimensionalization is done by dividing the each torque coefficient value to the OGE induced torque coefficient value. In Figure 6.11, CFD data is compatible with literature data.

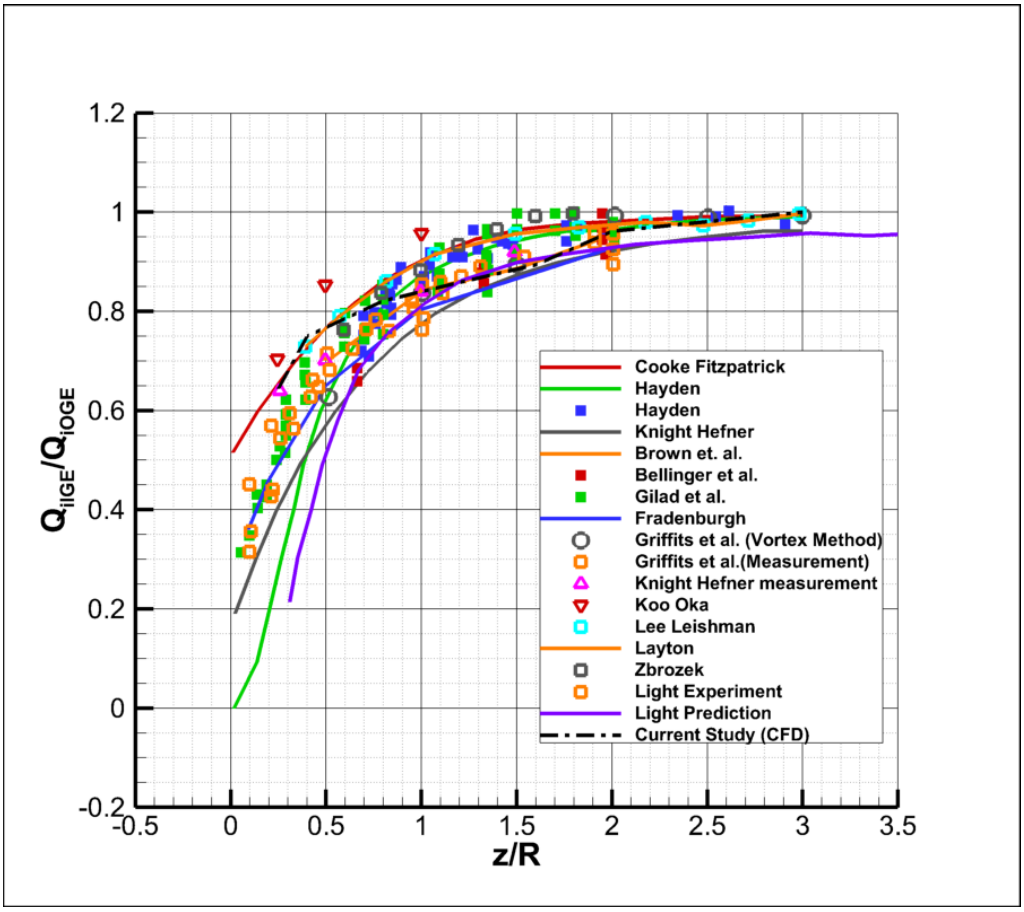

Figure 6.11 Non- dimensional induced torque change with respect to the ground proximity

In Figure 6.11, the induced power ratios tetrieved from Brown et al. [60], Hayden [61]. Griffits et al. [62] and other works retrieved from Leishman [1], shows good corellation with CFD data.

6.2.3 Tip Vortices

Figure 6.12 shows that the tip vortices are captured in the defined wake region which is an indicator for the rotor CFD solution accuracy.

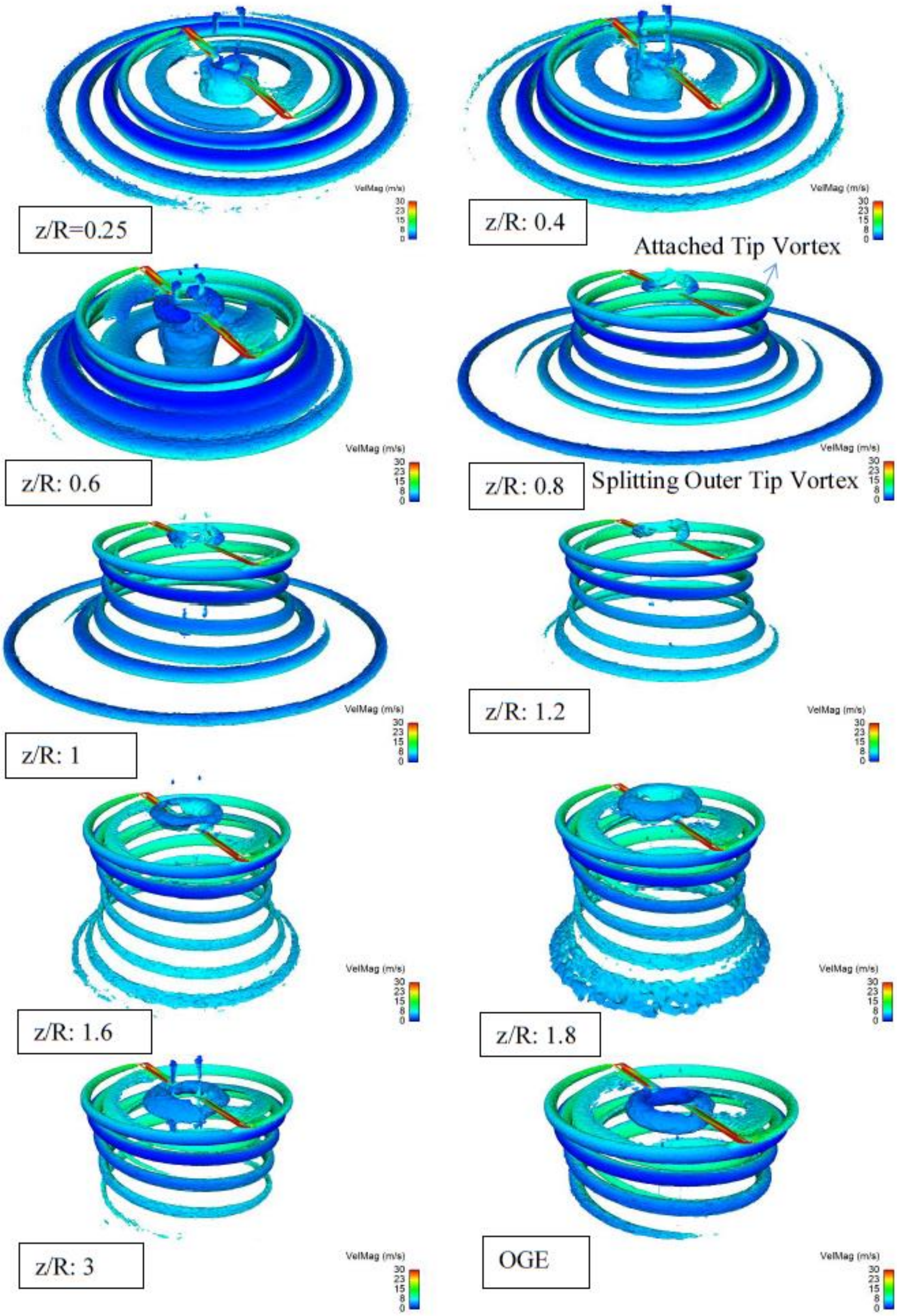

Figure 6.12 Q criterion iso surfaces coloured with velocity magnitude. Q=2000 s^{-2}

Tip vortex trajectories change with changing ground proximities. It is definite that, tip vortex refinement in volume grid has a great role on tip vortex visualization in all cases as stated in [52].

As vortex path structures are investigated, a splitting outer tip vortex ring is observed during z/R: 0.8 and z/R: 1. After z/R: 1.2, no splitting vortex ring is observed since these vortices are quite weak compared to the attached vortices. If Q criterion value reduces below 2000 s^{-2}. weak vortices will be visible for the higher z/R cases. From z/R: 1.2 to z/R: 1.6. attached helical vortex path is quite observable. After z/R:1.8, the effect of ground started to vanish which could be understood from quite weak lowermost vortices.

It is clear that, in ground effect, a vortex path is not contracted. On the contrary, it expands by trigger of reduced inflow [1]. This expansion is started to reduce when z/R is 1.8 and higher which is another clue that, groud effect is started to demise after a certain proximity ratio. Approximately, after z/R: 2, no ground effect is observable as defined by Leishman [1]. It is the first validated point of both test setup and CFD Method.

Figure 6.13 and Figure 6.14 show the radial and axial locations of the blade tip vortices for different ground proximities.

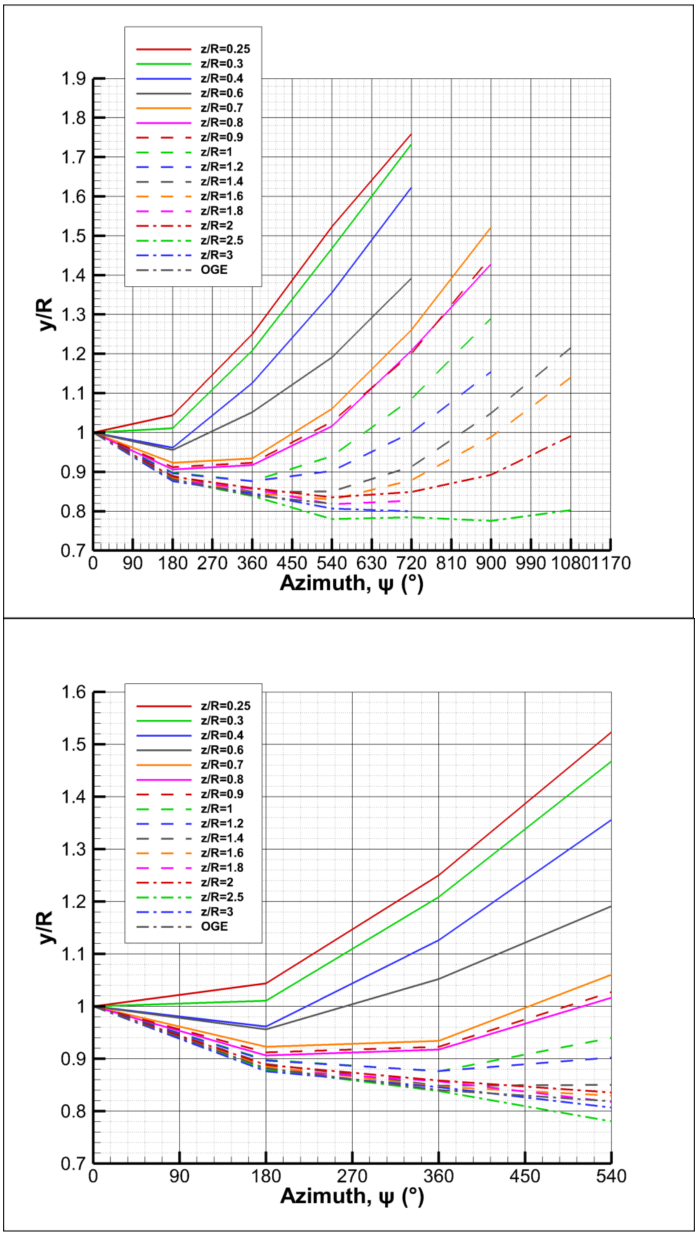

Figure 6.13 Radial location of blade tip vortices for each ground proximity value

In Figure 6.13, with increasing proximity (decreasing z/R value) , the expansion of rotor downwash is evident. Maximum, 0.75R expansion is observed when z/R: 0.25. This expansion decreases till ground proximity decreases hence, during the out of ground effect, rotor downwash becomes contracted. The vortex age is detected till 540° azimuth angle. For some cases. vortex ages up to 1080° azimuth are available. With this wide range of plot, the possible locations of uncaptured vortices could be estimated for azimuth values higher than 540°, in ground effect.

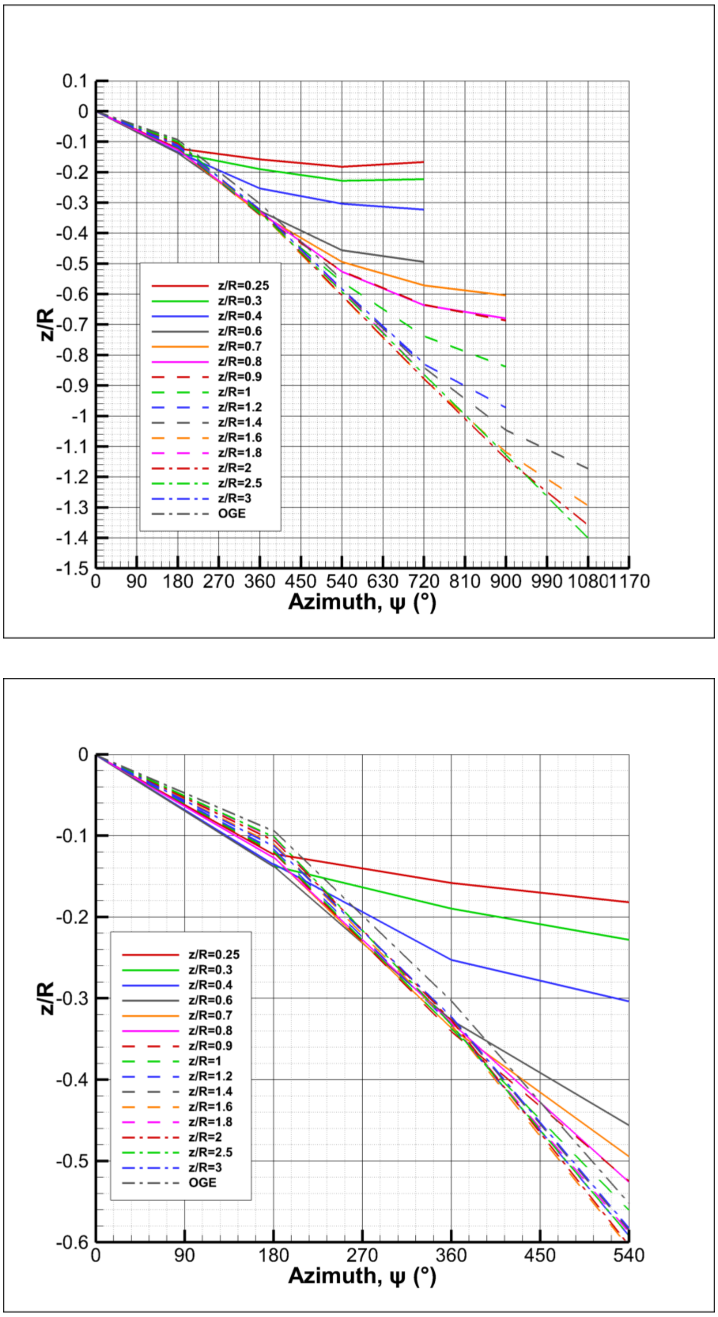

Figure 6.14 Axial location of blade tip vortices for each ground proximity value

Figure 6.14 shows the axial locations of the blade tip vortices for each ground proximity value with changing azimuth. For low z/R values. axial location reaches a steady value due to the ground presence. When z/R increases, the axial location increases beneath the rotor tip path plane and reaches a constant trend after z/R: 2.

which shows the demise of the ground effect after this proximity value. Figure 6.13 and Figure 6.14 are valid for 10° blade collective angle only.

6.3 Ground Effect Cases with Inclined Ground

The solution parameters are shown in Table 6-5:

Table 6-5 Solution parameters

z/R	0.8, 1.2, 1.6, 2
Inclination Angle (β)	5° ,15°,25°
Volume Grid Sizes	20 Millions – 30 Millions

6.3.1 Results

Results are classified with selection of non - dimensional distance (z/R) or inclination angle (β) as independent variable similar to the application in section 5.

6.3.1.1 The Change of Inclination Angle (β)

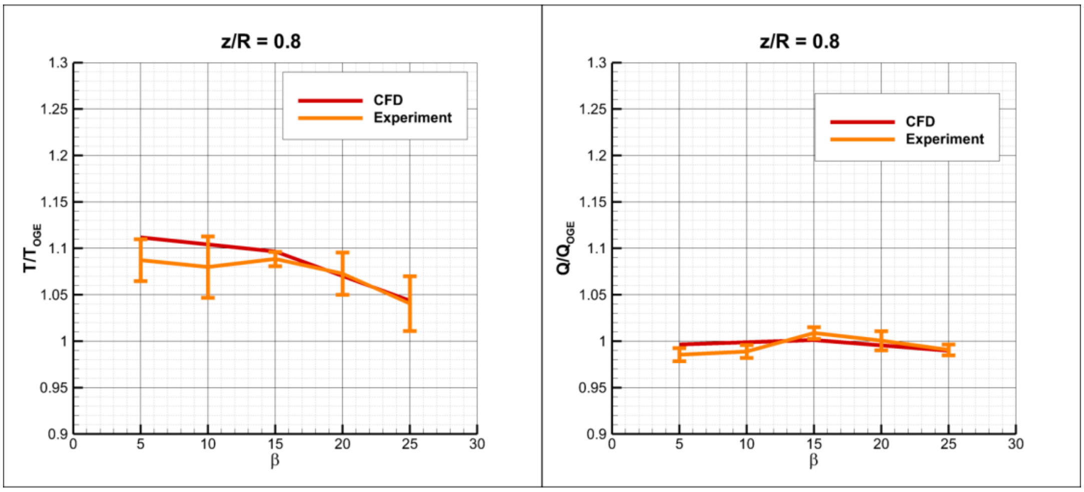

Figure 6.15 Non – dimensional thrust and torque values for z/R: 0.8

In Figure 6.15, at first glance, results are strongly dispersed. However, for non - dimensional thrust, values are located in the errorbar bounds of experimental results. The dispersion is at most 2% for thrust case. For torque values, %1.5 acceptable difference is observed. As explained in previous section, at most 2% oscillation is acceptable for steady torque trend. Torque is almost oscillating around the Q/Q_{OGE} :1 value which is expected since with constant RPM, constant power is supplied into system

Thrust reduction with increasing angle (β) is apparent. This reduction is only 6% approximately.

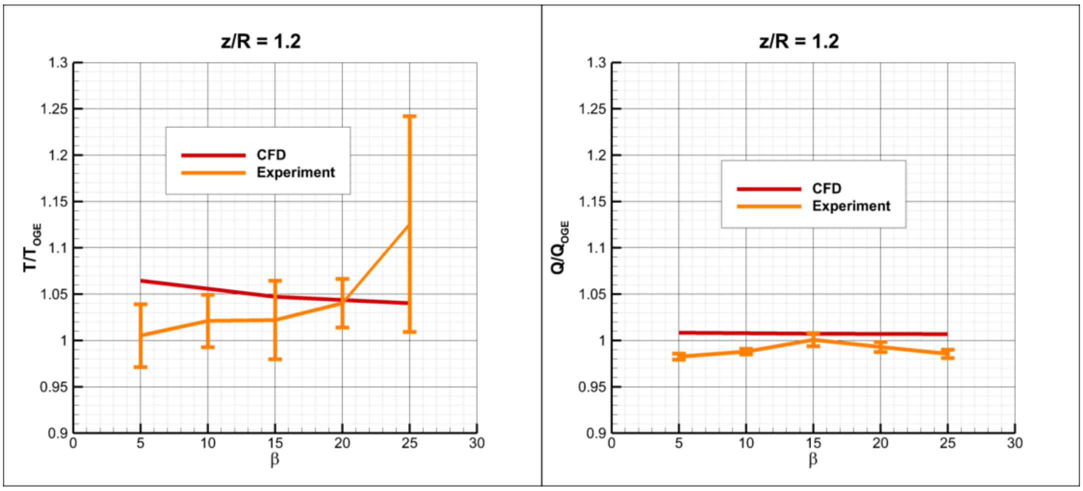

Figure 6.16 Non – dimensional thrust and torque values for z/R: 1.2

In Figure 6.16, for z/R:1.2, especially for cases of 15° and 20°, consistency could be seen. However, for thrust value of 5° inclination, %2-%3 dispersion is apparent. For 15° torque value, accuracy is achieved. For the thrust value of 25°, almost %7 difference attracts the attention. However, as described in previous section, CFD simulations are conducted without hub and any other external part. The existence of these parts could increase the thrust values. This shifting is %4 increment in ground effect without inclination. If complex and asymmetric nature of the downwash of inclined ground effect is considered, thrust/torque increment value higher than 4% is expected condition. Torque has maximum difference of 2.2% which could be acceptable for steady torque trend.

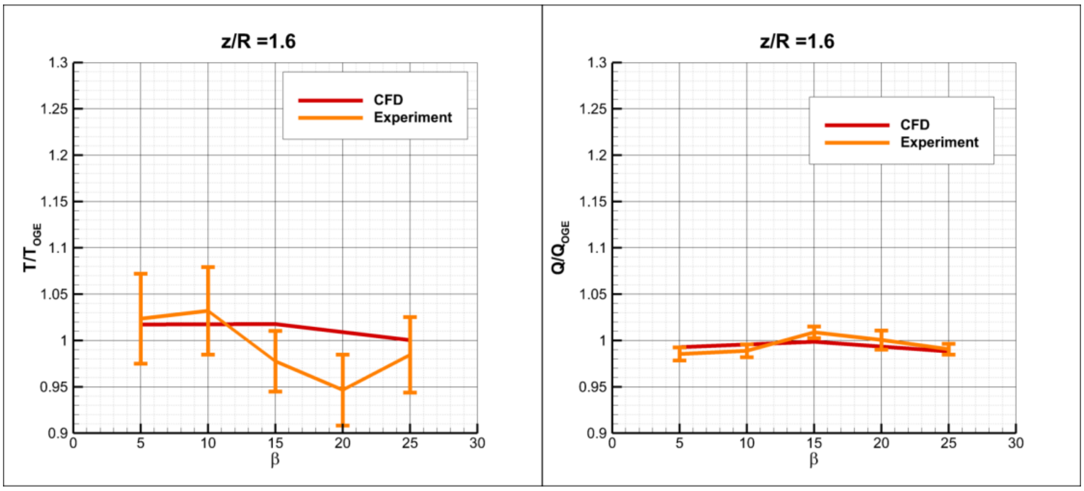

Figure 6.17 Non – dimensional thrust and torque values for z/R: 1.6

In Figure 6.17, thrust values are lying in the range defined by error bars and trends are similar. Decreasing thrust profile is observed. For torque values, the trends are similar but CFD overestimates the solutions with %1.5 difference which is acceptable.

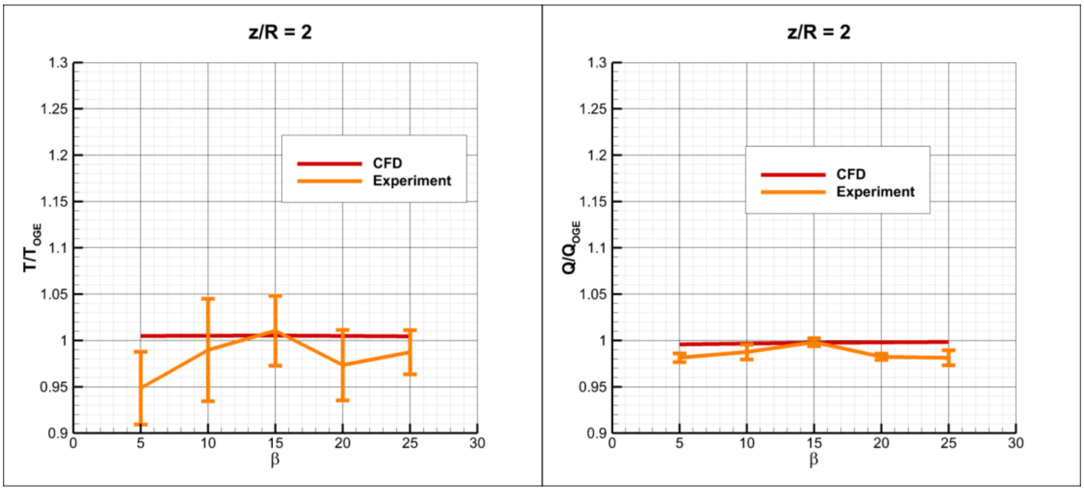

Figure 6.18 Non – dimensional thrust and torque values for z/R: 2

In Figure 6.18, normally, z/R 0.2 is a distance that ground effect vanishes. Even in inclined cases, out- of- ground- effect characteristics are dominant. Experimental data does not shape any trend curve but thrust results located in the region defined with errorbars. Torque results have a difference lower than 2% which is acceptable.

6.3.1.2 The Change of Non – Dimensional Distance (z/R)

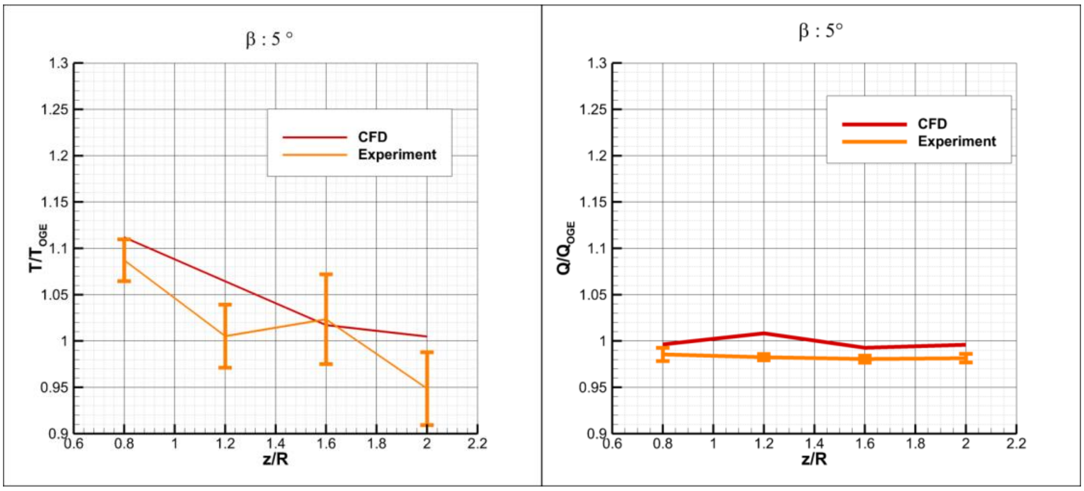

Figure 6.19 Non – dimensional thrust and torque values for β = 5

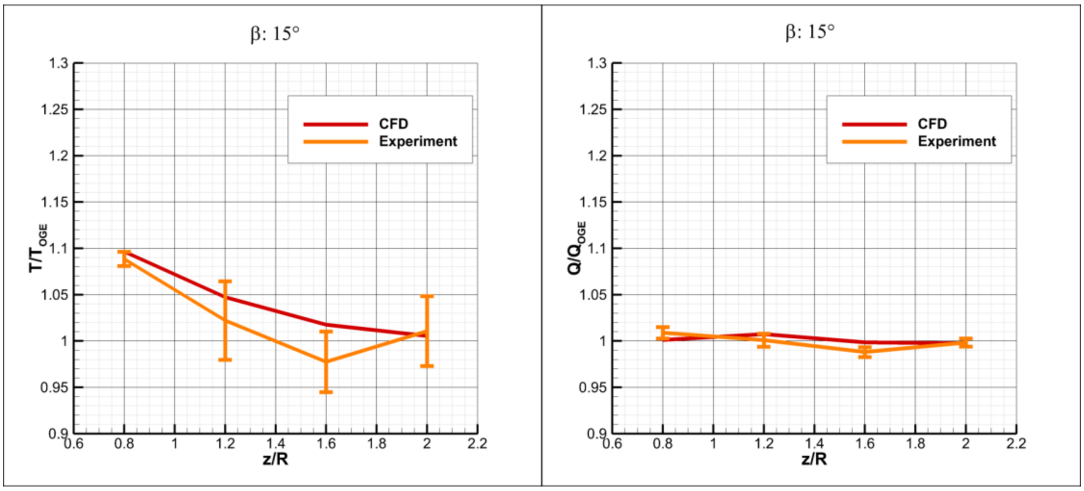

Figure 6.20 Non – dimensional thrust and torque values for β = 15

In Figure 6.19 and in Figure 6.20, acceptable accuracy and trend similarity is observed for thrust values with increasing proximity. For torque values, 2% difference is detected which is acceptable. The torque trends are almost similar. However, overestimation of the torque value of z/R: 1.2 is apparent. However, it stays in the 2% range which could be denoted as acceptable.

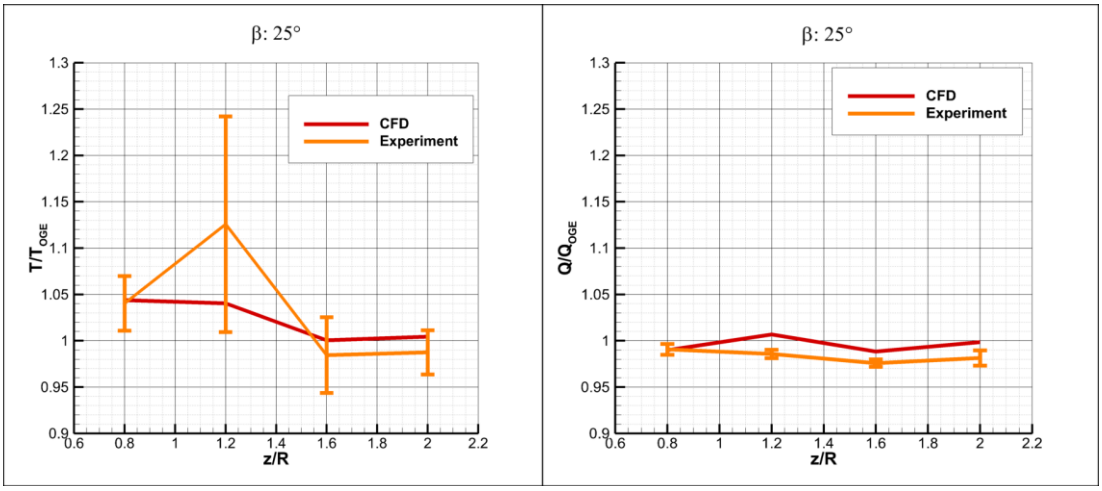

Figure 6.21 Non – dimensional thrust and torque values for β = 25

In Figure 6.21. thrust accuracy and trend are almost satisfying. The data dispersion of z/R: 1.2 on thrust curve shows that, possible experimental errors arise, since this data seperation is not observed for the other proximities.

For this reason, The dataset seperations figured in section 6.3.1.2. may have the same experimental error problem, since variety of experimental error sources are available in experimental facility. Although test setup is sensitive to the outer effects, still, most of the results are acceptable.

Test setup shows almost satisfactory corellations with CFD results for ground effect cases without inclination. Little accuracy reduction is inspected during inclination. The possible reason is, combination of experimental errors eith the complex nature of rotor downwash during ground inclination.

Table 6-6 Thrust increment from z/R: 1.6 to z/R: 0.8 relative to OGE with respect to the inclination

β	(%)
0	12
5	10
15	7.5
25	5

As seen from Table 6-6, increasing inclination leads reduction in thrust increment with respect to the OGE which accurately shows ground effect reduction with increasing inclination angle. However, even for 25° inclination, thrust is still higher than the OGE value which is the clear prrof that ground effect still exist.

6.3.2 Flowfield Analysis

Figure 6.22 shows the flowfield and velocity magnitudes for z/R: 0.8 with changing inclination angle

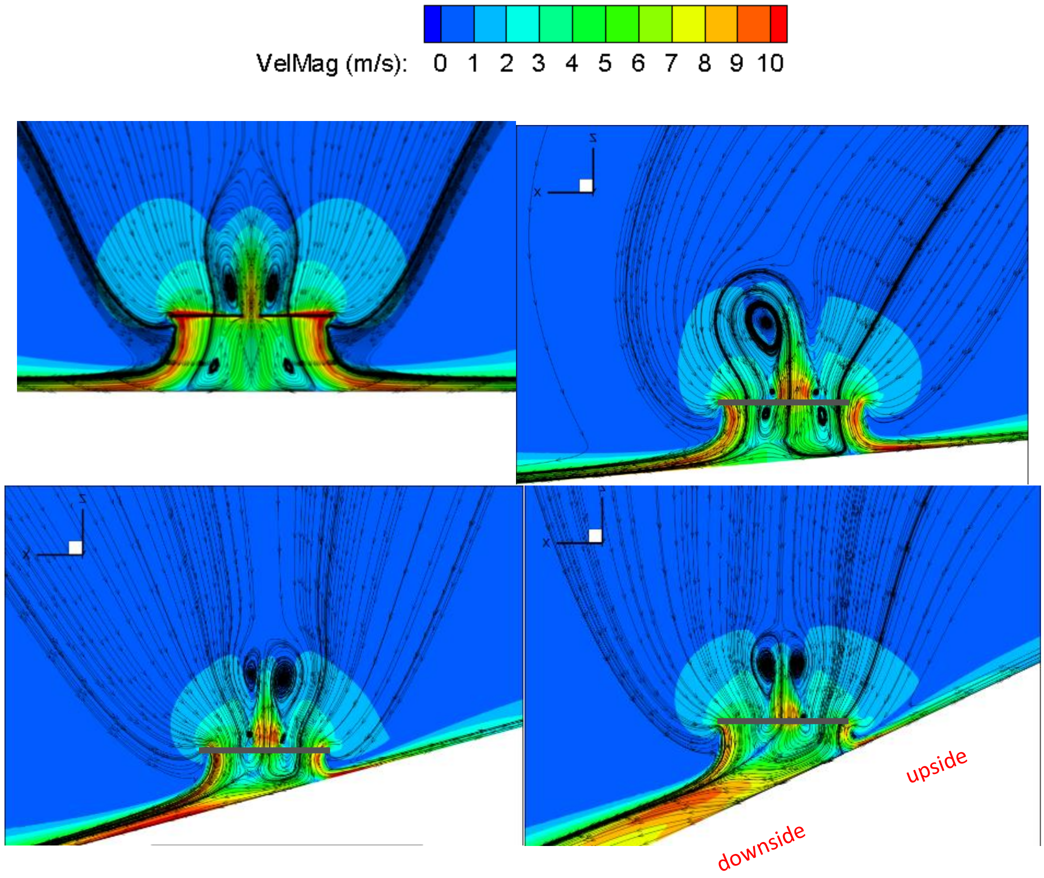

Figure 6.22 Velocity magnitude and streamlines for z/R: 0.8 and β: 0°, 5° ,15°, 25°

Figure 6.23 shows the flowfield and velocity magnitudes for z/R: 1.2 with changing inclination angle

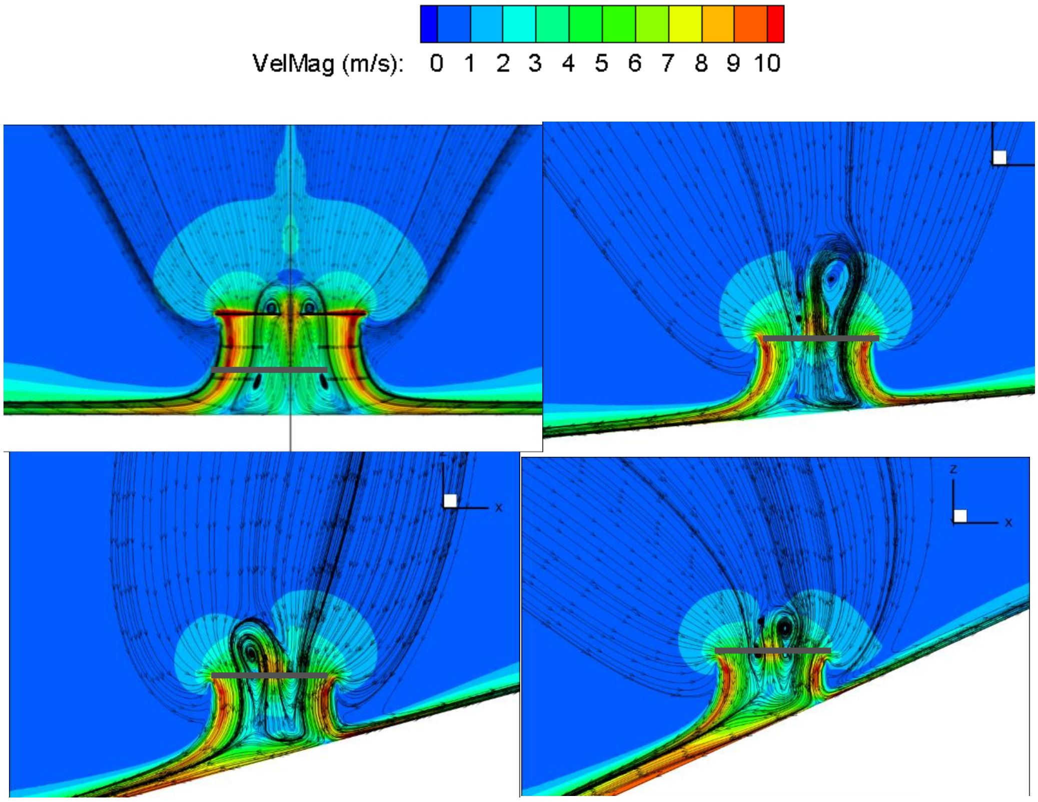

Figure 6.23 Velocity magnitude and streamlines for z/R: 1.2 and β: 0°, 5° ,15°, 25°

The ground inclination generates further complications on rotor downwash, in Figure 6.22 and in Figure 6.23. The strong upper vortex is seen on cases z/R: 0.8 and z/R: 1.2. Increasing inclination angle reduces the flow circulations in the downwash which is the reason for the ground effect reduction with inclined ground. The upper strong vortex is seen when inclination is 5°. When β increases, the upper vortex divided into two smaller parts. The reduction in flow recirculation at the closer part of the ground may lead this division.

Figure 6.24 shows the flowfield and velocity magnitudes for z/R: 1.6 with changing inclination angle.

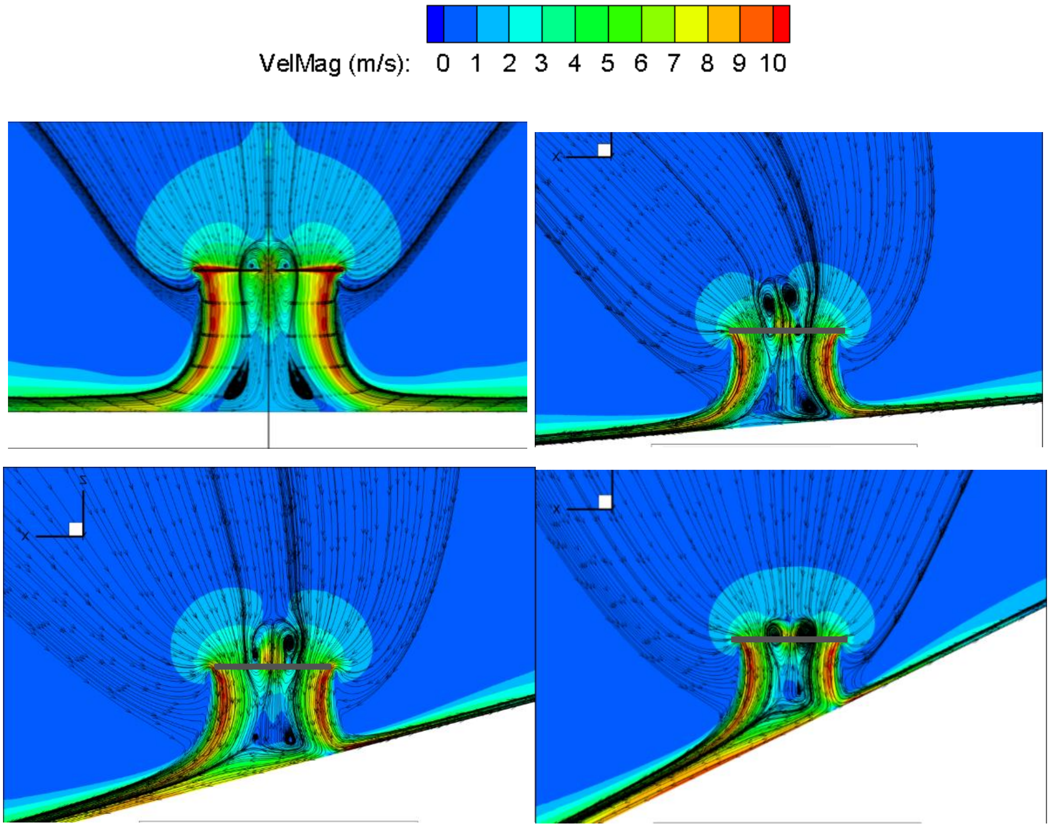

Figure 6.24 Velocity magnitude and streamlines for z/R: 1.6 and

β: 0°, 5°,15°, 25°

In addition. the upper vortex loss leads to higher inflow as shown in Figure 6.24 and in Figure 6.25. As inclination increases, the flow velocity at the downside increases which reduces the ground effect in overall rotor with prevention of flow recirculation at this zone.

The reduction of upper vortices, increases the overall inflow with increasing ground distance.

In Figure 6.24 and in Figure 6.25, for z/R: 1.6 and for z/R: 2, new ground vortex emerges from downside to the upside of the surface inclination. This ground vortex is in cooperation with the increasing root vortex and it is getting stronger with increasing inclination.

Figure 6.25 shows the flowfield and velocity magnitudes for z/R: 2 with changing inclination angle

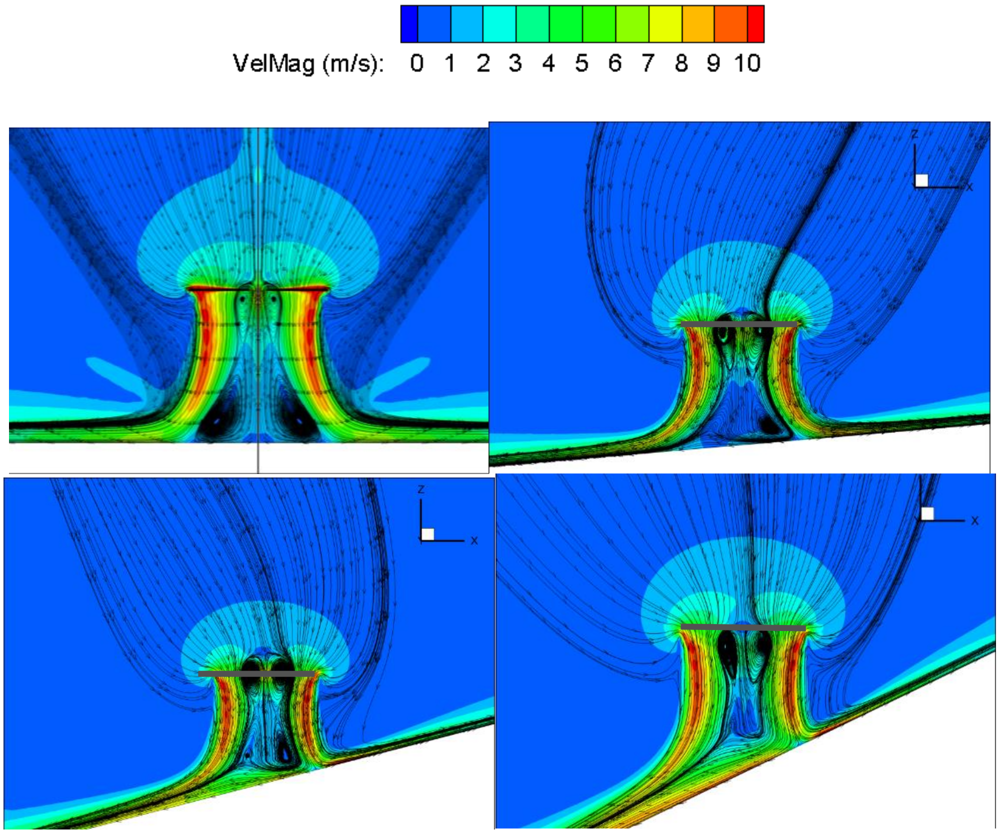

Figure 6.25 Velocity magnitude and streamlines for z/R: 2 and

β: 0°,5° ,15°, 25°

The root vortex is stronger when ground proximity is higher. When z/R: 0.8, due to the higher recirculation than the case of z/R: 1.6, an upper vortex emerges in the vicinity of the blade root. However, when z/R: 1.6, this upper vortex is not available since recirculation is weak. In addition, inclination change at the higher proximity (z/R: 0.8), creates higher downwash decay due to the stronger root and ground vortices.

Inclined surface creates abundant asymmetry on the rotor inflow where the risk of the loss of helicopter control may be emerged. This is actual when flowfields are inspected, the one half of the rotor has a normal downwash whereas other half of the rotor enters the vortex ring state which is critic phase for rotor flow and helicopter stability as explained by Leishman [1].

6.3.3 Inflow Analysis

Figure 6.26 shows the inflow distribution for z/R:0.8 with different inclination angles.

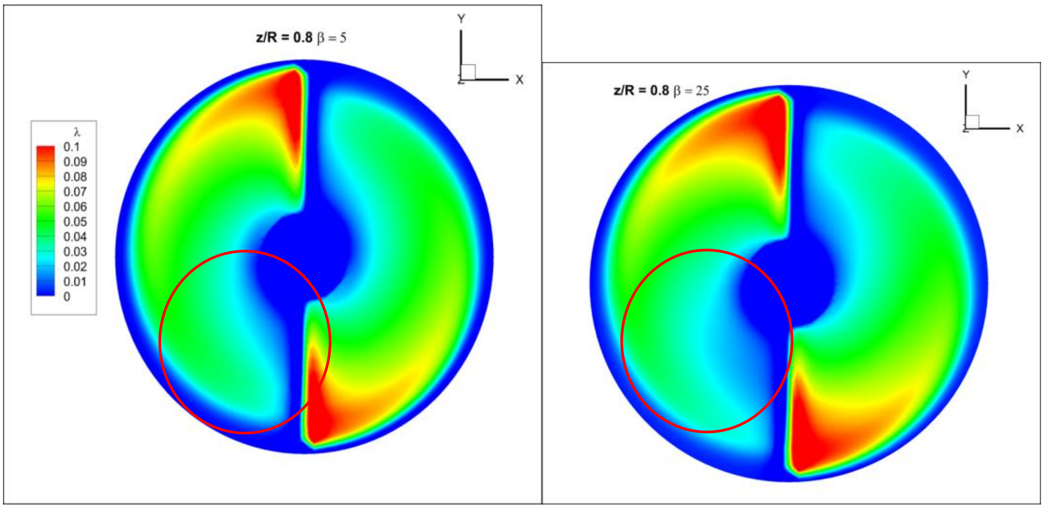

Figure 6.26 Inflow distribution for z/R : 0.8 β:5 and β:25

As inflow pattern of ground effect without inclination cases are inspected, only half of the rotor disk is enough to inspect inflow. The other half is just the symmetry of the described inflow and the overall inflow could be calculated by taking the double of it. since flow symmmetry does not spoil. However. during ground inclination. asymmmetry is apparent. When Figure 6.26 is inspected, asymmetric regions enclosed with red circles appear with increasing β.

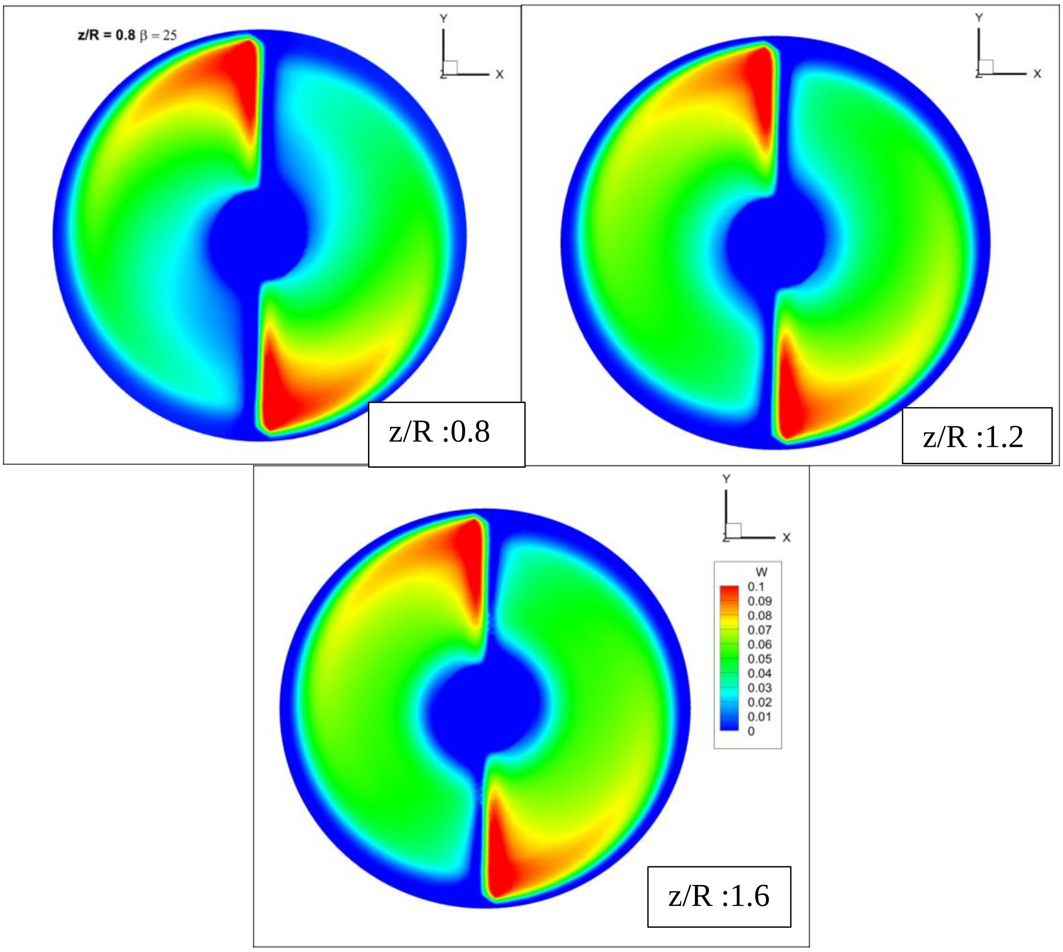

Figure 6.27 Inflow distributions of β:25 for z/R: 0.8, z/R: 1.2 and z/R :1.6

For highest β value, when ground distance increases from z/R: 0.8 to z/R:1.6. asymmetric profile transforms into a more symmetric condition as seen from inflow distributions in Figure 6.27.

In conclusion, inclined ground effect results in asymmetry on rotor inflow, hence, straightforward issues of ground effect without inclination are changing. For different cases, rotor may behave like in-ground-effect or our-of-ground-effect conditions. However, after a certain proximity, asymmetry and overall ground effect vanishes and out-of-ground-effect phenomenon takes the scene.

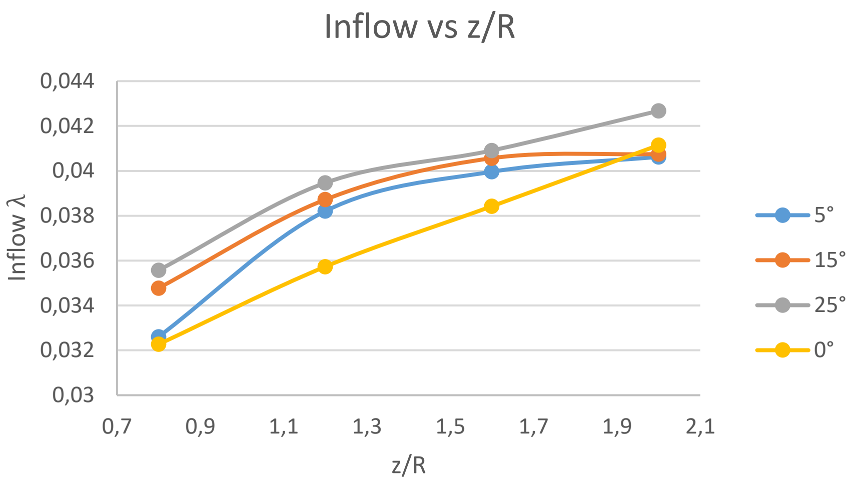

Figure 6.28 Inflow vs z/R for different β

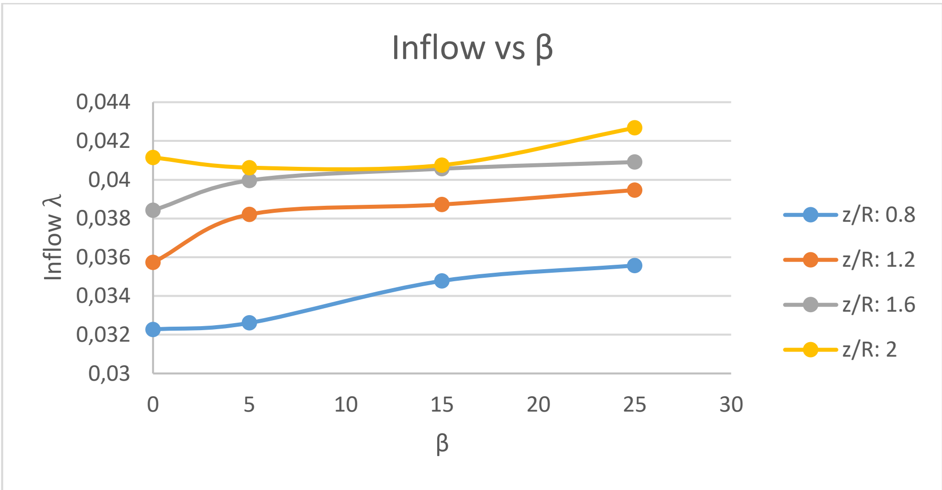

Figure 6.29 Inflow vs β for different z/R

Figure 6.28 shows the variation of inflow with respect to the ground proximity for different inclination angles. Alternatively, the variation if inflow with respect to the inclination angle could be plotted in Figure 6.29. There is a direct proportion between the inflow and increasing inclination. The increasing inclination leads reduction in ground effect due to the inflow increase as declared by Iboshi et al [8,16]

6.4 Empirical Relations

As Figure 5.8 for ground effect without inclination, and Figure 6.19 - 6.21 for inclined cases are inspected, sample 3rd order polynomial curves and empirical equations are obtained. Empirical relations are shown in Figure 6.30.

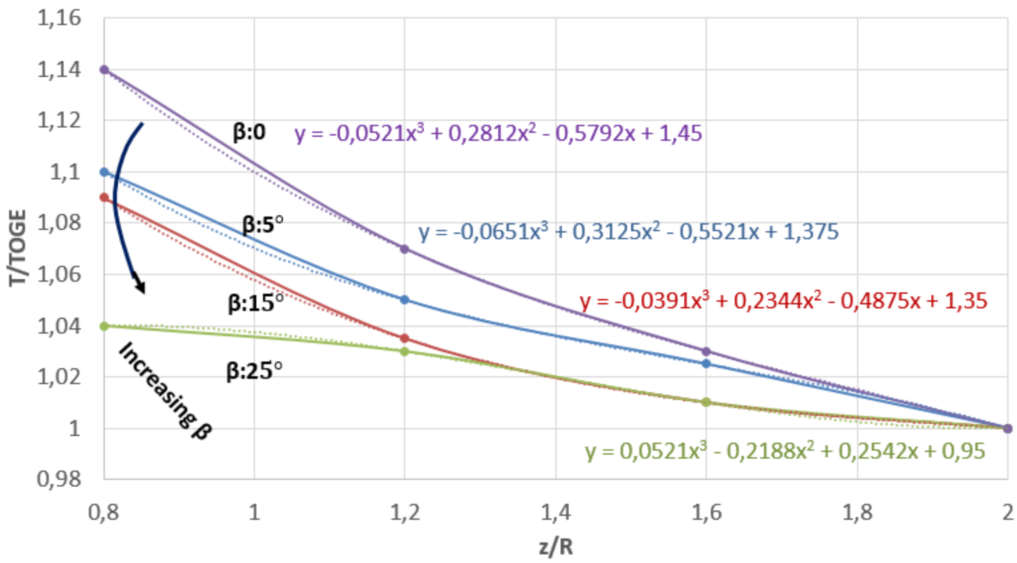

Figure 6.30 Empirical relations for ground effect with/without Inclination for non - dimensional thrust.

With help of Figure 6.30, the non - dimensional thrust value could be estimated for specified ground inclination angle and ground proximity. If thrust value for out of ground effect is known, then desired dimensional thrust could be estimated. Since torque has a constant trend in the interval of z/R:08 – OGE. there is no need to establish an empirical relation for torque.

CHAPTER 7

CONCLUSION AND FUTURE WORK

Ground effect is the change in helicopter rotor performance during the ground presence below the rotor. The recirculating flow from ground to the blades, changes the inflow of the rotor hence, induced power changes which is advantageous that same thrust value is obtained with lower power consumption. This condition is validated with both test setup and CFD method. Accurate tip vortex iso-surfaces and thrust figure shows the validity of the solution procedure.

As ground is inclined, asymmetric condition is imposed on the rotor flow and this asymmetry removes the advantages of ground effect thus, flow field becomes more chaotic. Asymmetry is observable when rotor flow during inclined surface is investigated. The one half of the rotor struggles with vortex ring whereas other half is exposed to quite clean flow during the close distance to the ground. The asymmetry in rotor inflow is totally dangerous since it may spoil the overall stability of helicopter hence, catashtropic results may be inevitable. The fatality risk is higher than the out-of- ground-effect (OGE) condition. During the out of ground effect phase, pilot has a chance to regain the attitude and stability of aircraft due to the altitude and time advantages. Neverthless, during the in-ground-effect (IGE) condition, the distance is very close to the ground, and any corruption in flow like unsymmetric vortex, may create a sudden change in stability and helicopter may go down in a very short time on account of the close distance to the ground. When inclination increases in ground effect, rotor performs out of ground effect characteristics hence, efficiency of rotor decreases.

In this study, fuselage effect is not investigated. However, the occurrence region of the ground vortex is the possible location of any helicopter fuselage which increases the risk of fatality since recirculating flow may rotate the fuselage and this rotation may be a contribution to the overall stability corruption. For this reason, rotor and fuselage design must be resistive to any stability spoiling objects especially in ground effect with inclination. The unsymmetry in rotor flow and downwash must be taken into account during the stability analyses.

Ground effect requires a minimum rpm value in order to initiate a sufficient inflow reduction. For this work, 2000 RPM does not create any ground effect since corresponding tip Reynolds number is not adequate to create sufficient inflow for ground effect aerodynamically.

The fidelity of the test setup is high since similar results are obtained for ground effect with no inclination.

Inclined ground effect creates transient changes in inflow and tip vortex distribution over the rotor. This situation creates sudden changes in thrust and torque values.

The fidelity of CFD methodology is acceptable since test data is validated. Besides, with proper flowfield inspection, the reasons behing the performance losses and gains are evident. Flow field is inspected with tip vortex propagation and velocity magnitude distribution.

A phase locked Particle Image Velocimetry (PIV) application can be planned in order to gain better insight about the flow behaviour during the extreme ground effect cases. The Ground effect tests with partial ground can be performed with the same experimental setup.

For enhancement of CFD simulations, multi moving reference frame, sliding mesh, overset grid can be used in order to reach a result with better convergence rates and better precision.

REFERENCES

[1] Leishman J.G., "Principles of Helicopter Aerodynamics", 2nd Edition. Cambridge Aerospace Series . July 2006

[2] Darling. D. (2017), helicopter. [online] Daviddarling.info. Available at: http://www.daviddarling.info/encyclopedia/H/helicopter.html. 2017

[3] Helicopter Anti-Torque Systems - Helicopter Training Videos (HTV), (2017), Helicopter Training Videos (HTV). Retrieved 27 September 2017, from http://www.helicoptertrainingvideos.com/2013/09/helicopter-anti-torque-systems/

[4] Garden. H. (2017), "How Helicopters Work. The Heart of the Helicopter: The Rotor Assembly", Retrieved 27 September 2017.from http://science.howstuffworks.com/transport/flight/modern/helicopter5.htm

[5] "What are these circles around the propeller?". Aviation.stackexchange.com. Retrieved 27 September 2017. from https://aviation.stackexchange.com/questions/21626/what-are-these-circles-around-the-propeller

[6] FAA “Helicopter Flying Handbook’’. FAA-H-8083-21A

[7] Biot - Savart Law . Retrieved from the website:"http://farside.ph.utexas.edu/teaching/em/lectures/node39.html"

[8] Hayata. Y.,Iboshi. N., Itoga. N., Prasad. J.V.R. ,2002. Ground Effect and Blade Flapping Motion of a Rotor Hovering above Finite Inclined Ground Plane. Journal of the Japan Society for Aeronautical and Space Sciences

[9] Hefner R.A., Knight M.,1941. Analysis of a Ground Effect on the Lifting Airscrew, Daniel Guggenheim School of Aeronautics , Georgia School of Technology, Washington December 1941.

[10] Fradenburgh. E.A. (1960) “The Helicopter and the Ground Effect Machine’’ Sikorsky Aircraft Division, Stratford, Connecticut. Journal of the American Helicopter Society. Volume 5. Number 4. 1 October 1960. pp. 24-33(10)

[11] Bolanovich M., "Experimental Downwash Velocity, Static Pressure, and Temperature Distributions in Ground Effect for a 75-Foot Jet Driven Rotor"

[12] Light. J.S. (1993) "Tip Vortex Geometry of a Hovering Helicopter Rotor in Ground Effect" NASA Ames Research Center, Moffett Field, CA. Journal of the American Helicopter Society, april 1993.

[13] Xin H., Prasad J.V.R., Peters D.A. "An Analysis of Partial Ground Effect on the Aerodynamics of a Helicopter Rotor", AIAA 00-0262

[14] Tanner P., Overmeyer A.D., Jenkins L.N., Yao C.S., Bartram S.M. "Experimental Investigation of Rotorcraft Outwash in Ground Effect". AHS 71st Annual Forum May 5-7 2015, Virginia.

[15] Iboshi. N., Itoga. N., Prasad. J.V.R., Sankar. L.M. (2014) "Ground Effect of a Rotor Hovering above a Confined Area" FAE Journal, Frontiers in Aerospace Engineering Volume 2 Issue 1. February 2014.

[16] Hayata. Y.,Iboshi. N., Itoga. N., Prasad. J.V.R. ,2003. "Hovering Performance of a Rotor in an Inclined and Partial Ground Effect". Journal of the Japan Society for Aeronautical and Space Sciences,Volume 51, Issue 595, pp. 433-440, 2003

[17] Yeager. W.T. Jr., Young. W.H. Jr., Mantay. W.R. (1974) "A Wind Tunnel Investigation of Parameters Affecting Helicopter Directional Control at Low Speeds In Ground Effect''. NASA Technical Note D-7694 Washington D.C. November 1974

[18] Gilad. M., Chopra. I., Rand. O. (2011) "Performance Evaluation of a Flexible Rotor in Extreme Ground Effect" Alfred Gessow Rotorcraft Center, Department of Aerospace Engineering, Maryland USA. 37th European Rotorcraft Forum. Milan, Italy, 2011.

[19] Caradonna. F.X., Tung. C.,1981 "Experimental and Analytical Studies of a Model Helicopter Rotor in Hover". NASA Ames Research Center. Sep. 1981.

[20] Leishman. J.G., Rauleder J., 2012. "Measurements of Organized Turbulence in the Dual-Phase Flow Below a Rotor" Department of Aerospace Engineering, ERF 2012.

[21] Leishman. J.G., Rauleder J., 2013. "Turbulence Modifications and Phase Couplings in Ground Effect under Simulated Brownout Conditions", Department of AEE University of Maryland, American Helicopter Society

[22] Leishman. J.G., Sydney. A., 2013. "Measurements of Rotor/Airframe Interactions in Ground Effect Over a Sediment Bed" Department of AEE, American Helicopter Society

[23] Leishman. J.G., Sydney. A.,2014. "Measurements of the Plume-Like Three Dimensionality of Rotor Induced Dust Fields", Department of Aerospace Engineering, American Helicopter Society

[24] Lee. T. E., and Leishman. J. G. and Ramasamy. M. (2008). "Fluid Dynamics of Interacting Blade Tip Vortices With a Ground Plane." American Helicopter Society 64th Annual Forum Proceedings, Montreal. Canada. April 29–May 1. 2008.

[25] Hanker. Jr. E.J., Smith. R.P. (1985) "Parameters Affecting Helicopter Interactional Aerodynamics in Ground Effect". Journal of the American Helicopter Society, January 1985.

[26] Balch D.T., Sacullo A., Sheehy T.W., 1983. "Experimental Study of Main Rotor/Tail Rotor/Airframe Interactions in Hover -Volume1", NASA Contractor Report 166485, June 1983.

[27] Curtiss. Jr. H.C., Sun. M., Putman. W. F., Hanker. Jr. E.J. (1984) "Rotor Aerodynamics in Ground Effect at Low Advance Ratios". Journal of the American Helicopter Society, January 1984.

[28] Ganesh. B., Komerath. N. (2004) "Unsteady Aerodynamics of Rotorcraft in Ground Effect". AIAA Paper 1004-2431 Fluid Dynamics Meeting Portland, OR. June 2004.

[29] Flemming R. J. "RSRA Vertical Drag Test Report". NASA Ames Research Center ,Contractor Report 166399, 1981

[30] Wadcock A.J., Ewing L.A., Solis E., Potsdam M., Rajagopalan G., "Rotorcraft Downwash Flow Field Study to Understand the Aerodynamics of Helicopter Brownout". U.S. Army Aviation and Missile Command, October 2008

[31] Doerffer P. , Szulc O. , 2008 "Numerical Simulation of Model Helicopter Rotor in Hover". Institute of Fluid Flow Machinery PAS , Gdansk, Poland.

[32] Kim J., Sankar L.N., Marpu R., Egolf T.A., Hariharan N.A "Parametric Study of Planform Effects on Rotor Hover Performance Using a Hybrid Navier Stokes – Free Wake Methodology". European Rotorcraft Forum Southampton UK. 2014

[33] Kang N. , Sun M. , 1997 . "Technical Note. Prediction of Flow Field of a Rotor in Ground Effect". Journal of American Helicopter Society, April 1997

[34] Fredsoe J. , Sumer B.M. , "Scour Below Pipelines in Waves", Journal of Waterway, Port, Coastal and Ocean Engineering" Vol. 116 Issue 3. American Society of Civil Engineers 1990.

[35] Menter. F. R. (1994). "Two -Equation Eddy Viscosity Turbulence Models for Engineering Applications ". AIAA Journal Vol. 32. No. 8, August 1994.

[36] Kao D.L., Ahmad J.U., Holst T.L., Allan B.G., 2013. "Visualization and Analysis of Vortex Features in Helicopter Rotor Wakes", 51st AIAA Aerospace Sciences Meeting 07-10 January 2013, Grapevine ,Texas.

[37] Kutz B. M., Günther T., Rumpf A., Kuhn A. 2014 "Numerical Examination of a Model Rotor in Brownout Conditions". AHS 70th Annual Forum Montreal, Canada, 2014.

[38] Rodriguez C. 2012 "CFD Analysis on the Main Rotor Blade of a Scale Helicopter Model using Overset Meshing". KTH Stockholm, Sweden, 2012

[39] Harten A., Yee H.C., Warming R.F. (1983). "Implicit Total Variation Diminishing (TVD) Schemes for Steady State Calculationss".NASA Technical Memorandum 84342

[40] Turkel, Eli, 1999 "Preconditioning techniques in computational fluid dynamics". Annual Review of Fluid Mechanics 31.1: 385-416.

[41] Amiraux M., Baeder J.D., Thomas S., 2013. "GPU-accelerated FVM – RANS Hybrid Solver for Simulating Two-phase Flow beneath a Hovering Rotor". AHS 2013.

[42] Filippone A. and Mikkelsen R. (2009) "Advances in CFD & Actuator Disk Models for Helicopter Aerodynamics". ERF 2009

[43] Tanabe Y., Saito S., Ooyama N., Hiraoka K., 2008. "Study of a Downwash Caused by a Hovering Rotor in Ground Effect".

[44] Abras J. N., Hariharan N. 2015. "Comparison of CFD Hover Predictions on the S-76 Rotor". AIAA SciTech 5-9 January 2015 , Kissimmee ,Florida

[45] Kocurek J. D. and Tangler J. L. (1976) "A Prescribed Wake Lifting Surface Hover Performance Analysis". Journal of the American Helicopter Society , 14(4), pp. 20 – 32

[46] Haller G. (2005) "An Objective Definition of a Vortex". Journal of Fluid Mechanics vol. 525 pp 1-26 2009

[47] Baeder J., Duraisamy K., 2007 "High Resolution Wake Capturing Methodology for Hovering Rotors" Journal of the American Helicopter Society Vol.52 Number 2, 2007

[48] Baeder J.D., Kalra. T.S., Lakshminarayan. V. K., 2010. "CFD Validation of Micro Hovering Rotor in Ground Effect". Alfred Gessow Rotorcraft Center, University of Maryland, 66th Annual Forum and Technology Display of the American Helicopter Society International Phoenix, Arizona. May 11–May 13, 2010

[49] Lakshminarayanan V., Bush B., Duraisamy K., Baeder J. 2006 "Computational Investigation of Micro Hovering Rotor Aerodynamics". 24th AIAA Applied Aerodynamics Conference,San Francisco CA.

[50] Pandey K. M., Kumar G., Das D., Deka D., Surana A., Das H.J. "CFD Analysis of an isolated main helicopter rotor for a hovering flight". ESTIJ. 2011

[51] Bennett. W.E. and Cheeseman. I.C. (1955) "The Effect of the Ground on a Helicopter Rotor in Forward Flight". ARC R & M 3021.

[52] Hayden. J.S. (1976) "The Effect of the Ground on Helicopter Hovering Power Required". 32th Annual National V/STOL Forum of the American Helicopter Soc.. Washington DC. 10-12May 1976

[53] Layton D.M., "Helicopter Performance" . Matrix Publishers, 1984.

[54] Bensing F., Kessler M., Kramer E., Kutz B., 2010. "CFD calculation of a helicopter rotor hovering in ground effect". STAB Conference, November 2010. Berlin

[55] Bensing F. , Embacher M., Hollands M., Kutz B., Kessler M., Kramer E. 2012. "Numerical Simulation of Helicopter Wake Evolution, Performance and Trim". Institut für Aerodynamik und Gasdynamik, Universitat Stuttgart. Pfaffenwaldring 21. D-70569,Stuttgart, Germany

[56] Zhao J., He C. 2014 "Physics – Based Modeling of Viscous Ground Effect for Rotorcraft Applications". AHS Forum, Montreal, Canada, May 20-22, 2014.

[57] Kurtuluş D.F. "AE547 Experimental Aerodynamics Lecture Notes" .Department of Aerospace Engineering . METU

[58] Şahbaz M., Uzol N.S., Kurtuluş D.F., "Model Helikopter Döner Kanat Sistemi için Yer Etkisi Durumunda Performans ve Akış Araştırması". 6th National Aerospace Conference, UHUK-2016-014. 28-30 September 2016, Kocaeli, Turkey

[59] Şahbaz M., Uzol N.S., Kurtuluş D.F. "Computational Analysis of a Model Scale Helicopter Rotor In Ground Effect". 9th Ankara International Aerospace Conference, 20-22 September 2017

[60] Brown R.E.,Whitehouse G.R., "Modelling Rotor Wakes in Ground Effect" Journal of the American Helicopter Society, July 2004.

[61] Hayden J.S. "The effect of ground on helicopter hovering power required" Proceedings of the American Helicopter Society. 32nd Annual Forum. Washington DC. 1976.

[62] Griffiths D.A., Ananthan S., Leishman J.G., "Predictions of Rotor Performance in Ground Effect Using a Free Vortex Wake Model". Journal of the American Helicopter Society, October 2005.

[63] ATI GAMMA F/T Sensor Ranges . Retrieved from the website: "http://www.ati-ia.com/products/ft/ft_models.aspx?id=Gamma"

APPENDIX A

GROUND TUFT VISUALIZATION

In this part, tuft visualizations for sample ground proximities and inclination angles are given. The corresponding CFD results will be presented for each experimental visualization. As seen from the Figure A.1, Figure A.2 and Figure A.3, both CFD and experimental flowfields are relevant. The flow profile on the ground has a variable profile with respect to the ground invlination angle (β).

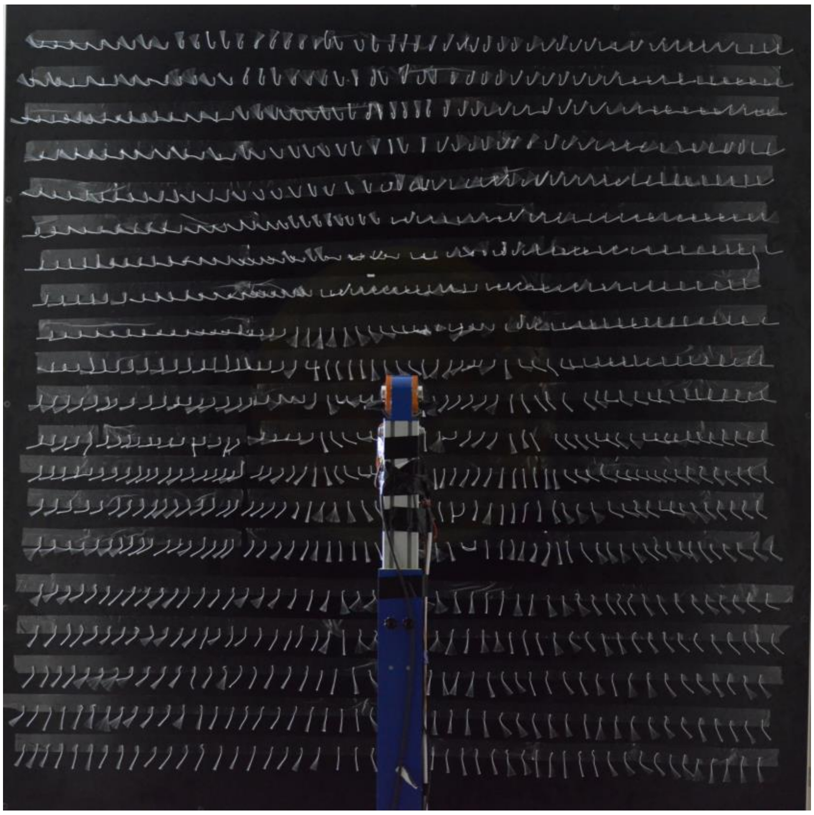

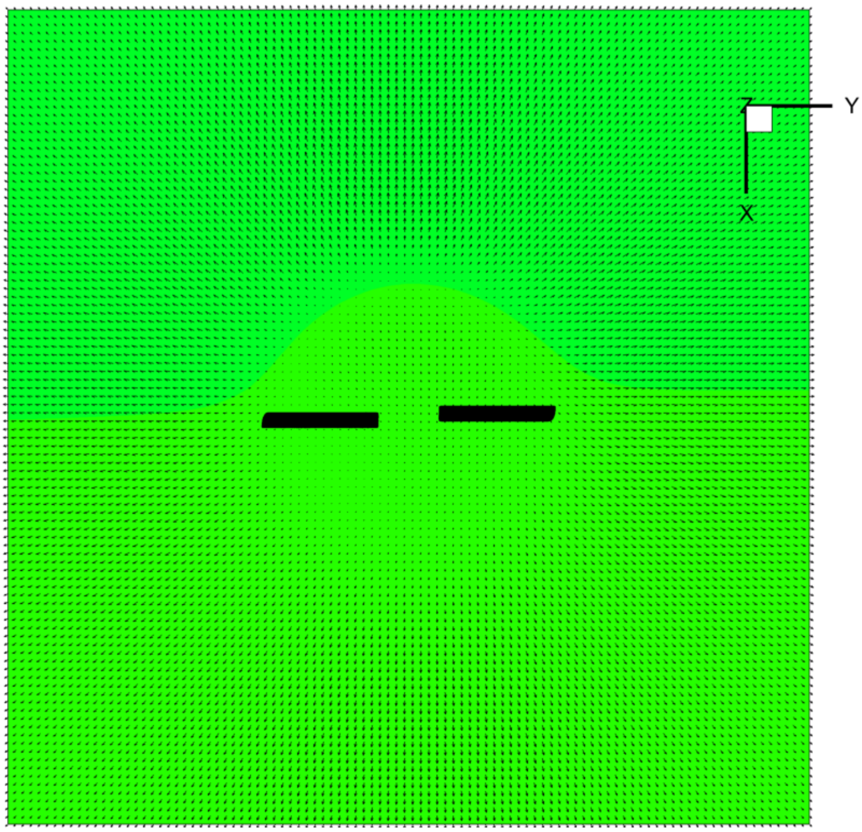

Figure A.1 Tuft visualization for z/R: 1.6 and β: 5°

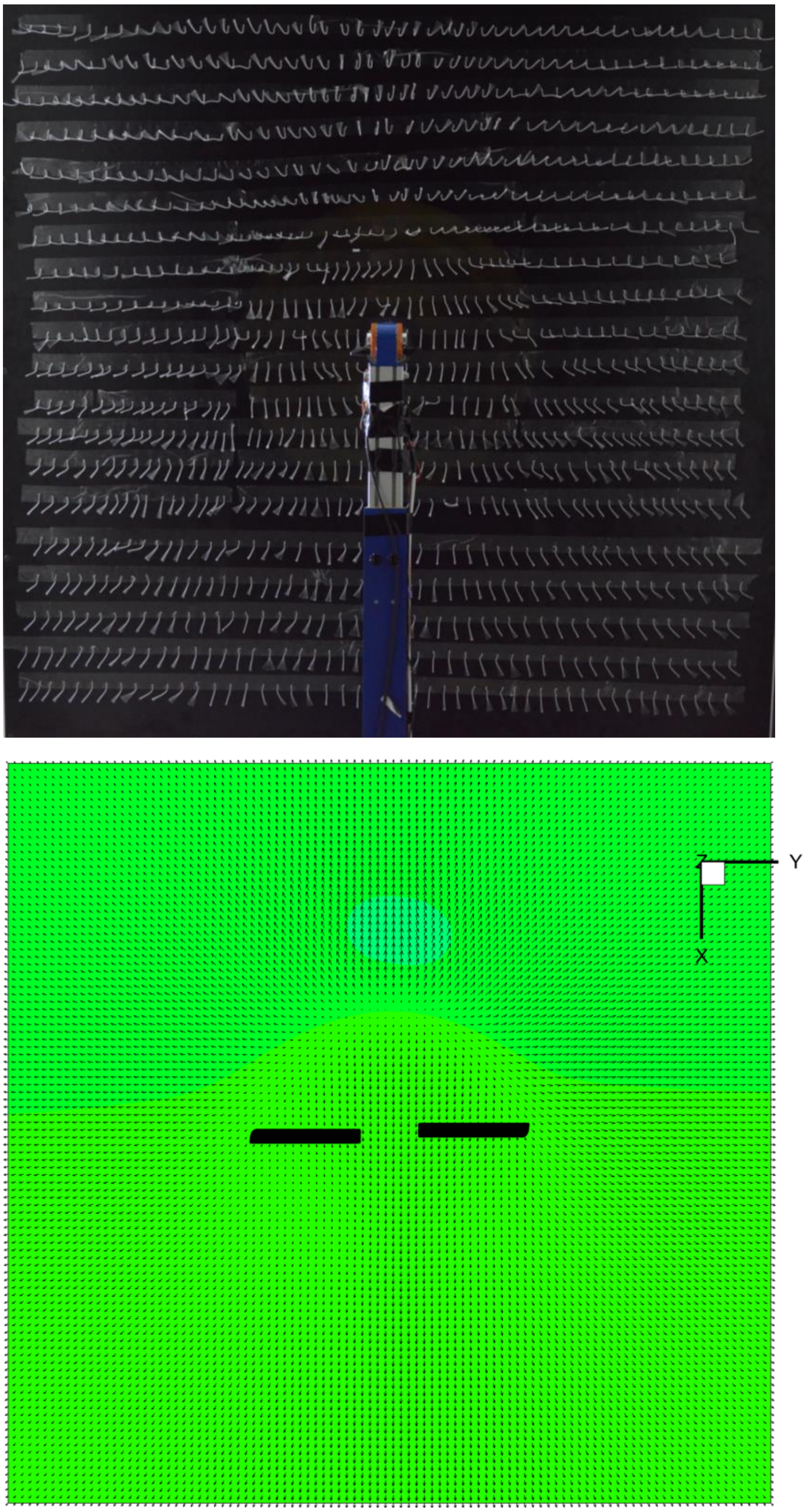

Figure A.2 Tuft visualization for z/R: 1.6 and β: 15°

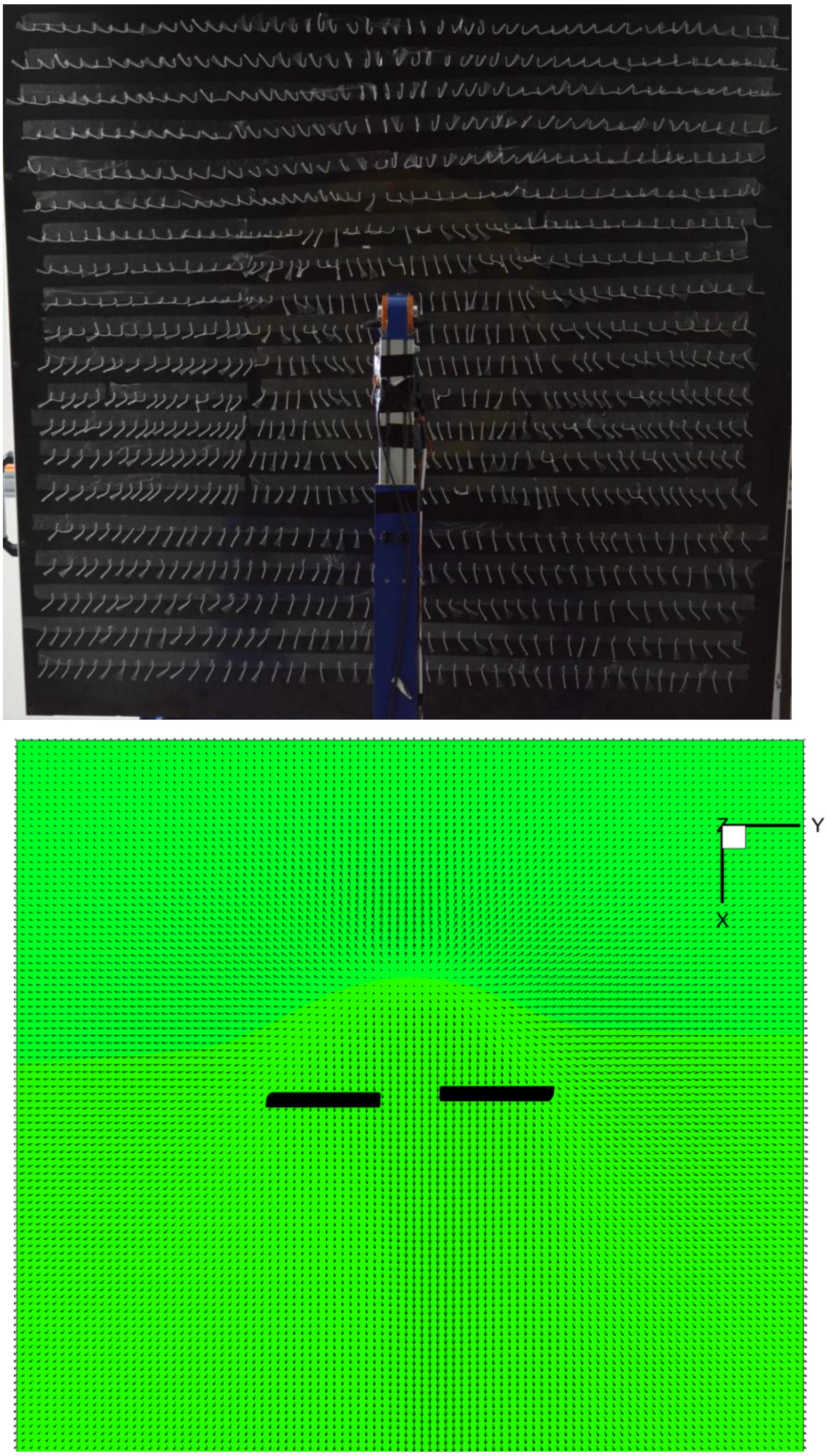

Figure A.3 Tuft visualization for z/R: 1.6 and β: 25°